2 International Conference on Rheology

Presentation

Poster

A-10-234-12

2nd International Conference on Rheology

14 & 15 December 2021, Tehran, Iran

EFFECT OF RHEOMETRICAL PARAMETERS OF EPDM IN FLEXIBLE ELASTOMERIC FOAMING

P. Ezzati[1*], A. Mohammadi[2], N. Taremi[2], M. Hashemi[2] and M R Alizadehfard[1]

1. OSMOTEC, PO BOX 571, Turramurra NSW 2074 Sydney Australia
2. LINKRAN Industrial Group, PO Box 90210, Tehran Iran

peyman@osmotec.com.au

Abstract

In this study rheometrical behavior of EPDM compound in closed cell flexible elastomeric foam (FEF) was investigated. In manufacturing of EPDM FEF, rheometrical parameter shown that production are based on curing and blowing behavior. Studies of rheometric diagram of EPDM foam with different kind of formulation show curing and blowing occurred.

The parameters that showed difference in formulations are such as scorch time, curing rate index (CRI), minimum torque (ML) and maximum torque (MH). Scorch time studies has shown that process must be start with progress of blowing and curing must occur at the second. CRI in highest level helps cells with N_2 gas cur simultaneously with help of ultrafast curing acceleration. MH and ML are the parameters with different volume in diverse of formulation and must be check for each product. MH: 300% modulus, ML: viscosity, MH-ML: Chain Length Duration (CLD)

Keywords: EPDM, RHEOLOGIC, RHEOMETRIE, DIAGARM, CLOSED CELL, FEF

Introduction

Closed-cell elastomeric insulation is one of the most modern insulations in the world, which provides thermal, cooling and acoustic insulation properties. In this regard, their up-to-date production has special sensitivities. Elastomeric Insulations In addition to being a low-density swollen foam, they are also an elastomeric piece that has elastic properties. This piece of elastic foam has millions of closed-cells containing nitrogen gas, which is made in the production process and performs the main load of insulation. EPDM is commonly used as a base elastomer in the fabrication of closed-cell elastomeric insulation. In this research, an attempt has been made to study and obtain the best form of insulation that has both of this properties such as low density and uniformity and complete closed-cells by examine the torques graph had shown in rheometrical test.

Raw materials and testing

In this study EPDM from, Keltan Company with 3430G grade was used. ADC was used as a foaming agent. Sulfur was used as the curing agent and fast curing systems were used as accelerators. DOP oil was used as a softener of mixture. Soot with grade 330 was used.

Results and discussion

A rheometer is a laboratory measuring instrument that, unlike viscometers, is used to measure some augmentation parameters such as dynamic viscosity, shear velocity and shear stress. The operation mechanism of this device is by examining the power required to rotate a stirrer inside the sample, parameters such as dynamic viscosity are measured by this test. It is a tool for determining the characteristics of rubber and vulcanized (baked) compounds. As you know, the raw materials of rubbers in raw form have low properties that cannot be used in industries, but when combines with additives and bakes create a uniform, stable mixture. The important obstacle is the appropriate time of curing these materials which is not stable, according to the type of material and additives in it and due to the lack of re-deformation after curing rubber, it is necessary to provide appropriate information before injection or molding. Timing is very important in this mold of rubber forming process or in injecting, since the material shaping does not change after baking, the curing agent must be in the final stage and after adding all the necessary additives should be added. To perform rheometric tests from the MDR rheometer of the GDM Turkey Company. In the temperature of 180 Celsius degree in 10 minutes. The arch-density of the produced foams was measured by device made in China. Curing agent must be in the final stage after adding all the necessary additives. The scenario of flexible elastomeric closed-cell Insulation foam production is that the compound which enters the furnace moves from a low temperature from 130 °C to a high temperature as 180 °C inside the furnace. Upon the first entering temperature zone, nitrogen gas is releases slowly from ADC. This gas must be trapped inside the final cells and then it cooks to keep the gas inside with no evacuation. The scorch time should be accurate so compound cooking start at last as all the nitrogen gas releases. After that, the cooking process must be fast enough to cook the cell quickly to makes millions of cells at the same time. In order of making flexible closed cells with such elastic properties so that bursting does not occur in the cell under tensile and compressive stresses. To meet all the expectations, three samples of mixtures with three different amounts of sulfur were produced. In the sample with the highest sulfur, the maximum torque was accord, indicating a modulus value of 300% higher. But the values of the torque were same and it cannot be considered effective in the production of closed cell foam because the mooney viscosity of the compounds had the same values. The cooking speed of all three mixes was almost the same because a kind of static cooking system was used with the same accelerators from the fast family. But to some extent, with the increase of sulfur, the cooking speed almost increased. In the three mixtures produced, the difference between the maximum and minimum torque, which indicates the length of the cross joints, increased.

This higher value in sulfur indicates that the C-Sn-C bond length is longer and more elastic in trapping more nitrogen gas. Therefore, the best state of production of closed cell elastomeric insulation was seen in sample No. 3, density was 44 kg/m^3. But samples number 2 and 3 were 65 and 95 kg/m^3.

Acknowledgment

We would like to thank the Board of Directors and the Managing Director of Linkran Industrial Group for investing in research on Linkran elastomeric insulation.

Reference

1- Kass K, Blumberga A, Blumberga D, Zogla G, Kamenders A, Kamendere E. Pre-assessment Method for Historic Building Stock Renovation Evaluation. Energy Procedia 2017;113:346–353.
2- Dylewski R, Adamczyk J. The environmental impacts of thermal insulation of buildings including the categories of damage: A Polish case study. Journal of Cleaner Production 2016;137:878–887.
3- Blumberga A, Timma L, Blumberga D. System Dynamic Model for the Accumulation of Renewable Electricity using Power-to-Gas and Power-to-Liquid Concepts. Environmental and Climate Technologies 2015;16:54–68.
4- Kamenders A, Vilcane L, Indzere Z, Blumberga D. Heat Demand and Energy Resources Balance Change in Latvia. Energy Procedia 2017;113:411–416.
5- Adityaa L, Mahliaa TMI, Rismanchic B, Nge HM, Hasane MH, Metselaare HSC, Oki M, Aditiyab HB. A review on insulation materials for energy conservation in buildings. Renewable and Sustainable Energy Reviews 2017;73:1352–1365.
6- Fanga Z, Lia N, Lia B, Luod G, Huanga Y. The effect of building envelope insulation on cooling energy consumption in summer. Energy and Buildings 2014;77:197–205.
7- Schuchardt GK. Integration of Decentralized Thermal Storages Within District Heating (DH) Networks. Environmental and Climate Technologies 2016;18:5–16.

Table 1 Formulation of FEF based on EPDM in Phr*

Sample	FEF 1	FEF2	FEF 3
EPDM	100	100	100
C.B. 330	10	10	10
DOP	50	50	50
ADC	75	75	75
S	1	3	5
Accelerators	8.5	8.5	8.5
*Phr: per hundred			

Table 2 Rheometerical parameters of samples

Sample	FEF 1	FEF2	FEF 3
MH (n.m)	2.57	2.08	1.65
ML (n.m)	0.24	0.23	0.22
S2 (min: sec)	5	5	5
S90 (min: sec)	1:54	2:05	2:41
CRI	25	20	18
Density (Kg/m^3)	95	65	44

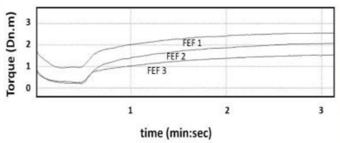

Figure 1: Rheometer diagram based on data from table (1)

Article code: A-10-234-12

2nd International Conference on Rheology

14 & 15 December 2021, Tehran, Iran

EFFECT OF RHEOMETRICAL PARAMETERS OF EPDM IN FLEXIBLE ELASTOMERIC FOAMING

P. Ezzati[1*], A. Mohammadi[2], N. Taremi[2], M. Hashemi[2], and M R Alizadehfard[1]

1. OSMOTEC, PO BOX 571, Turramurra NSW 2074 Sydney Australia
2. LINKRAN Industrial Group, PO Box 90210, Tehran Iran

peyman@osmotec.com.au

Abstract

In this study, rheometrical behavior of EPDM compound in closed-cell flexible elastomeric foam (FEF) was investigated. In the manufacturing of EPDM FEF, rheometrical parameters shown that products are based on curing and blowing behavior. Studies of rheometric diagram of EPDM foam with a different kind of formulation show curing and blowing occurred. The parameters that showed differences in formulations are such as scorch time, curing rate index (CRI), minimum torque (ML), and maximum torque (MH). Scorch time studies have shown that process must start with the progress of blowing and curing must occur at the second. CRI at the highest level helps cells with N2 gas cur simultaneously with help of ultrafast curing acceleration. MH and ML are the parameters with different volumes in diverse formulations and must be check for each product. MH: 300% modulus, ML: viscosity, MH-ML: Chain Length Duration (CLD)

Keywords: EPDM, RHEOLOGIC, RHEOMETRIE, DIAGARM, CLOSED CELL, FEF

Introduction

Closed-cell elastomeric insulation is one of the most modern insulations in the world. which provides thermal, cooling and acoustic insulation properties. In this regard, their up-to-date production has special sensitivities. Elastomeric Insulations In addition to being a low-density swollen foam, they are also an elastomeric piece that has elastic properties. This piece of elastic foam has millions of closed-cells containing nitrogen gas, which is made in the production process and performs the main load of insulation. EPDM is commonly used as a base elastomer in the fabrication of closed-cell elastomeric insulation. In this research, an attempt has been made to study and obtain the best form of insulation that has both of this properties such as low density and uniformity and complete closed-cells by examine the torques graph had shown in rheometrical test.

Raw materials and testing

In this study EPDM from, Keltan Company with 3430G grade was used. ADC was used as a foaming agent. Sulfur was used as the curing agent and fast curing systems were used as accelerators. DOP oil was used as a softener of mixture. Soot with grade 330 was used.

Results and discussion

A rheometer is a laboratory measuring instrument that, unlike viscometers, is used to measure some augmentation parameters such as dynamic viscosity, shear velocity and shear stress. The operation mechanism of this device is by examining the power required to rotate a stirrer inside the sample, parameters such as dynamic viscosity are measured by this test. It is a tool for determining the characteristics of rubber and vulcanized (baked) compounds. As you know, the raw materials of rubbers in raw form have low properties that cannot be used in industries, but when combines with additives and bakes create a uniform, stable mixture. The important obstacle is the appropriate time of curing these materials which is not stable, according to the type of material and additives in it and due to the lack of re-deformation after curing rubber, it is necessary to provide appropriate information before injection or molding. Timing is very important in this mold of rubber forming process or in injecting, since the material shaping does not change after baking, the curing agent must be in the final stage and after adding all the necessary additives should be added. To perform rheometric tests from the MDR rheometer of the GDM Turkey Company. In the temperature of 180 Celsius degree in 10 minutes. The arch-density of the produced foams was measured by device made in China. Curing agent must be in the final stage after adding all the necessary additives. The scenario of flexible elastomeric closed-cell Insulation foam production is that the compound which enters the furnace moves from a low temperature from 130 °C to a high temperature as 180 °C inside the furnace. Upon the first entering temperature zone, nitrogen gas is releases slowly from ADC. This gas must be trapped inside the final cells and then it cooks to keep the gas inside with no evacuation. The scorch time should be accurate so compound cooking start at last as all the nitrogen gas releases. After that, the cooking process must be fast enough to cook the cell quickly to makes millions of cells at the same time. In order of making flexible closed cells with such elastic properties so that bursting does not occur in the cell under tensile and compressive stresses. To meet all the expectations, three samples of mixtures with three different amounts of sulfur were produced. In the sample with the highest sulfur, the maximum torque was accord, indicating a modulus value of 300% higher. But the values of the torque were same and it cannot be considered effective in the production of closed cell foam because the mooney viscosity of the compounds had the same values. The cooking speed of all three mixes was almost the same because a kind of static cooking system was used with the same accelerators from the fast family. But to some extent, with the increase of sulfur, the cooking speed almost increased. In the three mixtures produced, the difference between the maximum and minimum torque, which indicates the length of the cross joints, increased. This higher value in sulfur indicates that the C-Sn-C bond length is longer and more elastic in trapping more nitrogen gas. Therefore, the best state of production of closed cell elastomeric insulation was seen in sample No. 3, density was 44 kg/m^3. But samples number 2 and 3 were 65 and 95 kg/m^3.

Acknowledgment

We would like to thank the Board of Directors and the Managing Director of Linkran Industrial Group for investing in research on Linkran elastomeric insulation.

Reference

1- Kass K, Blumberga A, Blumberga D, Zogla G, Kamenders A, Kamendere E. Pre-assessment Method for Historic Building Stock Renovation Evaluation. Energy Procedia 2017;113:346–353.

2- Dylewski R, Adamczyk J. The environmental impacts of thermal insulation of buildings including the categories of damage: A Polish case study. Journal of Cleaner Production 2016;137:878–887.

3- Blumberga A, Timma L, Blumberga D. System Dynamic Model for the Accumulation of Renewable Electricity using Power-to-Gas and Power-to-Liquid Concepts. Environmental and Climate Technologies 2015;16:54–68.

4- Kamenders A. Vilcane L, Indzere Z, Blumberga D. Heat Demand and Energy Resources Balance Change in Latvia. Energy Procedia 2017;113:411–416.

5- Adityaa L, Mahliaa TMI, Rismanchic B, Nge HM, Hasane MH, Metselaare HSC, Oki M, Aditiyab HB. A review on insulation materials for energy conservation in buildings. Renewable and Sustainable Energy Reviews 2017;73:1352–1365.

6- Fanga Z, Lia N, Lia B, Luod G, Huanga Y. The effect of building envelope insulation on cooling energy consumption in summer. Energy and Buildings 2014;77:197–205.

7- Schuchardt GK. Integration of Decentralized Thermal Storages Within District Heating (DH) Networks. Environmental and Climate Technologies 2016;18:5–16.

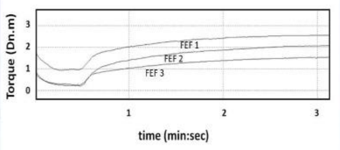

Figure 1: Rheometer diagram based on data from table (1)

Table 1 – Formulation of FEF based on EPDM in Phr*

Sample	FEF 1	FEF2	FEF 3
EPDM	100	100	100
C.B. 330	10	10	10
DOP	50	50	50
ADC	75	75	75
S	1	3	5
Accelerators	8.5	8.5	8.5
*Phr: per hundred			

Table 2 – Rheometerical parameters of samples

Sample	FEF 1	FEF2	FEF 3
MH (n.m)	2.57	2.08	1.65
ML (n.m)	0.24	0.23	0.22
S2 (min: sec)	5	5	5
S90 (min: sec)	1:54	2:05	2:41
CRI	25	20	18
Density (Kg/m3)	95	65	44

A-10-234-16

2nd International Conference on Rheology

14 & 15 December 2021, Tehran, Iran

EFFECT OF RHEOMETRICAL PARAMETERS OF NBR IN FLEXIBLE ELASTOMERIC FOAM

P. Ezzati[1*], A. Mohammadi[2], N. Taremi[2], M. Hashemi[2] and M R Alizadehfard[1]

1. OSMOTEC, PO BOX 571, Turramurra NSW 2074 Sydney Australia
2. LINKRAN Industrial Group, PO Box 90210, Tehran Iran

peyman@osmotec.com.au

Abstract

In this study rheometrical behavior of NBR compound in closed cell flexible elastomeric foam (FEF) was investigated. In manufacturing of NBR, FEF curing and blowing affected on production which shown in rheometrical parameters. Rheometer diagram studies of different FEF foamed formulation based on NBR showed curing and blowing phenomenon simultaneously. These parameters were such as scorch time, curing rate index (CRI) minimum torque (ML) and maximum torque (MH). Scorch time showed that process must be design in the way that blowing should start at first and after blowing curing must occur. Blown cells whit N_2 gas contains must cure simultaneously so that it needs ultrafast curing acceleration and CRI in highest level. MH and ML parameters, must be check for each and individual product. MH, ML, MH-ML despite 300% modulus, viscosity, chain length duration (CLD) respectively.

Keywords: NBR, RHEOLOGIC, RHEOMETRIE, DIAGARM, CLOSED CELL, FEF

Introduction

Closed-cell elastomeric insulation is one of the most modern insulations in the world, which provides thermal, cooling and acoustic insulation properties. In this regard, their up-to-date production has special sensitivities. Elastomeric Insulations In addition to being a low-density swollen foam, they are also an elastomeric piece that has elastic properties. This piece of elastic foam has millions of closed-cells containing nitrogen gas, which is made in the production process and performs the main load of insulation. NBR is commonly used as a base elastomer in the fabrication of closed-cell elastomeric insulation. In this research, an attempt has been made to study and obtain the best form of insulation that has both of this properties such as low density and uniformity and complete closed-cells by examine the torques graph had shown in rheometrical test.

Raw materials and testing

In this study NBR from, Kumho Company with 3430G grade was used. ADC was used as a foaming agent. Sulfur was used as the curing agent and fast curing systems were used as accelerators. DOP oil was used as a softener of mixture. Soot with grade 330 was used.

[

Results and discussion

A rheometer is a laboratory measuring instrument that, unlike viscometers, is used to measure some augmentation parameters such as dynamic viscosity, shear velocity and shear stress. The operation mechanism of this device is by examining the power required to rotate a stirrer inside the sample, parameters such as dynamic viscosity are measured by this test. It is a tool for determining the characteristics of rubber and vulcanized (baked) compounds. As you know, the raw materials of rubbers in raw form have low properties that cannot be used in industries, but when combines with additives and bakes create a uniform, stable mixture. The important obstacle is the appropriate time of curing these materials which is not stable, according to the type of material and additives in it and due to the lack of re-deformation after curing rubber, it is necessary to provide appropriate information before injection or molding. Timing is very important in this mold of rubber forming process or in injecting, since the material shaping does not change after baking, the curing agent must be in the final stage and after adding all the necessary additives should be added. To perform rheometric tests from the MDR rheometer of the GDM Turkey Company. In the temperature of 180 Celsius degree in 10 minutes. The arch-density of the produced foams was measured by device made in China. Curing agent must be in the final stage after adding all the necessary additives. The scenario of flexible elastomeric closed-cell Insulation foam production is that the compound which enters the furnace moves from a low temperature from 130 °C to a high temperature as 180 °C inside the furnace. Upon the first entering temperature zone, nitrogen gas is releases slowly from ADC. This gas must be trapped inside the final cells and then it cooks to keep the gas inside with no evacuation. The scorch time should be accurate so compound cooking start at last as all the nitrogen gas releases. After that, the cooking process must be fast enough to cook the cell quickly to makes millions of cells at the same time. In order of making flexible closed cells with such elastic properties so that bursting does not occur in the cell under tensile and compressive stresses. To meet all the expectations, three samples of mixtures with three different amounts of sulfur were produced. In the sample with the highest sulfur, the maximum torque was accord, indicating a modulus value of 300% higher. But the values of the torque were same and it cannot be considered effective in the production of closed cell foam because the mooney viscosity of the compounds had the same values. The cooking speed of all three mixes was almost the same because a kind of static cooking system was used with the same accelerators from the fast family. But to some extent, with the increase of sulfur, the cooking speed almost increased. In the three mixtures produced, the difference between the maximum and minimum torque, which indicates the length of the cross joints, increased. This higher value in sulfur indicates that the C-Sn-C bond length is longer and more elastic in trapping more nitrogen gas.

Therefore, the best state of production of closed cell elastomeric insulation was seen in sample No. 3, density was 44 kg/m³. But samples number 2 and 3 were 65 and 95 kg/m³.

Acknowledgment

We would like to thank the Board of Directors and the Managing Director of Linkran Industrial Group for investing in research on Linkran elastomeric insulation.

Reference

1- Kass K, Blumberga A, Blumberga D, Zogla G, Kamenders A, Kamendere E. Pre-assessment Method for Historic Building Stock Renovation Evaluation. Energy Procedia 2017;113:346–353.

2- Dylewski R, Adamczyk J. The environmental impacts of thermal insulation of buildings including the categories of damage: A Polish case study. Journal of Cleaner Production 2016;137:878–887.

3- Blumberga A, Timma L, Blumberga D. System Dynamic Model for the Accumulation of Renewable Electricity using Power-to-Gas and Power-to-Liquid Concepts. Environmental and Climate Technologies 2015;16:54–68.

4- Kamenders A, Vilcane L, Indzere Z, Blumberga D. Heat Demand and Energy Resources Balance Change in Latvia. Energy Procedia 2017;113:411–416.

5- Miezis M, Zvaigznitis K, Stancioff N, Soeftestad L. Climate Change and Buildings Energy Efficiency – the Key Role of Residents. Environmental and Climate Technologies 2016;17:30–43.

6- Zamovskis M, Vanaga R, Blumberga A. Mathematical Modelling of Performance of New Type of Climate Adaptive Building Shell. Energy Procedia 2017;113:270–276.

7- Fortuna S, Mora TD, Peron F, Romagnoni P. Environmental Performances of a Timber-concrete Prefabricated Composite Wall System. Energy Procedia 2017;113:90–97.

Table 1 – Formulation of FEF based on NBR in Phr*

Sample	FEF 1	FEF2	FEF 3
NBR	100	100	100
C.B. 330	10	10	10
DOP	50	50	50
ADC	75	75	75
S	1	3	5
Accelerators	8.5	8.5	8.5
* Phr: per hundred			

Table 2 – Rheometerical parameters of samples

Sample	FEF 1	FEF2	FEF 3
MH (n.m)	2.57	2.08	1.65
ML (n.m)	0.24	0.23	0.22
S2 (min: sec)	5	5	5
S90 (min: sec)	1:54	2:05	2:41
CRI	25	20	18
Density (kg/m³)	95	65	44

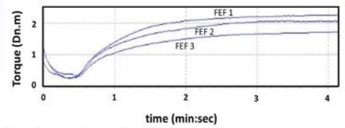

Figure 1: Rheometer diagram based on data in Table (1)

Article code: A-10-234-16

A-10-240-1

2nd International Conference on Rheology

14 & 15 December 2021, Tehran, Iran

Preparation and Evaluation of TPV nanocomposites based on Polycaprolactone /ethylene propylene diene monomer rubber (PCL/EPDM) using dynamic vulcanization and presence of sepiolite nanoparticles

Ali Moshkriz[1], Reza Darvishi[2]*, Fatemeh Naderi[3]

1. Department of Chemical Engineering, Faculty of Engineering, Arak University, Arak, 38156-8-8349, Iran.
2. Department of Gas and Petroleum, Yasouj University, Gachsaran, 75918-74831, Iran.
3. Department of polymer Engineering, Faculty of Engineering, Amirkabir University, Tehran, 15875-4413, Iran.

Abstract

The following research is about the preparation of a nanocomposite base on polycaprolactone /ethylene propylene diene monomer rubber (PCL/EPDM) compound with 2,5-Bis(tert-butylperoxy)-2,5-dimethylhexane (DHBP)-induced dynamic vulcanization and addition of sepiolite nanoparticles (SN). The rheological behavior of the nanocomposites was investigated in order study the properties. SN were localized mostly in the EPDM droplets and at the interface where a layer of particles was formed with a small amount dispersed in the PCL matrix. The incorporation of SN or DHBP induced compatibilization, causing a significant reduction in the size of EPDM droplets in addition to improving the interfacial adhesion. On the other hand, synchronic dynamic vulcanization and SN incorporation synergistically affected the compatibilization of EPDM and PCL phases. The elongation at break and impact strength of the PCL/EPDM compound containing 5% SN showed a significant increase from 18% to 195% and 8.1 to more than 98.3 kJ/m2, respectively as compared to the neat sample.

Keywords: Compatibilization, dynamic vulcanization, SN, Polycaprolactone (PCL), rheology.

Introduction

Today, the wide-spreading application of common petroleum-based polymers has led to environmental contaminations, highlighting the need for novel alternative polymers with high biodegradability [1]. As a biodegradable polymer, Polycaprolactone (PCL) has been benefited from various advantages such as ease of processability, excellent biocompatibility, compared to the conventional polymers, bio-based nature, which have introduced it as a alternative to petroleum-based polymers [2]. However, PCL suffers from inherent brittleness, which has limited its commercial applications [3]. In this research, toughening of PCL has been the subject of some industrial projects. Different approaches have been developed to resolve the brittleness of PCL among which, copolymerization, and blending can be mentioned. As a cost-effective material with elastomeric nature, EPDM has been employed as a toughening agent in different polymers [4]. EPDM is also known for its high flexibility, oil resistance, weather resistance, transparency, and proper affinity toward fillers and pigments. These features have made EPDM a good option to cope with the mechanical drawbacks of PCL as reported by several researchers [5].

Experimental

The weight ratio of PCL to EPDM (PCL/EPDM) was maintained at 75/25. Four series of blends were provided including neat PCL/EPDM and SN containing blends labeled as PCL/EPDM/Nx in which x represents the weight fraction of SN (x = 0%, 1%, 3%, and 5%) with respect to the polymer content. The specimen with DHBP was showed by TPVx (x–varied from 1 to 5). The DHBP content of the compatibilized samples was set at 0.1 wt% (with respect to the total polymers). For instance, PCL/EPDM/DHBP/Nx is representative of the blend containing 75 wt% PCL, 25 wt% EPDM, 0.1 wt% DHBP, and 1 wt% SN is shown by TPV1. The melt mixing approach was utilized to obtain the specimens using a lab internal mixer (Brabender Plastirecord) at 180°C and a rotor speed of 80 rpm for 15 min. First, PCL was incorporated into the mixing chamber. About 2 min later, the EPDM was added. After 1 min, the desired amount of SN nanoparticles was added to the samples. After about 8 min from the beginning of the mixing process, DHBP was added to initiate the dynamic vulcanization process. The samples were obtained using 5 min of compressive molding (400S Polystat model, Germany) at 190 °C.

Results and Discussion

Rheological behavior

Figure 1(a,b) shows the variation of dynamic modulus, G' and G'', with frequency for PCL/EPDM blend and crosslinked PCL/EPDM blends with and without nanoparticles.

The neat PCL/EPDM sample showed terminal behavior trend by a shoulder at the storage modulus at low frequencies which could be assigned to the contribution of the interface to the blend elasticity as well as the shape relaxation of the EPDM droplets within the PCL matrix.In presence of 1 wt% nanoparticles, the modulus increased at all frequencies especially at lower values, and deviated from terminal behavior. The enhancement of both $G'_{components}$ and $G'_{interface}$ contributed to the increase of total G'. The incorporation of SN and DHBP exhibited a synergistic effect in compatibilization of the droplet and matrix phases leading to a considerable enhancement in the interfacial strength and reducing droplet size which increased $G'_{interface}$. As discussed above, due to the higher affinity, the SN nanoparticles are located mainly in the EPDM droplets and some are localized in the PCL phase. Then, the G' components is also enhanced.

Presence of SN in PCL phase restricts short-range dynamics of polymer chains especially in the entanglement length scales contributing to enhanced storage modulus at high frequencies. Nonetheless, SN contents above 5 wt% led to a drastic enhancement in the low-frequency storage modulus making it almost independent of frequency (a plateau). Such a trend suggests a solid-like viscoelastic feature. In other words, SN established a percolated network in the PCL matrix, spanning the sample and restraining the long range motions of polymer chain. This demonstrates that SN got "saturated" in the EPDM phase beyond 5 wt%, and the excess amount of NPs will remain in the PCL phase during the mixing process.

Conclusion

In this research, super toughened PCL/EPDM blend was successfully prepared with synchronic dynamic vulcanization and the addition of nanoparticles. At optimal loading of 5 wt% SN and 0.1% DHBP, the highest enhancement of mechanical properties was observed. However, synchronic incorporation of SN and DHBP at optimal levels led to a super toughened PCL/EPDM blend. Rheological measurements revealed a low crosslink density induced by dynamic vulcanization. For SN contents of 5 wt% and above, a substantial increment was detected in the low-frequency storage modulus, making it almost frequency-independent (a plateau). Such a phenomenon demonstrates that NPs got "saturated" in the EPDM phase beyond 5 wt%, and the excess amounts of SN remained in the PCL phase during the mixing process.

References

[1]. Han, Jin-Lin, Sun-Mou Lai, and Yu Ting Chiu. "Two-way multi-shape memory properties of peroxide crosslinked ethylene vinyl-acetate copolymer (EPDM)/polycaprolactone (PCL) blends." Polymers for Advanced Technologies 29.7 (2018): 2010-2024.

[2]. Burgoa Beitia Azieti "Design and development of high-performance thermoplastic vulcanizates with vibration damping properties." (2020).

[3]. Palau, Carmen V., et al. "Promotion Items EPDM Cheering Foam Hand for Sports Events." Engenharia Agricola 38.6 (2018): 893-900.

[4]. Deng, Wangde, et al. "Adsorption recovery of phosphate from waste streams by Ca/Mg-biochar synthesis from marble waste, calcium-rich sepiolite and bagasse." Journal of Cleaner Production 288 (2021): 125638.

[5]. Deng, Wangde, et al. "Adsorption recovery of phosphate from waste streams by Ca/Mg-biochar synthesis from marble waste, calcium-rich sepiolite and bagasse." Journal of Cleaner Production 288 (2021): 125638.

Figures and Graphs

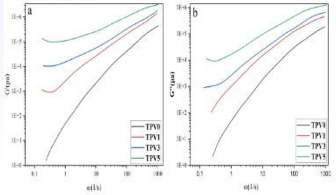

Figure 1-(a,b). Variation of (A) storage modulus and (B) loss modulus with frequency for different samples.

Article code: A-10-240-1

2nd International Conference on Rheology

14 & 15 December 2021, Tehran, Iran

Rheological investigation of binary EPDM/PA blend processed via Reactive Extrusion

Fatemeh Naderi[1], Reza Darvishi*[2], Ali Moshkriz[3]

1. Department of polymer Engineering, Faculty of Engineering, Amirkabir University, Tehran, 15875-4413, Iran.
2. Department of Gas and Petroleum, Yasouj University, Gachsaran, 75918-74831, Iran.
3. Department of Chemical Engineering, Faculty of Engineering, Arak University, Arak, 38156-8-8349, Iran.

Abstract

Tough EPDM/PA blends were compatibilized by in situ reactive extrusion. This study deals with evaluation of the influences of blend composition on the rheological properties. In low frequency region, Elastic behavior of PA shifted to viscose behavior in the presence of dispersed and grafted EPDM droplets. Increasing content of EPDM in the blend, led to lower compatibility and dilatant fluid behavior moved to lower frequencies until this behavior disappeared in presence of 25% EPDM.

Keywords: in situ copatibilization– reactive extrusion – dilatant fluid – psudoductile fluid -Toughness

Introduction

One of the most common engineering plastics with excellent properties is PA. but its low impact strength restricts applications [1,2]. The very basic toughening method is to incorporate rubber particles [3,4]. However, their incompatibility reduces these properties. Therefore, interface interaction should be promoted. The effects of the viscoelastic behavior of blends on their final mechanical has been noticed in the past few decades [5,6]. Also, the rheology is an effective way to study morphology and the interface properties and of the blends. On the other hand, Reactive extrusion is considered as a common method to manufacture polymer blends with special properties. The rheological properties of EPDM/PA blends are investigated in this study to provide the relationship between structure and performance.

Experimental

In the conducted reactive extrusion, various amounts of EPDM was dissolved in molten CL at 160 °C under mechanical stirring and 1 wt. % KOH and 0.5 wt. % TDI were added to two distinct equal parts of the EPDM/CL molten mixture, following by reactive extrusion which was carried out in an co-rotating twin screw extruder at the temperatures of the 200 °C. Different blends with 5, 15 and 25 wt. % contents of EPDM were produced, respectively.

Results and discussion

Blend composition, interfacial adhesion, morphology and molecular weight are significantly affecting properties of blends. 25 the complex viscosity of the both PA and EPDM decreased as the frequency increased, and exhibited shear-thinning characteristic. However, an increase in the η* value of the reactive blends is observed at low frequencies and then decreased gradually in the high-frequency region. This diagram illustrated that this behavior us quite different from the dilatant fluid behavior in the whole-frequency region. In low frequency region, the dilatant fluid behavior attributes to the uniform distribution of EPDM droplets, and the enhanced compatibility between PA and EPDM. Gradually moving of the dilatant fluid behavior to the lower frequencies with increasing amount of EPDM is a noticeable point in the diagram. This behavior is disappeared at 25% of the EPDM based on increased diameter of droplets and decreased compatibility. Also, the complex viscosity of reactive blends increased with the EPDM content at a fixed frequency. Based on enhanced interfacial interaction, the reactive blends showed higher complex viscosities than the values predicted by linear superposition. Because of high viscosity of the reactive melting mixture of caprolactone and EPDM based on inhibited diffusion of the active ionic centers of polymerization, molecular weight decreased in the blend by increasing EPDM amount, figure1-A. The storage modulus (G) as PA/EPDM blends with different amounts of ABS is illustrated, figure 1-B. As shown in the figure, the storage modulus curves for EPDM and PA followed a linear mixing rule. The storage modulus of these blends gradually increased with the increasing amount of EPDM. Notably, G' diagram showed a similar trend. As a result, the storage modulus showed an increase in the low frequency region and followed linear mixing rule in the high frequency region. Therefore, the compatibility of reactive blends is proven, which leads to an enhancement in the interfacial adhesion, Figure1-B. The loss modulus diagram for the reactive blends with different contents showed that the 25 wt% blends has the maximum loss modulus, indicating a higher energy dissipation that for the other blends with lower EPDM contents, Figure 1-C. The increase in EPDM or the rubber phase content increased the loss modulus of the EPDM/PA blends. Therefore, the rubbery phase in the EPDM strongly controls the viscoelastic behavior and loss modulus of the reactive blends.

Conclusion

The rheological properties of the EPDM/PA blends prepared by reactive extrusion were studied. The uniform distribution of EPDM droplets led to dilatant fluid behavior and a transition from viscous to elastic behavior in the low frequencies. Also, by increasing EPDM content, the diameter of EPDM droplets raise and the compatibility decreased, resulting in the disappearance of the dilatant behavior.

Refrences

1. Hale, W.; Lee, J.-H.; Keskkula, H.; Paul, DR. Effect of PBT melt viscosity on the morphology and mechanical properties of compatibilized and uncompatibilized blends with ABS. Polymer 1999, 40, 3621-3629.
2. Ozkoc, G.; Bayram, G.; Bayramli, E. Effects of polyamide 6 incorporation to the short glass fiber reinforced ABS composites: an interfacial approach. Polymer 2004, 45, 8957-8966.
3. S. Wu, "Control of Intrinsic Brittleness and Toughness of Polymers and Blends by Chemical Structure: A Review," Polym. Int., vol. 29, no. 3, pp. 229–247, 1992.
4. XU, Chuanhui, et al., Dynamically vulcanized PP/EPDM blends with balanced stiffness and toughness via in-situ compatibilization of MAA and excess ZnO nanoparticles: Preparation, structure and properties. Composites Part B: Engineering, 2019, 160: 147-157.
5. Mungall, J. E. Interfacial Tension in Miscible Two-Fluid Systems with Linear Viscoelastic Rheology. Phys. Rev. Lett. 1994, 73, 288-291.
6. Maani, A.; Blais, B.; Heuzey, M.-C.; Carreau, P. J. Rheological and morphological properties of reactively compatibilized thermoplastic olefin (TPO) blends. J. Rheol. 2012, 56, 625-647.

Figures and Graphs

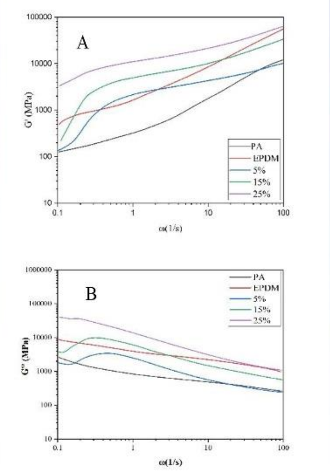

Figure 1 diagrams of G' (A) & G'' (B) of different samples: (PA), (EPDM), PA with 5%EPDM (figure 5%) , 15% EPDM (figure15%) and 25% EPDM(figure25%).

Article code: A-10-240-2

www.icor-sor.com

A-10-244-2

2nd International Conference on Rheology
14 & 15 December 2021, Tehran, Iran

Investigating the Degradation of PLA/ PCL/ ZnO Nanocomposites by Viscoelastic models

Parsa Dadashi[1], Amir Babaei[2]
1. School of Chemical Engineering, College of Engineering, University of Tehran, Tehran, Iran
2. Department of Polymer Engineering, Faculty of Engineering, Golestan University, Gorgan, Iran

Abstract
For the first time, the degradation of a polymer blend in the presence of nanoparticles by considering the effect of nanoparticles on the degradation was investigated using Lee and Park model and fractional Zener model in this research. Poly (lactic acid)/ poly (caprolactone)/ zinc oxide nanocomposite blends were prepared by melt mixing method. Interface complex shear modulus for the neat polymer blend and its nanocomposites were calculated by using Lee and Park model in a range of frequencies. All of factors imposing elasticity on the systems including the solid-like behavior and also degradation catalytic activity of ZnO nanoparticles in the presence of polyesters were considered. Accordingly, most of the samples with a high amount of ZnO exhibited low elasticity which was attributed to the overcoming of the degrading role of ZnO. Additionally, the results obtained from the fractional Zener model was in a good harmony with the Lee and Park model analysis.

Keywords: Lee and Park model- Fractional Zener- hydrolytic degradation- Nanocomposites- PLA- ZnO nanoparticles.

Introduction

In recent decades, many researches are devoted to developing degradable polymeric systems due to the environmental pollution of petroleum-based polymers[1,2]. One of the most promising biodegradable polymers with extraordinarily bio-applications is Poly (lactic acid) (PLA)[3–9]. PLA brittleness is a very important disadvantage, in spite of its bio-applications advantage[10–16]. Therefore, blending the PLA with other biodegradable polymer such as polycaprolactone (PCL) for improving PLA mechanical properties by toughening mechanism has been recommended[17]. In addition to the importance of mechanical properties of biomaterials, controlling the degradation time is a significant parameter in bio-applications such as drug delivery, tissue engineering and so on[18]. Hence, using a third component as a degradation rate controller in PLA/ PCL blend is a technical approach. Zinc Oxide (ZnO) as an antibacterial nanofiller has an effect on hydrolytic degradation on polyesters[19]. Significance of the polymer blends interface on the mechanical properties is an inevitable issue, and mechanical-microstructure correlation of the polymer blends was investigated many times but the applicability of the rheology Provide opportunities for researchers to look into various fields[11,20–22,22,23]. Accordingly, investigating the degradation was carried out with rheological emulsion models and fractional Zener model for the first time due to the role of degradation on the interfacial viscoelastic properties of PLA/ PCL polymer blends.

Experimental

PLA with Ingeo 2003D trade name supplied by NatureWorks Co.Ltd. (USA), has a density of 1.24 g/cm³, a melting point of 210 °C, a tensile strength at brea of 53 MPa and a melt flow index of 6 g/10 min (210°C, 2.16 Kg). PCL, Capa® 6800 with melting point of 58-60 °C, melt flow rate of 3 g/10 min (1" PVC die at 160C,2.16Kg), density of 1.1 g/cm³ was supplied by Perstrop Sweden.

Samples were Melt mixed by HAAKE internal mixer model SYS 90 drive (USA). PLA as matrix phase and PCL as disperse phase form 80 wt.% and 20 wt.% of the PLA/PCL blend, respectively. The Mixing was performed at 170 c and 60 rpm for 8 min. Rheology assessment was performed at 170 under a Nitrogen atmosphere by instAnton Paar USD200 (Austria) rheometer. The morphology of cryo-fractured samples was investigated by using a field emission scanning electron microscope (FE-SEM) MIRA3 model from Tescan (Czech Rep).

Results and Discussion

Morphology

Fig.1a-f shows the FE-SEM micrographs of PLA/PCL blend and its nanocomposites containing 2,4 and 6 wt. % ZnO nanoparticles. FE-SEM micrographs demonstrate droplet-matrix morphology in which PLA and PCL are matrix and droplet with (80/20 w/w), respectively.

Viscoelastic emulsion models

Lee and Park have developed Doi and Ohta model for immiscible polymer blends. Equation (1) is Lee and Park model.

$$G^* = \left(1 + \frac{6(G_d^* - G_m^*)}{10(G_m^* + G_d^*)}\varphi\right) G_m^* + G_{interface}^* \quad \text{Equation 1}$$

Where $G_h^*(\omega)$, $G_m^*(\omega)$, G_d^* and $G_{interface}^*$ are the blend system complex modulus, matrix complex modulus, disperse complex modulus, and interface complex modulus, respectively[24–26].

Fig. 2 shows $G_{interface}^*$ versus frequency for the PLA/PCL (80/20 w/w) samples with various ZnO nanoparticles loading obtained from Lee and park model.

As observed in fig. 2, The following $G_{interface}^*$ values are arranged in decreasing order:

$$G_{i-PLAPCL}^* \gg G_{i-ZnO2}^* > G_{i-ZnO4(1)}^* \cong G_{i-ZnO4(2)}^* > G_{i-ZnO6}^* \quad \text{Equation 2}$$

As mentioned above, PLA/PCL sample had maximum $G_{interface}^*$ value, but by increasing ZnO contents, they almost decreased. The following results are possible reasons for this decreasing trend:

a) Probably, ZnO was migrated from PLA phase to PLA/PCL interface after degradation and play interfacial tension reduction role in non-degraded regions. Moreover, by increasing ZnO nanoparticles contents, the accumulation of nanoparticles in the interface might be increased and leads to coalescence suppression due to nanoparticles acting as barriers at the interface that results in interfacial tension decrement[23,27].

b) PLA/PCL hydrolytic degradation is associated with carboxylic acid, lactic acid, caprolactone, and other functional oligomers generation as a consequence of chain breakup. Therefore, these kinds of residues (carboxylic acid, lactic acid, and so on) could act as compatibilizers when degradation promotes through ZnO nanoparticles incorporation[28–30].

Fractional Zener model

Fractional Zener, which is based on the standard Zener model, has been extensively applied for the evaluation of the viscoelastic properties of composite systems. Equation (11) is the following constitutive equation.

$$G'(\varpi) = G_e + G_0\varpi^{\beta} \frac{\cos\left(\frac{\beta\pi}{2}\right) + \varpi^{\alpha}\cos\left(\frac{(\beta-\alpha)\pi}{2}\right)}{1 + 2\varpi^{\alpha}\cos\left(\frac{(\alpha)\pi}{2}\right) + \varpi^{2\alpha}} \quad \text{Equation 3}$$

(2)

$$\varpi = \omega\tau_0$$

Where β_i, α, τ_0 and G_0 denote the fractional exponents, a characteristic time, and the modulus of the fractional elements, respectively[31].

By fitting Eq. (2) to the experimental data using the genetic algorithm for different samples were calculated, and the results are showed in fig 3.

As it demonstrates, Ge and τ_0, from Zno-2 to Zno-4(1), ZnO-4(1) to Zno-4(2), ZnO-4(2) to Zno-4(3), and ZnO-4(3) to Zno-6 have decreasing, increasing, decreasing, increasing trend, respectively. this decreasing trend in these two parameters (Ge and τ_0) demonstrates increasing viscose nature due to the sample degradation and increasing trend in these two parameters (Ge and τ_0) attributes to increasing elastic nature in consequence of hydrodynamic interactions induced by ZnO nanoparticles. As observed, by increasing ZnO-NPs amounts, degradation almost increases and leads to increasing viscose nature, but Zno-6, in spite of the high amount of ZnO, has a more elastic nature than zno4(3) due to predominated hydrodynamic interactions or agglomeration or its special localization in PLA/PCL blend. In addition, G0 has an inverse trend compared to Ge that confirms mentioned phrase. It implies that increasing G0 parameter values demonstrate increasing viscose nature due to degradation of sample and decreasing trend attributes to increasing elastic nature due to hydrodynamic interactions of ZnO nanoparticles.

Conclusion

In this work is Lee and Park model and fractional Zener micromechanical models were used to describe the relationship between viscoelastic properties and hydrolytic degradation of PLA/ PCL/ ZnO nanocomposites. The viscoelastic properties of PLA/ PCL/ ZnO nanocomposites were fitted well by Lee and Park model. Subsequently, nanocomposites interface complex modulus was calculated from Lee and Park model. Decrement trend was almost observed in interface complex modulus by incorporation ZnO that it was ascribed to migration of ZnO to the interface as a consequence of

References

1. Haji Abdolrsaouli, M.; Babaei, A.; Kaschta, J.; Nazockdat, H. *J. Vinyl Addit. Technol.* **2019**, *25*, 48.
2. Jamshidian, M.; Tehrany, E. A.; Imran, M.; Jacquot, M.; Desobry, S. *Compr. Rev. Food Sci. Food Saf.* **2010**, *9*, 552.
3. DeStefano, V.; Khan, S.; Tabada, A. *Eng. Regen.* **2020**, *1*, 76.
4. Garlotta, D. *J. Polym. Environ.* **2001**, *9*, 63.
5. Auras, R.; Harte, B.; Selke, S. *Macromol. Biosci.* **2004**, *4*.
6. Dugan, J. S. *Int. Nonwovens J.* **2001**, *os-10*, 155892500108.
7. Lun, Y. K.; Kim, K.; Hsiao, B. S.; Chu, B.; Hadjiargyrou, M. *J. Control. Release* **2003**, *89*, 341.

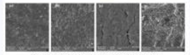

Fig 1. FE-SEM micrographs of a) PLA/PCL (80:20 w/w) blend, b) ZnO-2, c) ZnO-4, f) ZnO-6.

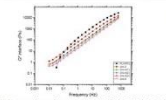

Fig 2. $G_{interface}$ Versus frequency for the PLA/PCL (80/20 w/w) samples with various ZnO loadings obtained Lee and park model after modification of G_m^* values.

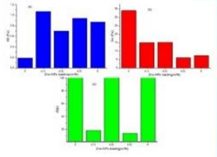

Fig 3. a) G0, b) Ge, and c) τ_0 fractional zener parameters at different ZnO NPs loadings in PLA/PCL-based nanocomposites.

2nd International Conference on Rheology

14 & 15 December 2021, Tehran, Iran

A New Rheological Model for Investigating the Polymer/ Filler Interfacial Properties for binary Polymer Blends

Parsa Dadashi[1], Amir Babaei[2]

1. School of Chemical Engineering, College of Engineering, University of Tehran, Tehran, Iran

2. Department of Polymer Engineering, Faculty of Engineering, Golestan University, Gorgan, Iran

Abstract

Interfacial tension between polymer and filler is an important issue for characterizing the rheological, mechanical, electrical, thermal and optical properties in polymer blends due to the role of nanoparticles localization on the microstructure of phase segregated nanocomposites. Hence, the models that are used are not appropriate for these systems due to the negation of kinetic parameters. In this study, a new model based on Palierne emulsion model is proposed for calculating the polymer/ nanoparticle interfacial tension. The proposed model is validated for Poly (Methyl Meta Acrylate)/ Poly (Styrene)/ Multiwalled Carbon Nanotubes (PMMA/ PS/ MWCNTs) systems with droplet/ matrix morphology.

Keywords: Polymer Blend- Palierne model- Interfacial tension- LVR rheology- Interphase.

Introduction

Polymer/ particle interface properties play a crucial role on the mechanical, electrical, optical and thermal properties specially in binary polymer blends. interface properties are identified by a characteristic parameter that is called interfacial tension[1-4]. In this regard, Wu proposed a static model that is based on thermodynamic equilibrium state. Wu model is not appropriate in melt state that convection is dominated in these systems due to the negation of Wu model assumptions[5]. Palierne proposed a model for investigating the viscoelastic properties of emulsions based on Lorentz approach in electronic physics by accounting mechanical interactions between emulsion droplets and interface contribution[6]. However, Palierne model based on rheological assessments in dynamic states is an accurate model for calculating the polymer/ polymer interfacial tensions but it's not in agreement with polymer nanocomposites rheological results due to the negation of polymer/ particle interactions[6-8].

For the first time, the Palierne model (modified by pal type) was developed for binary polymer blends containing nanoparticles that is localized in droplet phase through considering the stress and strain amplification rate as polymer/ particle parameters.

The model is validated for PMMA/ PS/ MWCNTs nanocomposites as a case study. the parameters obtained from the developed model provided information about droplets crowding effect, nanoparticles amplification rate, and nanocomposite interfacial tension in addition to polymer/ particle interfacial tensions in dynamic states.

Experimental

NC-7000 MWCNTs with 90% carbon purity, 250-300 m^2/g specific surface area was provided from Nanocyl Company (Belgium). PMMA with grade of IH830 and MFI of 2.5 (g/10min) (230°C, 3.8 kg) was purchased from LG chemical Co. PS with grade of Solarene G114 and MFI of 8.5 (200°C, 5 kg) was obtained from DongbuHannong Chemical Co (Korea). PMMA/ PS blend with 80/ 20 weight percent composition containing 1 wt% MWCNTs with matrix- droplet morphology was prepared by brabender internal mixer (D-47055 model (Germany)) at temperature of 220 °C and mixing time of 12 min. oscillatory shear rheological measurements was carried out at the temperature of 220 °C by Physica Anton Paar (MCR 301). Morphology assessments of cryo-fractured samples were carried out by FE-SEM (S-4160) made in Hitachi.

Results and Discussion

Fig 2 depicted morphology of PMMA/ PS polymer blend with 80/ 20 weight percent composition in the presence of 1wt% MWCNTs.
According to the FE-SEM figure, the droplet-matrix morphology is dominated in this system with PMMA droplet phase. Volume average radius of droplets was obtained equal to 1570 nm from FE-SEM morphology images.
Fig 3 demonstrated Transmission electron microscopy image of PMMA/ PS polymer blend with 80/ 20 weight percent composition in the presence of 1wt% MWCNTs. It is observed in figure 3 that MWCNTs is localized in droplet phase.
According to the fig 4, the developed emulsion model is proposed in equation (1).

$$G_c^* = G_m^*\left(\left(\frac{1+3\psi\phi H_1^*}{1-2\psi\phi H_1^*}\right) + a_r a_s\left(\frac{1+3\psi\phi H_2^*}{1-2\psi\phi H_2^*}\right)\right) \quad \text{Equation (1)}$$

$$H_1^* = \frac{4\left(\frac{\alpha}{Ra}\right)[2G_m^* + 5G_{d1}^*] + [G_{d1}^* - G_m^*][16G_m^* + 19G_{d1}^*]}{40\left(\frac{\alpha}{Ra}\right)[G_m^* + G_{d1}^*] + [2G_{d1}^* + 3G_m^*][16G_m^* + 19G_{d1}^*]}$$

$$H_1^* = \frac{4\left(\frac{\alpha}{Ra}\right)[2G_m^* + 5G_{d0}^*] + [G_{d0}^* - G_m^*][16G_m^* + 19G_{d0}^*]}{40\left(\frac{\alpha}{Ra}\right)[G_m^* + G_{d0}^*] + [2G_{d0}^* + 3G_m^*][16G_m^* + 19G_{d0}^*]}$$

$$\psi\phi = 1 - \exp\left[\frac{-\phi}{1-\left(\frac{\phi}{\phi_m}\right)}\right]$$

G_m^*, G_{d1}^*, G_{d0}^*, ϕ, ϕ_m, α, R, ar and as are matrix complex shear modulus, droplet containing nanoparticles complex shear modulus, droplet without nanoparticles complex shear modulus, volume fraction, maximum packing volume, interfacial tension and droplet radius, strain amplification rate and stress amplification rate, respectively.

Fig 4 demonstrated the fitting result of the proposed model (equation (1)) with experimental results that was obtained from rheometer analysis in a graph.
According to the graph, experimental results is in a good agreement with the model.
$\gamma_{PMMA/PS}$, $\gamma_{PS/MWCNTs}$, ϕ_m and aras were obtained from model
is equal to 1.57 mN/m, 13.7 mN/m, 0.37 and 1. Comparison between experimental results and model is summarized in table 1.

Table 1 demonstrated that the model results was in a good agreement with semi-experimental results due to considering droplets crowding effect and amplification rate effect. In addition to the ability of the model for predicting the experimental results, it
provides the supplementary details about the polymer/ nanoparticle interfacial tension due to the accounting amplification and crowding effects parameters.
is equal to 1.57 mN/m, 13.7 mN/m, 0.37 and 1. Comparison between experimental results and model is summarized in table 1.
Table 1 demonstrated that the model results was in a good agreement with semi-experimental results due to considering droplets crowding effect and amplification rate effect. In addition to the ability of
the model for predicting the experimental results, it provides the supplementary details about the polymer/ nanoparticle interfacial tension due to the accounting amplification and crowding effects parameters.

Conclusion

Due to the importance of polymer/ filler interphase on the mechanical, physical properties of polymer blend and lack of the accurate model for calculating the interface parameters, a new model is proposed by considering the polymer/ filler and filler/ filler hydrodynamic interactions in the term of stress and strain amplification rate effects. The model is validated by PMMA/ PS/ MWCNTs experimental data.

References

1. Bhattacharya, M.; Bhowmick, A. K. *Polymer (Guildf).* **2008**, *49*.
2. Buggy, M.; Bradley, G.; Sullivan, A. *Compos. Part A Appl. Sci. Manuf.* **2005**, *36*.
3. Fu, S.-Y.; Feng, X.-Q.; Lauke, B.; Mai, Y.-W. *Compos. Part B Eng.* **2008**, *39*.
4. Mamunya, E. P.; Davidenko, V. V.; Lebedev, E. V. *Compos. Interfaces* **1996**, *4*.
5. Wu, S. *J. Polym. Sci. Part C Polym. Symp.* **2007**, *34*.
6. Graebling, D.; Muller, R.; Palierne, J. F. *Macromolecules* **1993**, *26*.
7. Liao, H.; Liao, R.; Li, S.; Liu, C.; Tao, G. *Polym. Bull.* **2021**.
8. Dadashi, P.; Babaei, A.; Rostami, A. *Iran. J. Polym. Sci. Technol.* **2021**, *34*, 83.
9. Carriere, C. J.; Biresaw, G.; Sammler, R. L. *Rheol. Acta* **2000**, *39*.

Table 1. Comparison between parameters values obtained from new modified model and Semi-Experimental results.

Model parameters	Semi-Experimental	Model
$\gamma_{PMMA/PS}\left(\frac{mN}{m}\right)$ (At 220°C)	1.4 (Harmonic mean equation) [9] 0.7 (Geometric mean equation) [9] 0.564±0.05 (Experimental) [9]	1.57 (PMMA/PS/MWCNT nanocomposite containing 1wt% MWCNT)
$\gamma_{PS/MWCNTs}\left(\frac{mN}{m}\right)$ (At 220°C)	18.46 (Harmonic mean equation) [9] 10.45(Geometric mean equation) [9]	13.7
ϕ_m	0.4 (Krieger-Dougherty model) [9]	0.37
aras	1.32	1

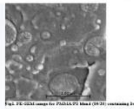

Fig2. FE-SEM image for PMMA/PS blend (80/20) containing 1wt% MWCNTs

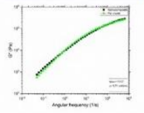

Fig 3. Comparison between experimental viscoelastic data (Complex shear modulus) and predictions of the modified palierne model (Pal model) for PMMA/PS/MWCNT nanocomposite.

Article code:

www.icor-sor.com

2nd International Conference on Rheology
14 & 15 December 2021, Tehran, Iran

Simulation of the filler weight fraction effects on rheological properties and process parameters of polypropylene melt in injection molding

Amirhosein Yazdanbakhsh[1*], Alireza Behzadi[2]

1. PhD candidate in polymer Engineering-School of Chemical Engineering -College of Engineering -University of Tehran
2. Master's degree in polymer Engineering-School of Chemical Engineering -College of Engineering -University of Tehran

*a.yazdanbakhsh@ut.ac.ir

Abstract

Polypropylene (PP) is one of the most widely used plastics for the production of various parts in the injection molding process. Calcium carbonate ($CaCO_3$) is one of the most common mineral fillers that is added to PP to enhance its properties. In this study, the process of injection molding of a Toyota wheel cap was simulated by selecting PP with different weight percentages of caco3 by Autodesk Moldflow software. The results showed that increasing the filler weight percentage affects the rheological properties of the melt and the injection process parameters. In general, with increasing filler percentage, melt viscosity, injection pressure, clamping force and shear stress had higher values.

Keywords: Polypropylene, Injection molding, Viscosity, Filler, Simulation

Instruction

Polypropylene (PP) is a plastic used in the injection molding process to produce a variety of parts. Calcium carbonate ($CaCO_3$) is a common additive for PP reinforcement that increases elastic modulus, decreases yield stress, increases impact resistance, reduces crystallinity and reduces its price. PP/$CaCO_3$ composite is used in the production of plastic shelves, shoes and sandals, automotive industries, home appliances, etc. [1,2].
Dynamically, increasing the $CaCO_3$ particles, enhances the storage modulus and the loss modulus of melt and decreases the damping (tan δ). Thus, increasing the weight fraction of $CaCO_3$ changes the rheological properties of PP melt and therefore, changes the process considerations of injection molding [3]. Today, Autodesk Moldflow is the most well-known software for simulating injection molding and analyzing process conditions and defects. In this study, this software has been used to investigate the effects of increasing the weight fraction of $caco_3$ on melt rheological properties and injection conditions.

Theoretical

Autodesk Moldflow software analysis is based on meshing, so the type and size of meshes are effective in the accuracy of results and analysis speed. Due to the complexity of engineering problems, numerical methods are often used. In this software, two methods of Finite Element or Finite Difference are used to perform calculations.
The meshing of the part (a Toyota wheel cap) was done according to its dimensions (140×43×135) mm of Dual Domain type and with the value of Global edge length equal to 3.99 mm. Finally, 15,690 triangular meshes were created with a maximum aspect ratio of 20.15 and a 99% mesh matching percentage. The polymer used in this work is pp, a product of Ferro company, which once selected a grade of 20% filler ($CaCO_3$) and the next time a grade with 35% filler was selected from the software database. Gate Location, Molding Window, and Fill+Pack analyzes were performed on the mesh piece, the results of which are described below.

Results and Discussion

The simulation results showed that at the same shear rate and temperature, the viscosity of the pp melt increase with increasing weight percentage of caco3, which is shown in Fig 1.
Increasing the weight percentage of filler and consequently growth the viscosity of the plastic melt can affect the injection process conditions. Table 1 compares the various important parameters in the injection molding process for the PP+20% filler and the pp+35% filler. In general, with increasing filler weight percentage, injection pressure, clamping force and shear stress showed higher values. Also, in PP with higher filler percentage, less injection time was observed, which can be related to the higher shear stress applied to this plastic by the injection machine screw, but the reduction of injection time with increasing filler percentage cannot be expressed as a general rule. Cooling time is one of the important parameters of the injection process, which indicates the residence time of the part from the beginning of filling the mold to the ejection time. Fig 2 shows the cooling time diagram in terms of mold temperature for plastics with different filler percentages. According to this figure, with increasing the percentage of filler in the PP + $caco_3$ composite, the cooling time at different temperatures decreases. As expected, in general, the cooling time increases with increasing mold temperature.

Conclusion

In this study, the process of PP injection molding with different weight percentages of $caco_3$ (20% and 35%) was simulated and their rheological and process parameters were compared with each other. The effect of filler increase on viscosity, injection pressure, clamping force, shear stress, melt and mold temperature, injection time and cooling time were also investigated.

References

1. Thenepalli, T., Jun, A. Y., Han, C., Ramakrishna, C., & Ahn, J. W., A strategy of precipitated calcium carbonate ($CaCO_3$) fillers for enhancing the mechanical properties of polypropylene polymers, *Korean. J. Chem. Eng.*, **39**, 1009-1022, 2015.
2. Mao, H., He, B., Guo, W., Hua, L., & Yang, Q., Effects of nano-$CaCO_3$ content on the crystallization, mechanical properties, and cell structure of PP nanocomposites in microcellular injection molding, *Polymers*, **10**, 1160, 2018.
3. Karamipour, S., Ebadi-Dehaghani, H., Ashouri, D., & Mousavian, S., Effect of nano-$CaCO_3$ on rheological and dynamic mechanical properties of polypropylene: Experiments and models, *Polym. Test.*, **30**, 110-117, 2011.

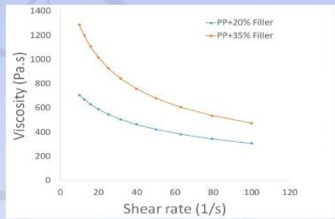

Fig 1. Viscosity diagram vs shear rate

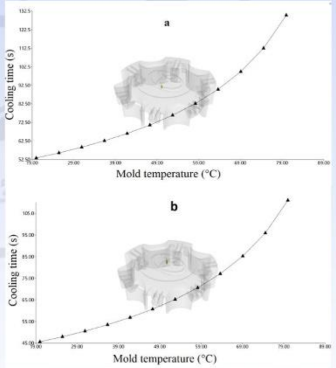

Fig 2. Cooling time vs mold Temperature: a) PP+20% $CaCO_3$, b) PP+35% $CaCO_3$

Table 1. Injection process considerations (For different filler percentages)

Parameter	PP+20% Filler	PP+35% Filler
Maximum Clamp Force (tonne)	1.7	2.3
Maximum Injection Pressure (MPa)	1.8	2.5
Recommended Melt Temperature (°C)	278	241
Recommended Mold Temperature (°C)	80	80
Injection time (s)	2.5	2.3
Shear stress (MPa)	0.26	0.34

Article code: A-10-246-1

A-10-248-1

2nd International Conference on Rheology
14 & 15 December 2021, Tehran, Iran

Effect of sulfur curing accelerators on the combination of sulfur curing and metal oxide in CR/CSM rubber blending

Farshad taghavian, Mohammadreza pourhossainy*
1. student of Malek Ashtar University of Technology
2.Faculty of Materials and Manufacturing Technologies, Malek Ashtar University of Technology.

Abstract

In this research, preparation, description and applications Chlorosulfonate polyethylene (CSM) and Polychloroprene (CR) rubber blend are discussed. CSM rubber is highly reactive, and reactivity is due to the SO_2Cl groups. Which have a sulfur curing. For these reasons, this type of rubber has a low scorching time, which can cause problems for subsequent processes such as molding. Polychloroprene rubber also have a metal curing and have a low scorching time too. In this research, an attempt has been made to achieve better curing by changing the curing system. The effect of using PbO instead of ZnO can also be seen in some mechanical and thermal properties.

keywords: CSM - blend - scorch time - PbO - accelerator.

Introduction

Blends of rubbers are of technological and commercial importance, since they allow the user to access properties of the final blended and vulcanized rubber that is not accessible from a single, commercially available rubber alone [1]. Detailed studies of the mechanisms of scorch delay have been illustrated with studies based on sulphenamide accelerators. Chloro sulfonated poly ethylene (CSM) is an important rubber which has been frequently used in many applications [2]. Chloroprene rubber (CR) can be cross-linked with metal oxides.

Experimental

Rubbers used for composite preparation: CR rubber, Baypren 110, CSM rubber, Hypalon 40S. other rubber ingredients were: stearic acid, and PbO; sulfur obtained from Chemmin Corporation, MgO, ETU, TMTD, CBS. Compounding was done on a laboratory size two roll mixing mill. CRI, were calculated using Eqs. (1) and (2), respectively:

$$MDR = \frac{90(M_{Max}-M_{Min})}{100} + M_{Min} \quad (1)$$

$$CRI = \frac{100}{t_{C90}-t_{S2}} \quad (2)$$

where M_{Min} and M_{Max} are minimum and maximum torque; t_{S2} is the optimum cure time; and t_{C90} is the scorch time.

Results and Discussion

Rheographs of the mixes are given in Figs1. in Table 1 also shows the consumption of each accelerator. CR/CSM rubber blends with TMTD have higher values than CR/CSM compounds with CBS accelerators. The torque difference values of ΔM increase with increasing TMTD concentration and decrease with increasing concentration of CBS accelerators for CR/CSM rubber blends. The CR/CSM rubber blends with TMTD accelerator have ΔM maximum. The scorch time t_{S2} is also improved slightly with increasing CBS (within a few seconds). that the CRI of the compounds increases with increasing accelerator. CBS provides the best processing safety in this compound In addition, TMTD and MBTS also provide superior mechanical properties. Due to their lower reactivity, the MBTS accelerator gives a relatively low state of cure. Therefore, the vulcanizates obtained possess low modulus and hardness as well as elasticity [3].

Conclusion

The chosen accelerator affects the cure rate and scorch safety as well as the number and type of the crosslinks formed. The blends with TMTD possess relatively have the highest CRI and the lowest scorch time. Due to the fact that no filler is used in the compound, it can be noted that adding CBS accelerator to the compound greatly reduces the maximum torque.

References

[1] G. Marković, V. Jovancovic, *Curing and mechanical properties of chlorosulphonated polyethylene rubber blends*, Chem.Ind. Chem. Eng. Q. 17 (3) 315−321 (2011).
[2] Flory PJ (1946) Ind Eng Chem 38(4):417–436.
[3] G. Marković, B. Radovanović, *The Effect of Accelerators on Curing Characteristics and Properties of Natural Rubber/Chlorosulphonated Polyethylene Rubber Blend*, Materials and Manufacturing Processes 2014, 24:10-11, 1224-1228.

Table 1. The content of accelerators (phr) in different rubber compounds based on CR/CSM (50:50) rubber blend with out of any filler.

Accelerators	Sample name		
	A	B	C
CBS	1.5	0	2.5
TMTD	1	1	1
MBTS	0	0.5	0

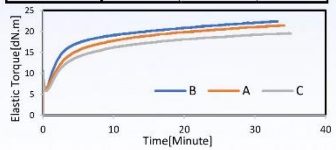

Figure 1. Rheographs of CR/CSM rubber blend compounds cured with accelerator TMTD, MBTS & CBS.

Article code:

www.icor-sor.com

2nd International Conference on Rheology
14 & 15 December 2021, Tehran, Iran

Tuning pressure-sensitive adhesion in blend adhesives using viscoelastic properties

As'ad Zandi and Somayeh Ghasemirad*
Polymer Engineering Department, Faculty of Chemical Engineering, Tarbiat Modares University, P.O. Box 14115-114, Tehran, Iran

Abstract
Despite their generally high shear strength, thermoplastic polyurethane pressure-sensitive adhesives (TPU-PSAs) suffer from low tack. Herein, a synthesized TPU-PSA containing 17.5% hard segment was blended with a synthesized acrylic copolymer PSA comprised of 82 wt. % butyl acrylate and 18 wt. % methyl methacrylate. The puropse of the research was to control the pressure-sensitive adhesion using Chang's viscoelastic window and Chu's criteria. The blend PSAs generally demonstrated shear strengths and loop tack values in between and more than those of the pure components, respectively. The loop tack of the blend PSA was maximized at the TPU content of 40 wt. % in the blend.

Keywords: Thermoplastic polyurethane; Pressure-sensitive adhesive; Chang's viscoelastic window; Loop tack; Shear strength

Introduction

Pressure-sensitive adhesives (PSAs) are able to bond various substrates under light pressure in a short time, and they must be debonded without leaving residue on the substrate [1]. PSAs are used in labels, tapes, protective films, and medical products (patches, bandages, electrodes, plasters, etc.). Performance of PSAs are controlled by their viscoelastic properties due to the required balance between viscous and elastic components required for adequate bonding upon contact with the substrate and desired debonding. The performance of the PSAs are determined by three main characteristic properties, namely tack, shear strength, and peel strength.

According to the Dahlquist's criterion, an adequate tack in PSAs is obtained at G' values lower than 3×10^5 Pa at 25 °C and frequency of 1 Hz [2]. According to Chu, an adequate combination of adhesion (tack, peel) and cohesion (shear) properties in PSAs is expected when the G' value measured at 0.1 rad/s is $(2–4)\times10^4$ Pa and the (G' at 100 rad/s)/(G' at 0.1 rad/s) ratio is 5 to 300 [3].

Experimental

4,4-diphenylmethane diisocyanate (MDI) was kindly donated by Karoon Petrochemical Co. (Iran) and poly(propylene glycol) (PPG) with molecular weight of 2000 g/mol was supplied by Isfahan Copolymer Co. (Iran). Dibutyl tin dilaurate (DBTDL), 1,4-butanediol (BD), and N,N-dimethyl formamide (DMF) were obtained from Merck Co. (Germany). Methyl Methacrylate, Butyl acrylate and ethyl acetate were purchased from Merck (Germany) and 2,2'-azobisisobutyronitrile (AIBN) as an initiator were purchased from daejung (korea).

TPU-PSA was synthesized by using the prepolymer method in 250 mL flask under inert atmosphere (dried nitrogen) using an anchor impeller and overhead stirrer RZR-2102 (Germany). NCO/OH molar ratio of 1:1 were used considering also the OH groups of BD in the calculation [1]. MDI was melted at 80 °C in the flask, and the PPG, dried at 80 °C under reduced pressure (300 mbar) for 2 h, was added under stirring at 250 rpm. The reaction was continued for 30 min. Afterwards 0.02 mmol of catalyst (DBTDL) was added and the stirring was decreased to 80 rpm. The reaction lasted for 2 h and the amount of free NCO content was determined by dibutylamine titration. Then, the chain extender (BD) was added under stirring at 80 °C and 80 rpm for 5 min. DMF was used to dissolve the TPUs prior to coating on poly(ethylene terephthalate) (PET) films. For synthesizing acrylic PSA (Ac-PSA), the reactor was initially charged with MMA and BA (18:82 by weight), ethyl acetate, and AIBN solution [4]. The polymerization was carried out in a 250-mL four-necked flask, equipped with a reflux condenser and a nitrogen inlet. The reaction was conducted at 75 °C for 4.5 h. The blends of TPU-PSA and Ac-PSA were prepared at various compositions using a magnetic stirrer at 350 rpm. The mixing was carried out at 25 °C temperature for 5 h. The blends were coded with "TPUx-Ac" where x signifies the composition of TPU in the blend in wt. %.

The viscoelastic properties of the pristine TPU-PSA and Ac-PSA were measured using dynamic mechanical analysis (DMA) by Netzsch DMA 242 (Germany) at a strain of 30 µm, frequency of 0.1-50 Hz, and temperature range of -20-40 °C. The loop tack was investigated using a homemade universal testing machine using ASTM D6195-03 at a test speed of 300 mm/min. Static shear test was performed by hanging a weight of 1 kg to the PSA bonded to stainless steel in an area of 25 × 25 mm².

Results and discussion

Using the rheological mastercurve of TPU-PSA containing 17.5% hard segment, Fig. 1, it was located in the high shear zone of the Chang's viscoelastic window, Fig. 2. Moreover, its lower low-frequency G' than 3×10^5 Pa revealed its PSA character according to the Dahlquist's criterion. Blending of the Ac-PSA with lower storage and loss moduli with TPU-PSA led to preparation of PSAs with a generally higher shear strength than the Ac-PSA and a loop tack of interestingly higher than that of the primary components. The lower shear strength of the TPU20-Ac than the pristine Ac-PSA was probably due to the low content of TPU which could not compensate the phase separation between TPU and acrylic components. However, increase in the TPU content led to formation of interconnected microphase separated regions and an improved shear strength. The tack of the blend PSAs increased up to 40 wt. % and decreased at higher TPU contents. The negative impact of the low-acrylic content in the blend, namely 20 wt. %, was also observed in the tack.

Conclusions

The blend PSAs were comprised of high-shear moduli TPU and low-shear moduli acrylic copolymer. The blending of high-shear strength TPU and high-tack acrylic copolymer components showed a shear strength in between and a high synergy in tack. The blends far from the middle concentration range showed deterioration in the property expected from the lower-in-concentration component.

References
1. M. Fuensanta and J.M. Martín-Martínez "Influence of the hard segments content on the structure, viscoelastic and adhesion properties of thermoplastic polyurethane pressure sensitive adhesives" J. Adhes. Sci. Technol. **2020**, 1-20
2. C. A. Dahlquist, Pressure-sensitive adhesives. In: R. L. Patrick (Ed.). Treatise on adhesion and adhesives. New York: Marcel Dekker Inc.; **1969**. pp. 219-260.
3. S. G. Chu. Dynamic mechanical properties of pressure-sensitive adhesives. In: L. H. Lee (Ed.). Adhesive bonding. New York: Plenum Press; **1991**. pp. 97-137.
4. S. Taghizadeh and D. Ghasemi "Synthesis and Optimization of a Four-Component Acrylic-Based Copolymer as Pressure Sensitive Adhesive" Iranian Polymer Journal, 19, **2010**, 343-352

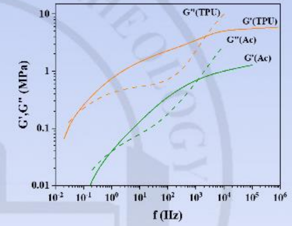

Fig. 1. Rheological mastercurve of TPU-PSA and Ac-PSA

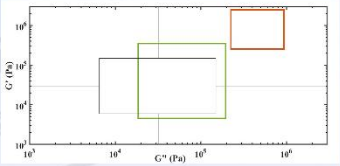

Fig. 2. Chang's viscoelastic window of TPU-PSA (orange) and Ac-PSA (green)

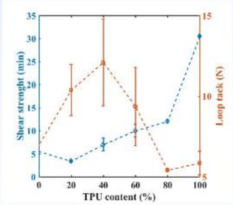

Fig. 3. Shear strength and loop tack of the PSAs versus the TPU content

Article code: A-10-253-1

2nd International Conference on Rheology
14 & 15 December 2021, Tehran, Iran

Preparation of composite with high damping using nitrile-butadiene rubber / phenolic resin

As'ad Zandi[a]*, Mohadeseh Jafarzadeh[b] and Sahar Tavosi[a]

a. Polymer Engineering Department, Faculty of Chemical Engineering, Tarbiat Modares University, P.O. Box 14115-114, Tehran, Iran
b. Caspian Faculty of Engineering, College of Engineering, University of Tehran, Guilan, Iran

Abstract
Rubber is the most important damping material because of its unique viscoelastic properties. The damping principle of rubber damping material is to use the viscoelastic property of the polymer to absorb vibration energy .In this research work, NBR and phenolic resin(P55) in with a mass ratio of 80:20 and three different values of Carbon black were used. According to the resilience test The sample with 70 phr carbon black had a damping value of 91% And according to the DMA test at 10 Hz, tan δ peak showed 0.8 at a temperature of about 25 degrees.

Keywords: Rubber; viscoelastic properties; vibration energy; nitrile-butadiene rubber; phenolic resin

Introduction

Damping materials have been widely used in the vibration and noise control to reduce their harmful consequences in the military and civil areas such as their application in the aerospace and naval vessels, transportation vehicles, bridges and high buildings[1]. Polymer, especially rubber material, has unique high damping property around its glass transition temperature (Tg). During the relaxation process, part of the vibration energy dissipates as heat due to the friction between polymer chains. The loss tangent (tanδ), defined by the ratio of loss modulus (E") to storage modulus (E'), can be a measurement of the dissipation of the vibration energy. High performance damping materials should have a high loss factor (tanδ > 0.3) over a broad temperature range of at least 60–80° C difference. However, a homopolymer usually only has effective damping performance below the room temperature with a narrow temperature range of only 20–30° C difference. Nitrile butadiene rubber/ phenolic resin (NBR/PR [NBPR]) was selected as matrix and different amounts of carbon black (0, 10 and 70 phr) were added to this system. NBR exhibits excellent damping performance due to the presence of polar cyan functional groups in its structure [2].

Experimental

NBR with an acrylonitrile weight content of 41% (N220S) was provided by Japan Synthetic Rubber Co., Ltd (Japan). Phenolic resin granols (P55) were obtained from Wuxi Mingyang Bonding Material Co., Ltd (China). Other rubber processing additives were of analytical grade and used without further purification.The NBPR composites were obtained by mixing the NBR and PR granols (the mass ratio of NBR and PR is 80:20) in φ152.4 mm two-roll mill at room temperature. Then, the compounding and crosslinking additives were added to the above mixtures, including 5.0 phr of zinc oxide, 2.0 phr of stearic acid, 0.2 phr of tetramethylthiuram disulfide, 0.5 phr of diphenyl guanidine, 0.5 phr of dibenzothiazole disulfide, and 2.0 phr of sulfur. Three samples were prepared with carbon block values of 0, 10 and 70 phr, which were named as follows, respectively CB (0 phr), CB (10 phr), CB (70 phr). Finally, the mixtures were hot pressed and vulcanized at 160°C and 15 MPa for their corresponding T90 (optimum cure time). The dynamic mechanical analysis (DMA) of the cured blend is performed on a NETZSCH Dynamic Mechanical Thermal Analyzer model DMA 242 with the tension sample holder. The dimensions of the specimens are 10 × 5 × 2 mm. The dynamic force on sample is 4 N, and it is used to produce oscillating amplitude of 30 μm. If this target amplitude cannot be achieved, the measurement will run with the maximum possible force. The sample is scanned from -150 to 160°C at a heating rate of 5°C/min, and the frequencies used in the measurement are 0.1, 0.5, 1, 5, 10 and 50 Hz., Resilience , Hardness and Tensile properties It was done according to the ASTM D1054 ,ASTM D2240 and D412 Respectively.

Results and discussion

Figure 1 shows that by increasing the amount of carbon black to 70 phr, the sample dampness has become 91%. Also, with increasing carbon black, the hardness of the samples increased, which is normal. Figure 2 shows that with increasing carbon black the modulus increased and the strain at break decreased which is reasonable. Figure 3 shows the tan δ in terms of temperature for the 70 phr carbon block sample, showing two tan δ peaks shifting to higher temperatures as the frequency increases.

Conclusions

According to DMA and resilience tests, the sample with 70 phr carbon block has a high damping. The tan δ peak is at 10 Hz in the ambient temperature range. According to the DMA results in the range of approximately 0 to 50 degrees, this sample has a suitable damp and can be used for applications in this temperature range. Of course, other properties should be considered according to the intended application.

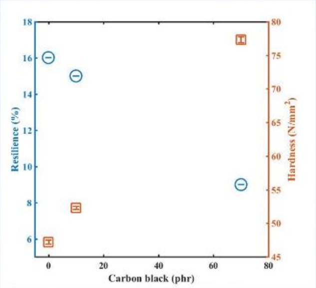

Fig. 1. Results of Resilience and Hardbess of CB (0 phr), CB (10 phr) and CB (70 phr) samples

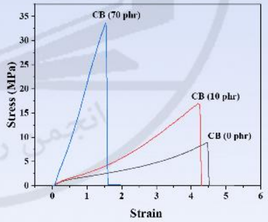

Fig. 2. stress vs strain for CB (0 phr), CB (10 phr) and CB (70 phr) samples

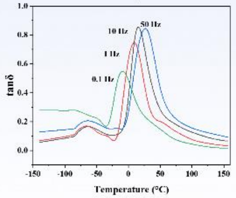

Fig. 3. tan δ vs temperature at frequencies of 0.1, 1, 10 and 50 Hz, for example with 70 phr carbon block

References

1. X. Lu, X. Li and M.Tian "Preparation of high damping elastomer with broad temperature and frequency ranges based on ternary rubber blends" J. Polym. Adv. Technol. **2014**, 25, 21–28
2. M. Song, X. Yue, X. Wang, M. Huang, M. Ma, W.Pan, Q.Qin "Improved high-temperature damping performance of nitrilebutadiene rubber/phenolic resin composites by introducing different hindered amine molecules" J. e-Polymers ,**2020**, 20, 482–490

Article code: A-10-252-1

A-10-254-2

2nd International Conference on Rheology
14 & 15 December 2021, Tehran, Iran

Mechanical Behavior and Rheological Properties of Two Differently Synthesized Double Network Hydrogels: A Comparative Study

Sara Tarashi1, Hossein Nazockdast1, Saeid Safaghsorkh2

1. Department of Polymer Engineering, Amirkabir University of Technology, Tehran, Iran.
2. Mechanical Engineering Department, University of Kashan, Kashan, Iran.

Abstract
Double network (DN) hydrogels have been well recognized as new tough materials. However, a comprehensive study on the effect of synthesis methods of DN hydrogels is very critical as they influence their properties. This study is aimed at investigating the effect of two different synthesis methods of thermal-curing and UV-curing on the mechanical and rheological properties of the κ-carrageenan /polyacrylamide DN hydrogel. Compared to the thermal-cured DN, the UV-cured DN hydrogel has exhibited different mechanical behavior (plastic-like with localized necking vs. elastomeric-like) and excellent mechanical properties. By focusing on the rheological results, it was demonstrated that the UV-curing method has resulted in much better thermo-reversibility.
Keywords: Hydrogel, Carrageenan, Mechanical Behavior, Rheological Properties.

Introduction
It has been known that single network hydrogels suffered from a poor mechanical performance. To overcome this drawback, physical-chemical double network (DN) hydrogels have been designed. In this hydrogels, the second chemical network is often fabricated by thermal or ultraviolet initiated radical polymerization. The properties of several DN hydrogels prepared by the thermal and UV curing method have been studied by some research groups [1,2]. It has almost been 8 years since the first physical-chemical DN hydrogel was developed, however most efforts have been made to investigate the mechanical properties of these DN hydrogels and a comprehensive attempt on the role of the synthesis method on the mechanical and rheological properties of these hydrogels is yet to be done. Therefore, in this work, we compare the effect of two different synthesis methods (thermal-curing and UV-curing techniques) of the physical-chemical DN hydrogels on mechanical and rheological properties.

Experimental
Materials
κ-Carrageenan (κ-Car), Potassium chloride (KCl), acrylamide (Am), N,N'-Methylenebis acrylamide (MBA), Ammonium persulfate (APS) and 2-hydroxy-4'-(2-hydroxyethoxy)-2-methylpropiophenone were purchased from Sigma-Aldrich. Graphene oxide (GO) was the product of Angstron Materials.
Sample Preparation
The UV-cured DN hydrogels were synthesized by a radical polymerization. Typically, κ-Car, Am, KCl, UV-initiator and MBA were dissolved in deionized water or GO suspension under stirring. Then, the solution was cooled and exposed to UV light to induce the photo-polymerization reaction of Am. Similarly, the thermal-cured DN hydrogels were obtained by replacing the UV-initiator with APS. In this method, first, κ-Car, Am, KCl, and MBA were added into the deionized water or GO suspension under stirring, then, APS was introduced. The obtained solution was then quickly poured into a mold. The sealed mold was cooled, and then placed into an oven at 60 °C for 24 hr. Samples were named as i-DN for double network hydrogel and i-DNGOx for double network containing GO. i = UV or Thermal represent the UV-curing or thermal-curing methods, and x is the weight percentage of GO.
Sample Characterization
Mechanical properties of hydrogels were measured on an Instron Machine. For tensile tests, the stretch rate of the upper clamp was kept constant. Rheological experiments were carried out by using a MCR301 rheometer with a parallel-plate system and temperature was controlled by a Peltier plate.

Results and Discussion
Tensile results (Figure 1) have demonstrated that although the UV-cured hydrogels exhibit a plastic-like behavior with pronounced localized necking, the thermally-cured one shows an elastomeric-like behavior. Moreover, the mechanical properties of the UV-DN hydrogel (σf = 0.42 MPa, εf = 2079 %, E = 0.1 MPa, and W = 3.54 MJ/m3) are greater than those of Thermal-DN hydrogel (σf = 0.12 MPa, εf = 722 %, E = 0.069 MPa, and W = 0.50 MJ/m3), which can be explained in terms of reducing the contribution of the κ-Car physical network and also reversible interactions in favor of increasing the cross-link density of PAm chemical network through grafting reaction in the thermally-cured hydrogel. Figure 1 also reveals that the addition of GO can have an enhancing effect on the mechanical performances of both hydrogels. The reinforcing efficiency of GO on the UV-cured hydrogel is higher than those of the thermal-cured hydrogel at the same GO content. This was attributed to the decrement in the GO interactions with individual networks as well as inter-network interactions as a result of the partial reduction of GO nanosheets in the thermal-curing method. By focusing on rheological measurements (Figures 2a and b), one may notice that although the G' and G" of the UV-cured hydrogels demonstrate a thermo-reversible behavior, the thermally-cured hydrogels exhibit no thermo-reversibility which can be attributed to the increasing the extent of physical network structural development caused by joining a fraction of grafted κ-Carmolecules into the physical network.

Conclusion
Tensile results demonstrated that although UV-cured hydrogels exhibit a plastic-like behavior, thermally-cured one shows an elastomeric-like behavior. Moreover, as evidenced by the rheology, UV-cured hydrogels exhibited better thermo-reversibility in comparison with thermally-cured hydrogels.

References
1. J. Wang, S. Su, J.Qiu, New J. Chem. 41, 3781–3789, 2017.
2. S. Liu, A.K. Bastola, L. Li, ACS Appl. Mater. Interfaces. 9, 41473–41481, 2017.

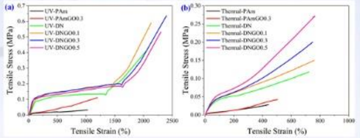

Figure 1. Tensile stress-strain curves for hydrogels prepared by (a) UV-curing and (b) thermal-curing methods.

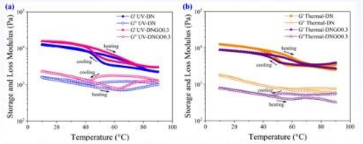

Figure 2. Dependence of G' and G" on temperature during a temperature sweep at a cooling and heating rate of 2 °C/min with a fixed angular frequency and strain amplitude.

Article code: A-10-254-2

2nd International Conference on Rheology
14 & 15 December 2021, Tehran, Iran

Evaluation of PLA functionalization process efficiently by using of FTIR, DMA and Tensile Technique

Elnaz Janjan, Gity Mir Mohamad Sadeghi and As'ad Zandi
a. Department of Polymer Engineering, Amirkabir University of Technology, Tehran, Iran
b. Polymer Engineering Department, Faculty of Chemical Engineering, Tarbiat Modares University, P.O. Box 14115-114, Tehran, Iran

Abstract
Poly(lactide)(PLA) has a relatively hydrophobic and neutral surface and lacks functional groups. There are different methods for functionalizition the surface. We used the chemical processing method to do this to functionalize the surface and then improve its applications by grafting heparin and so on. According to the tests performed, it was shown that the aminolysis process was performed and the PLA was functionalized.

Keywords: Poly(lactide); hydrophobic; functional groups; chemical processing method; aminolysis process

Introduction

PLA is a thermoplastic material, inert, with low interaction with cells, no functionality, and is resistant to acids, alkali, and fats[1]. PLA is often used in drug-delivery systems, like carriers, for the controlled delivery of different medicines Biopolyesters, with poly(lactide) (PLA) as the most prominent representative, are an excellent alternative to fossil-based materials. Sugar-based raw materials like corn and starchcan be used for the production of PLA, which makes it sustainable. PLA is biocompatible with the human organism and can be used in the production of implants as well as in other biomedical applications. As evidenced in works regarding PLA bionanocomposites, one of the challenges in the development of functional films or medical devices is to achieve a good dispersion of active components within the polymer matrix and, at the same time, maintaining their activity. Additionally, it is essential to ensure enough surface availability of the component in order to achieve the desired activity. Two main directions can be followed in the functionalization of materials: direct incorporation of active molecules into the material and physical or chemical bonding of actives molecules onto the surface of the material. One of the possible routes can be a surface modification of active compounds using some components with better compatibility with PLA, such as the "grafting from" method of modification. The grafting of the polymer chain on a solid surface is a very adaptable method for surface modification and functionalization. Polymer chains can be grafted to the solid substrate (grafting to), or the grafting reaction can be proceeded by polymerization from the surface (grafting from). Both methods are suitable for forming a thin layer on the solid surface with the desired physical and chemical surface properties. Falling into the category of wet chemical reactions, the aminolysis is usually characterized by attacking on the backbone ester bonds by small diamine molecules at the interface between the diamine solution and bulk polyester material, endowing the polyester surface with amino (–NH2) and hydroxyl groups (OH) [2]. The introduced NH2 and OH groups lay the foundation for subsequent conjugation of bioactive molecules. Compared to other surface modification methods, such as plasma or strong oxidation, the aminolysis has a clearer mechanism and predictable products. By adjusting the reaction parameters, the reaction rate and NH2 density can be accurately tuned. In addition, as a method based on wet chemistry, the aminolysis is suitable for modifying the interior of complex structures like 3D scaffolds. Thanks to these advantages, the aminolysis has been extensively studied and used in surface modification of polyester biomaterials in various forms. The schematic of the aminolyzed PLA is shown below.

Experimental

Poly(lactide))PLA (graide 4043d was from Nature Work Co. (USA) and Ethylene diamine from Merck Co. (Germany). Chloroform from CDH Fine Chemichal Co. (Dariya Ganj Dehli India).
PLA films were prepared using solvent casting method. 3g of PLA was mixed in 50ml of chloroform until a homogeneous mixture was mixed using a stirrer at room temperature. The homogeneous mixture was then cast in a petri dish and allowed to stand for 24 hours at ambient temperature. Then the prepared film was cut into 2cm x 2cm samples and washed with ethanol. To functionalize the ethanol-washed samples in a solution containing 10 g of ethylene diamine and 100 g of ethanol at room temperature, it was stirred until the samples were finally functionalized. The functionalized samples were then washed with deionized water to remove unstable amines (It should be noted that we prepared samples with different percentages, and our optimal sample is this sample). The pure sample with code PLA and the functionalized sample with code PLA10 are shown below. For Investigation of aminolysis process using DMTA by TTDMA (England), Tensile properties, ASTM D638 and ISO 527, ATR FTIR Tensor27 model by Brucker (Germany).

Results and discussion

According to Figure 1 and the appearance of peaks 3400 Cm-1 (amine) and 1510- 1580 Cm-1 (amide), the changes in the rheometric curves of the two samples, with differences in the curves of storage and loss modulus as well as tan δ can be seen in Figures 2 and 3.

The formation of a hydrogen bonding causes a shift in tan δ curve to higher temperatures. It can also be seen in Figure 4 that the strength of the PLA10 sample is reduced due to the breaking of the surface chain and a small amount of weight loss. The appearance of these two samples also changes. These results indicate that the Aminolysis process is performed

Conclusions

According to FTIR, DMA, and tensile tests, it is observed that the aminolysis process has been performed for PLA and this polymer has been functionalized and can be used to grafting with heparin, etc. and expand its applications. Because for these purposes we need to functionalize the PLA.

References

1. A. Mileti c, I. Risti c, M.Beatrice Coltelli and B. Pili c, s"Modification of PLA-Based Films by Grafting or Coating" J. J. Funct. Biomater. 2020, 11, 30,1-16

2. Y. Zhu, Z. Mao and Ch. Gao "Aminolysis-based surface modification of polyesters for biomedical applications" J. RSC Adv., 2013, 3, 2509 2519

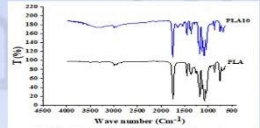

Fig. 1. Results of FT-IR of PLA and PLA10 samples

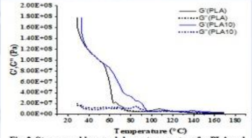

Fig. 2. Storage and loss modulus vs temperature for PLA and PLA10 samples

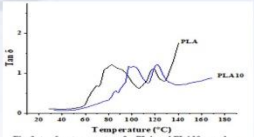

Fig. 3. tan δ vs temperature for PLA and PLA10 samples

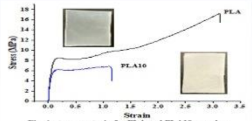

Fig. 4. stress vs strain for PLA and PLA10 samples

Article code: A-10-256-1

2nd International Conference on Rheology
14 & 15 December 2021, Tehran, Iran

The Impact of Nano Graphene Oxide on Rheological Properties of AM-co-AA Hydrogel as Drilling additive

F. Salmani1, A. Rabiee2*
1 Fateme Salmani, Iran Polymer and Petrochemical Institute, Tehran, Iran
2 Ahmad Rabiee, Faculty of Science. Department of Polymer Science. Iran Polymer & Petrochemical Institute, Tehran, Iran
*Corresponding Author's E-mail address: a.rabbii@ippi.ac.ir

Abstract

Drilling mud has different properties in different stages of drilling due to various roles so it should have good behavior in terms of rheological properties. In the present study, the polymer in drilling fluid was synthesized using acrylamide (AM) and acrylic acid (AA) monomers with constant molar ratios (0.7: 0.3 mole). Graphene oxide with different weight percentages (0.1, 0.3, 0.5 and 1 Wt %) was added to the polymer to synthesize the nanocomposite. The polymer and prepared nanocomposite was characterized by FT-IR, DMTA, TGA, TEM, rheometer, Fluid loss test and filter cake thickness analysis. According to the rheological properties, nanocomposite with 0.5% w/w of graphene oxide showed the best rheological properties. The addition of nanocomposite to drilling mud compared to polymer has a desirable property, such as reduction in fluid loss and thickness of mud cake which indicates a positive effect of presence of graphene oxide in drilling mud.

Keywords (Drilling mud, graphene oxide, Rheological behavior, nanocomposite, oil industry)

Introduction

Carboxymethylcellulose (CMC) is a cellulose derivative and is used as a fluid loss reducing agent in drilling operations. It acts as an important factor in improving the quality of drilling fluid and controls fluid loss, water absorption, and retention, type is used to increase the viscosity and the low well wall sealing, suspension builders and concentrators. The high viscosity type is used as a factor in reducing the waste filtering effluent from oil drilling. Although CMC is an effective viscosifying agent, but loses its properties at high temperatures [1,2]. Graphene oxide is a combination of carbon, oxygen, and hydrogen in variable proportions, which is obtained by reacting with strong oxidizers. The ratio of carbon to the oxygen of the oxidized product is C: O 1/2 and 2.9 [3].

In this study, we focused on preparation of graphene oxide modified nanocomposite for oil well drilling application containing nanoparticles with different concentrations. The applied polymer was synthesized using acrylamide (AM) and acrylic acid (AA) monomers (0.7 to 0.3 molar ratio in all experiments), and nanocomposite with different amounts of Go via the free-radical polymerization technique. The results showed that the addition of nanocomposite to drilling mud compared to polymer has more desirable rheological properties. fluid loss and thickness of mud cake which is an indication of positive effect of graphene oxide in drilling mud. The copolymers with graphene oxide structure possessed better rheological properties [4].

Resuts and discussions

Rheological behavior

Fig 1 shows the apparent viscosity of samples versus the shear rates with different amounts of graphene oxide in the nanocomposite. The apparent viscosity decrease with increasing shear rate which is an indication of shear thinning behavior. According to the results, the sample containing 0.5% of GO shows better resistance to shear and has the optimum rheological properties. Fig 2 Shows the storage modulus of samples versus angular frequency and a gradual increase in storage modulus with increasing angular frequency with the addition of GO. The nanocomposite containing 0.5 % GO has the highest storage modulus compared to the other samples due to well dispersion of nanoparticles in the polymer matrix.

TEM observation

TEM image of nanocomposite as shown in Fig 3 clearly illustrates that graphene oxide is well dispersed in polymer matrix without aggregation and any particle growth in the matrix at Nano-scale during polymerization, purification and drying. This may be due to the good
dispersion with ultrasound and interactions and formation of dipolar bonds between GO and functional groups of monomers, which can reduce macroscopic phase separation and stabilize the nanoparticles in
the polymer matrix [5].

Conclusion

Nanocomposite with different amount of Go (0.1, 0.3, 0.5 and 1 Wt %) were prepared by free-radical polymerization technique. The sample with 0.5% nanoparticle has the optimum rheological properties. Simultaneous use of polymers and nanomaterials in the resulting composites provided a synergistic effect and led to excellent mechanical strength and very high thermal stability. According to TGA results, the addition of graphene oxide to the main copolymer chains due to dipolar interactions has increased the heat resistance of nanocomposite. The storage modulus and glass transition temperature of nanocomposite was improved .The filter cake thickness and filtrates of samples at different time intervals were reduced in nanocomposite due to presence of nanoparticles compared with the copolymer.

References

[1] R. Caen, G. C.-J. of P. S. and Engineering, and U. 1996, "Drilling fluids: State of the art." Elsevier.

[2] V. C. Kelessidis, E. Poulakis, and V. Chatzistamou, "Use of Carbopol 980 and carboxymethyl cellulose polymers as rheology modifiers of sodium-bentonite water dispersions," Appl. Clay Sci., vol. 54, no. 1, pp. 63–69, Nov. 2011.

[3] W. S. Hummers and R. E. Offeman, "Preparation of Graphitic Oxide," J. Am. Chem. Soc., vol. 80, no. 6, pp. 1339–1339, Mar. 1958.

[4] A. A. Ahmadi and M. Monjazi, "Title : investigation of the effect of nono-silica particles onheat specific properties of water based drilling fluids and rheological properties Process:1 First trial (Field and check) 2 Peer review 3 Editing and three trials." no. 554864, 2018.

[5] Safari M., (2014), Variations in Wettability Caused by Nanoparticles. Petrol. Sci. Tech.32: 1505-1511

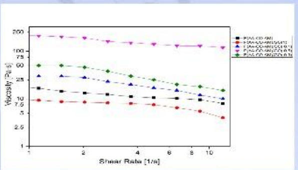

Fig 1. The dependence of viscosity on shear rates with different amounts of Go in nanocomposite.

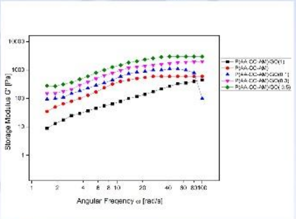

Fig 2. The dependence of storage modulus on angular frequency with different amounts of Go in nanocomposite.

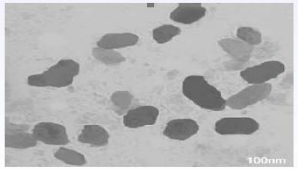

Fig 3. TEM images of nanocomposite with 0.5 wt% graphene oxide.

Article code: A-10-267.1

2nd International Conference on Rheology
14 & 15 December 2021, Tehran, Iran

The improved thermal sealing capability of polyethylene films by grafting lateral branches through a reactive extrusion process

F. Salmani1, A. Rabiee2*
1 F. Salmani[1], Sh. Ahmadi[2*],Gh.Nadri[3]

[1] *Fateme Salmani, Iran Polymer and Petrochemical Institute, Tehran, Iran*
[2] *Shervin Ahmadi, Iran Polymer and Petrochemical Institute, Tehran, Iran*
[3] *Ghaseme Naderi, Iran Polymer and Petrochemical Institute, Tehran, Iran*
[*] *Corresponding Author's E-mail address: Sh.ahmadi@ippi.ac.ir*
Sh.ahmadi@ippi.ac.ir

Abstract

The purpose of this study is to improve the adhesion strength and increase the heat sealing ability of polyethylene films by modifying their chemical structure. For this purpose, a substrate of density polyethylene alloy low/low-density linear polyethylene (LDPE / LLDPE = 30/70) with long side branches without gel formation through reactive extrusion process inside reactive twin extruder by combining different percentages of DCP primer 1-Octen and comonomer was prepared. The effect of change in the composition of the percentage of initiator and 1-Octen on the branching process and its effect on the viscoelastic behavior of polyethylene films with mechanical-rheological spectroscopic tests and dynamic properties mechanical-thermal was studied. Increased branching of the chains was accompanied by an increase in chain entanglements that caused increased elasticity of the melt was observed. in this regard, an increase in the storage modulus and viscosity of the polymer melt was observed.

Keywords: Rheology, Polyethylene, 1-Octane, Interfacial, Adhesion, Thermal sewing,peel

Introduction

Ethylene / alpha-olefin copolymers with a high percentage of comonomer. known as polyolefin elastomer, are one of the most widely used thermoplastic elastomers. These materials are a relatively new proportion of poly-parents that have been industrially produced with the development of metallocene hazard catalysts in the early 1990s. Compared to other types of thermoplastic elastomers, those thermoplastic elastomers that are based on polyolefins have attracted a lot of attention [1]. This is due to properties such as better chemical resistance, lower density, and lower price compared to similar materials. To achieve good elastomeric properties that include a low modulus against large deformations, the crystallinity of ethylene / alpha-olefin copolymer must be less than 20% by weight, which is important in the presence of alpha-olefins such as 1-propylene, butene, 1-hexene, and 1-octene. The structure of the main chain is realized. Most commercial polyolefins are elastomers of ethylene copolymers with butene or octane [1]. The accidental presence of these alpha-olefins in the chain structure prevents the crystallization of methylene sequences. Polyolefin elastomers can replace many commercial polymers such as ethylene-propylene rubber, ethylene vinyl acetate, styrene block copolymers, and polyvinyl chloride. Polyolefin elastomers have established themselves in applications such as the In general, three methods are used to create branches on polymer chains:

1. Use a suitable catalyst during the synthesis of the desired polymer.
2. Irradiation of high-energy gamma rays or high-energy gamma or electron beams to the polymer in the solid state.

Experimental

Materials

LDPE (low-density polyethylene) used in this project is prepared from Bandar Imam Petrochemical Grade 020. LLDPE polyethylene (low-density linear polyethylene) used in this project is prepared from Amirkabir Petrochemical with grade 0209. (DCP) is manufactured by Merck and organic peroxides are recognized as important initiators in free radicals to modify the structure and properties of polyethylene. One of the most important common peroxides, 2,5-Dimethyl-2,5-di(tert-butylproxy) hexane.

Results and discussion

Mechanical-rheological spectroscopy

Fig1 shows the behavior of the storage Modulus is shown in terms of the frequency of the control sample and the branched samples. As shown in the figure, none of the diagrams show the terminal behavior in the low-frequency range. In polymer alloys with interconnected morphologies, a polymer phase, such as three-dimensional lattice, is scattered throughout the alloy structure, and as a result, the behavior of the storage modulus in terms of angular frequency in this structure progresses to non- terminal in the low-frequency range. For all branched samples, the behavior of the storage terminal in the low-frequency range. For all branched samples, the behavior of the storage modulus in terms of angular frequency in the low-frequency range has shifted to non-terminal [3]. When the 1-octane comonomer is added to the alloy structure with 0.2% by weight of the peroxide primer, the storage modulus of the branched polymers is slightly increased and is observed at 0.2% by weight of the peroxide primer similar to the sample. This indicates that the amount of 1-1-Octen side bonds attached to the polymer is less than the samples in which 0.4% by weight of the primer was used. In most linear polymers at low frequencies, the change in viscous behavior is greater than in the elastic state, and as a result, the dissipation modulus is greater than the storage modulus. As the modulus of branching increases, the storage and loss modulus become closer together. Increasing the storage modulus indicates an increase in the elasticity of the specimens due to branching, which restricts the movement of the polymer chainsand increases the elasticity. According to table1 what was said in the analysis of the behavior of the storage module in terms of frequency, due to the increase of lateral branches, the bonding of the chains increases, and the elastic behavior of the material increases. Thus, the slope of the graph decreases in the low-frequency range. The highest slope is related to the curves of D0O0, D0.2O3, and. As mentioned, the D0.2O5 behavior deviation of the control samples from the terminal state (slope 2) is interconnected due to the proximity of the sample structure to the morphology. Also in examples, D0.2O3 and D0.2O5 Due to the lower rate of branching, less deviation from the terminal behavior occur, so the slope is higher [3].

Conclusions

1) The polyethylene branching process is a useful, efficient, and industrialized method to modify its adhesion properties in reactive extruders.
2) Rheological studies of the polymer melt showed the bonding of 1-actone comonomers to the polymer
chains and increasing the elasticity of the system without gel formation.
3) The formation of lateral branches on the chains by nucleation or regularity together was associated with increased crystallinity in branched specimens.

References

[1] Zhang K., Ye Z., Subramanian R., "Synthesis of block copolymers of ethylene with styrene and n-butyl acrylate via a tandem strategy Pd-diimine catalyst with atom transfer radical polymerization" , Macromolecules, 41, 3, 640 649, 2008.
[2] Wang J., Mao Q., "Methodology Based on the PVT Behavior of Polymer for Injection Molding", Adv. Polym. Technol., 32, 2013, 474 485, 2012.
[3] López-Barrón C. R., Macosko C. W., "Rheological and morphological study of co-continuous polymer blends during coarsening", J. Rheol. (N. Y. N. Y)., SOR, 56, 6, 1315 1334, 2012.

sample	storage module	loss module
(D_0O_0)	1.13	**0.74**
$(D_{0.2}O_0)$	0.73	**0.97**
$(D_{0.2}O_3)$	1.11	**0.77**
$(D_{0.2}O_5)$	1.22	**0.80**
$(D_{0.4}O_0)$	0.93	**0.73**
$(D_{0.4}O_3)$	0.90	**0.70**
$(D_{0.4}O_5)$	0.99	**0.71**

56, 6, 1315–1334, 2012.

Table1 loss values of storage and Loss module curves

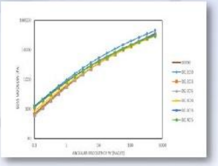

Fig1 Storage module behavior in terms of the angular frequency of control and branched specimens.

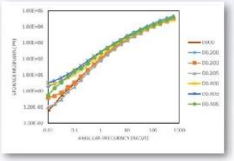

Fig2 Loss module behavior in terms of the angular frequency of control and branched specimen.

Article code: A-10-267-2

A-10-269-1

2nd International Conference on Rheology

14 & 15 December 2021, Tehran, Iran

Rheology and Mechanical Properties of PVC/EVA Nanocomposites Based Halloysite Nanotube

Soroush Shabani, Saman Ghaderzadeh

1. Research Laboratory of Green Organic Synthesis and Polymers, Department of Chemistry, Iran University of Science and Technology, 16846-13114 Tehran, Iran/ Ghazvin Granules Producing Co.
2. Department of Polymer Processing, Iran Polymer and Petrochemical Institute, 14965/115, Tehran, Iran/ Ghazvin Granules Producing Co.

Abstract

The innovation of this research was to study the effect of Halloysite Nanotube (HNT) amount on morphology, rheology and mechanical properties of the blends based on poly (vinyl chloride)/ethylene vinyl acetate copolymer (EVA). The impact resistance of PVC increased due to blending with EVA up to 90/10 while it experienced a reduction trend at the higher amount of EVA. From the rheological studies, it can be inferred that there was no strong interactions between HNT with PVC and EVA chains in the melt phase of PVC/EVA blend samples, so that the specific amount of HNT never affected on the rheological behavior and properties of the blend. It can be included from the Scanning Electron Microscopy (SEM) analysis that all the blend samples had a matrix-dispersed morphology and it was evolved by increasing HNT amount in the blend from the EVA dispersed phase size and its distribution viewpoint.

Keywords: Nanocomposites, PVC, Blend, HNT, Impact strength.

Instruction

The few studies are accomplished on thermoplastic/elastomer blend nanocomposites. Among the thermoplastics, PVC is one of the most commercial material (next to only a few more widely used plastics like PET and P.P.) which is due to its high stiffness, flame retardancy, chemical resistance and low cost [1].

In recent year, halloysite nanotubes (HNTs) have significantly been investigated as a leading nanofiller for advanced novelty of organic/inorganic composites due to their hollow structure, biocompatibility, cheap, and eco-friendly [26 28]. HNTs have been emphasized as an efficient filler to be combined with polymers for fabrication of polymer nanocomposites via performance improving. Herein we wish to report an easy and efficient approach for the preparation of PVC/EVA blend- halloysite nanocomposites by melt mixing. The structure, impact strength, thermal properties and morphology of the nanocomposites were also studied.

Experimental

PVC powder (suspension grade with K-value 65), Dioctyl terephthalate (DOTP) as plasticizer, Ba/Zn stearate and stearic acid used as thermal stabilizer and lubricant and EVA pellet (VA 28%). Ultrafine HNTs, in the form of the powder, with a density of 2.55 g/cm3 and cationic exchange capacity (CEC) of 10 meq/100 g were supplied by Imerys Tableware Asia Limited (New Zealand). Morphological figures of natural HNT, which illustrate a transparent central area that runs longitudinally along the nanotubes, indicating hollow and open-ended structure of HNT are given in our previous works.

PVC powder, EVA pellet, DOTP, Ca-Zn stearate, stearic acid and HNT were mixed according to the formulation shown in Table 1. The nanocomposites were produced by melt procedure into a two-roll mill at 170°C for 10 min and then forced molded into sheets at 170°C and 1000 psi for 7 min. The specimens, in dimensions 250 x 250 x 3 mm, were air cooled and obtained, then pellets were prepared for structure specification and properties measurements. Blending of PVC and EVA compared without HNT in the same process, regarding to properties the item P95E05 is chosen as an optimized blend to investigate by HNT.

Result and Discussion

Figure 1 gives information about the variation of impact strength of PVC/EVA blends and PVC/EVA/HNT nanocomposites, according to ASTM D256-04. From the blends, it is noticeable when 5 phr of EVA was added to PVC, Notched Izod impact strength rose from 5.2 kJ m-2 to 7.16 kJ m-2 of PVC, whereas the impact strength of nanocomposites declined gradually in present of the large content of EVA loading due to some agglomeration of EVA in the PVC matrix.

The nanocomposite of 95 PVC/5 EVA/5 HNT provides the highest impact strength by reaching to considerable improvement in comparison with other composites and net PVC. The notched impact strength of the nanocomposites has experienced a fall trend due to the further increase amount of HNT which cause to agglomeration of HNT in the PVC matrix, Figure 2. However, the nanocomposite of 95 PVC/5 EVA/5 HNT exhibits a synergism effect of the EVA and HNT that enhanced the toughness of the nanocomposite. The rheological properties of PVC/EVA/HNT nanocomposites illustrate increase in complex viscosity, Figure 3, especially at 5 phr HNT concentrations in comparison with the PVC/EVA composite and net PVC. Therefore, the low shear rate test method in composites determines that the variation of viscosity for composites are growing up at low angular frequency ω values. Approximation of the viscosity trend of the investigated nanocomposites at higher ω values indicates that not only the viscosity value, but module rate rose by increasing with the amount of HNT [2, 3].

Conclusion

The preparation of PVC/EVA/HNT nanocomposites was successfully carried out. The effect of EVA and HNT contents on the properties of the nanocomposites was studied. The results display that the impact test of the nanocomposites decreased with the adding of modified HNT into the PVC/EVA blend, whereas PVC was blended with 5 phr of EVA and 5 phr of HNT, synergistic improvement in notched impact strength happened. On the other hand, the EVA acts like a macromolecular plasticizer, while HNT treats as a nanoparticle reinforcing filler.

Acknowledgment

The authors gratefully acknowledge ***Ghazvin Granules Producing Co.*** for financial, material and instrument support.

References

1. Liu, Cong, et al., *Structure and properties of poly (vinyl chloride)/halloysite nanotubes nanocomposites*, Journal of Macromolecular Science, Part B 51.5: 968-98, 2012.
2. An, Q. F., et al., *Compatibility of PVC/EVA blends and the pervaporation of their blend membranes for benzene/cyclohexane mixture*, Journal of membrane science 222.1-2: 113-122, 2003.
3. Senthilvel, K., et al., *Studies the effect of halloysite nanotubes on the mechanical and hot air ageing properties of nitrile-polyvinyl chloride rubber nano-composites.*, Materials Today: Proceedings 43 (2021): 1730-1739

Table 1. Formulation of the PVC/EVA/HNT nanocomposites, unit is in phr, the abbreviations are P: PVC/E: EVA/H: HNT.

Sample code	PVC	EVA	Ca/Zn	HNT	DOTP
P95E05	95	5	4	0	25
P90E10	90	10	4	0	25
P95E05H1	95	5	4	1	25
P95E05H3	95	5	4	3	25
P95E05H5	95	5	4	5	25
P95E05H7	95	5	4	7	25

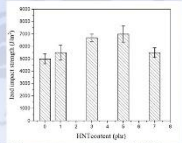

Fig 1. Izod impact strength of PVC/EVA/HNT nanocomposites

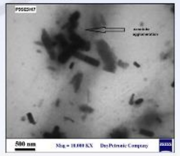

Fig 2. TEM of agglomeration of HNT in the PVC matrix

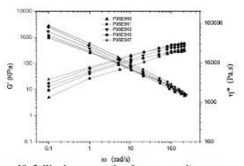

Fig 3. Rheology properties of nanocomposites.

Article code: A-10-269-1

2nd International Conference on Rheology
14 & 15 December 2021, Tehran, Iran

Viscoelastic Study of Biopolymer Hydrogels Applicable for Additive Manufacturing

Hossein Zehtab Minooei[1], Babak Kaffashi[2]*
1. Polymer Engineering Department, University of Tehran's Kish International Campus, Kish Island 7941639982, I.R. Iran
2. School of Chemical Engineering, College of Engineering, University of Tehran, Tehran 1417613131, I.R. Iran

Abstract

Application of biocompatible, biodegradable, inexpensive, non-toxic and edible naturally-occurring polymers in 3D printing process for biomedical and food industries are now taken into consideration. By virtue of increasing interest in 3D printing and need for the precise products with high production speed, this technology has been advancing and is considered as a state-of-the art and burgeoning technique. Keeping in view that water-soluble biopolymers behave in an intricate and time dependent way, so, predicting their rheological properties and applications in additive manufacturing process has been elusive and crucial. In this study, we investigate a novel ink made of gelatin/tragacanth hydrogel for Direct Ink Writing (DIW) and also we exhibit how formulation, preheating, amount of cross-linking agents and processing temperature influence on achieving essential time duration before clogging in nozzle. In the other hand, through study of time dependent viscoelastic measurements, we shed light on which the most optimal time for 3D printing without clogging is prior to gelation region. In fact, rheological parameters such as viscosity, storage and loss modulus, and damping factor are of vital importance to make a forecast on hydrogel behavior. In addition to assessment of printability through interconnected channels formed by filaments we suggest a new strategy by measuring the contact angle and cross-sectional area of droplet.

Keywords: biopolymer; 3D printing; ink; viscoelastic; stiffness; printability
*Corresponding author. E-mail address: kaffashi@ut.ac.ir

1 Introduction

The application of highly hydrophilic biopolymers in the Direct Ink Writing (DIW). 3D printing process is very challenging and ambiguous. In this research, we used tragacanth gum to moderate rheological properties of gelatin. Tragacanth gum, used as a thickening agent, provides thixotropy behavior. We selected the hydrogels with an elastic modulus of about 10kPa, which simulate tissue-like stiffness and are suitable for the culture of cells. During deposition of the hydrogel from the nozzle we encounter to serious issue of clogging in the nozzle tip due to the high rate of cross-linking and curing. Since these clumps affect the quality of the resolution and shape fidelity, therefore, we are willing to show how preheating, formulations, operating temperature, curing and preparation duration can influence the rheological and eventually, the printability properties. Through the contact angle measurement and the drop shape, one can estimate the printability of the hydrogels. It has been shown that the preheating of the gelatin and water mixture in a heat oven at 65℃ for 7 days increased the printing duration[1]. In this paper, we explored the preheating of the gelatin powder ca.1 to 2 hours at 65℃ which turns out to indicate the same or even better effects.

2 Experimental

2.1 Preparation of ink and hydrogel

Gelatin type A purchased from Merck, tragacanth gum was provided from locally extracted sample from Isfahan. Since the crosslinking agents with carbonyl group such as glutaraldehide are exclusively used for crosslinking gelatin, so we introduced an equal mixture of sucrose and borax into the gelatin/tragacanth blend. Distilled water is used as solvent. Suitable composition for our work achieved by trial and error. Solutions of gelatin (17%w/w), tragacanth (1.2%w/w), gelatin/tragacanth mixture (17/1.2%w/w) and gelatin/tragacanth hydrogel with 2.5 and 5%w/w crosslink agents were prepared. 2X10g gelatin powder preheated in the oven at 60-65℃ for 1 and 2 hours. Six samples were produced and named as 17, 17/1.2, 17/1.2/2.5, 17/1.2/2.5/1h, 17/1.2/5/1h and 17/1.2/5/2h

2.2 Rheometery

A rotational Physica MCR300 (Anton Paar) rheometer was used to measure the rheological parameters such as storage modulus (G'), loss modulus (G''), damping factor (tanδ) and viscosity using a plate-plate geometry measuring geometry (25 mm). According to this, time sweep, viscosity-time and amplitude sweep measurements with the control of strain and shear rate were conducted at 37℃.

2.3 Measurement of contact angle, droplet cross-section area and printability

The images of the droplet were taken with an 8MP camera, through the deposition of hydrogel drop on the surface of a petri dish. One equation which correctly determines the printability of the printed grid pattern formed by interconnected channels is as is as follows:[2]

$$Pr = L^2/16A \qquad (1)$$

Here A is the area and L is the perimeter of the interconnected channel formed by the filaments. Therefore, the acceptable printability would be from 0.9 to 1.1. In addition, we investigate cross section area of the droplet, so the printability area generally should be between being circularity (0.78) and being complete square (1).

$$\pi/4 \leq Pr \leq 1 \qquad (2)$$

3 Results and discussion

3.1 Rheological analysis

Considering the viscosity versus time data on three temperatures (25,32,37℃), as the slopes of the curves indicate, the pressure required to apply on ink in order to exit the nozzle, the appropriate temperature was chosen to be 37C. As is indicated in figures 1,2, the wider the initial plateau region of curve was, the longer the duration of 3D printing. The amplitude sweep measurement in the range of 1 to 300 % strain amplitude was also performed immediately after the time sweep measurement. The results show for all samples the both measurements equally increase until 1% then both measurements to decline which indicate a viscoelastic solid, the two moduli intersect after 100% strain (Figure 3). Considering the time sweep measurements, the best possible time for 3D printing will be under gelation condition. It can be said with a good approximation that the starting time of gelation is after the plateau region, say it is a viscoelastic liquid, and the end time is where the damping factor (tanδ) reaches the highest value as close to 1 (Figure 4-7).

3.2 Contact angle and printability

The measurement of the contact angles shows the lowest amount belongs to the pure gelatin and the highest one assigned to the hydrogel of 17/1.2/5/2h to be 21° and 89°, respectively (Figure 8). Furthermore, the values of cross sectional area increase from 0.4 to 0.79 for pure gelatin and hydrogel 17/1.2/5/2h, respectively (Figure 9). The measurement of the printability criteria was done in which printability increase from 0.83 for pure gelatin to 0.96 for hydrogel of 17/1.2/5/2h (figure 10).

Conclusion

The application of hydrogels in the direct ink writing 3D printing technique is a challenging issue in the biomedical and food industries. The high rate of cross-linking during the process can be facilitated by applying practical solutions to reach an appropriate formulation, preheating and suitable processing temperature. We add two other methods for determining printability, that is, measuring contact angle and the cross-section area compared to the common methods. The best results achieved for the sample of 17/1.2/5/2h. The whole strategies are essential but not sufficient. It may be suggested that the introduction of hydrophobic agent can improve the printability.

References

1. Yao Tan JJ, Pan Lee, Hashimoto M, Int J Bioprint, 6(4), 296, 118-129, 2020.
2. Ouyang L, Yao R, Zhan Y, Sun W, Biofabricat J., 8, 1-13, 2016.
3. Zhang B, Chung S.H, et al., Progress in Natural Science: Mat. Int J. 31, 180–191, 2021.
4. Wang C-H, Virgilio N, Wood-Adams PM, Heuzey M-C, Food Hydro. J, 79, 462-472, 2018.
5. Corker A, C-H Ng H, Poole RJ, Garcia-Tunon E.,Soft Matter J, 15, 1444-1456, 2019.
6. Aadil KR, Barapatre A, Jha H. Bioresour. Bioprocess J., 1-11, 3:27, 2016.
7. Nazarzadeh Z.E, Makvandi P, Tay F.R, Carbohydrate Polymers J, 212, 450–467, 2019.
8. Zhu S, Stieger MA., Van der Goot AJ, Schutysera M.A.I. Innov. Food Sci. and Energ. Tech. J 58, 102214, 2019.
9. Yanez M, De Maria C, Rincon J, and Boland T, Conf. NIP 27 and Digital Fabrication 632-635, 2011.
10. Li Voon S, An J, Wongb G, ZhangaY, Kai Chua C, Virt. Physic. Proto. J, 2019.
11. Rocha VG., Saiz E, Tirichenko I.S., Garcia-Tuñonc E, J. Mater. Chem A, 2020.
12. Hellio D, Djabourov M. Macromol. Symp., 241, 23–27, 2006.
13. Heidenreich AC, Perez-Recalde M, Wusener AG, Hermida EB, Polym. Test. 82, 106297, 2020
14. Zuidema JM., Rivet CJ., Gilbert RJ., Morrison FA., J Biomed Mater Res Part B,102B,1063–1073, 2014.
15. Baby DK., Rheology of Polymer Blends and Nanocomposites, chap. 9, Rheo. hydro., 2020.

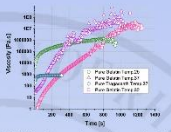

Fig 1. Viscosity versus time semi-log curve for gelatin at three temperatures 25, 32 and 37°C and tragacanth at 37°C. Decreasing slope of curve and expanding plateau region before a sharp increase in viscosity in order to achieve optimal time is essential.

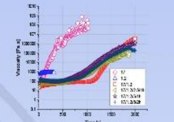

Fig 2. Viscosity versus time semi-log curve for six samples.

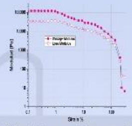

Fig 3. Amplitude sweep log-log curve for hydrogel 17/1.2/5/2h. Linear viscoelastic region (LVE) to strain 1% is indicated, flow stress and yield stress can be calculated.

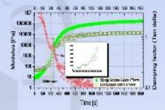

Fig 4. Time sweep test on pure gelatin, gelation region shows short time available before clogging takes place.

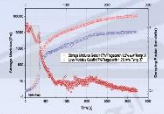

Fig 5. Time sweep test on gelatin/tragacanth blend, gelation region shows short time in which time is more than pure gelatin.

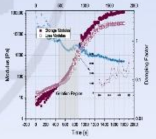

Fig 6. Time sweep semi-log curve for hydrogel 17/1.2/2.5/1h. Effect of increasing preheating duration and amount of crosslink agents on time available before clogging is distinctly shown.

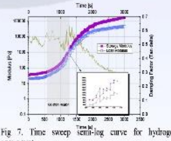

Fig 7. Time sweep semi-log curve for hydrogel 17/1.2/5/2h.

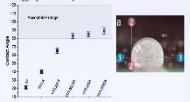

Fig 8. Contact angle of sample 17/1.2/5/2h(a). Printability based on measurement of contact angle average of the droplet on the surface of petri dish(b).

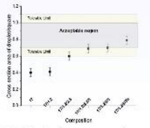

ig 9. Printability based on measurement of cross section average of the droplet on the surface of petri dish.

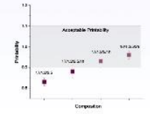

Fig 10. Printability based on average area of interconnected channels formed by the filaments after 1h deposition on the petri dish at 37C.

Article code: A-10-270-1

A-10-271-1

2nd International Conference on Rheology

14 & 15 December 2021, Tehran, Iran

Effect of atmospheric pressure cold plasma (ACP) treatment on the technological characteristics of quinoa flour

Leila Zare[1], Sarah Sanaei Nasab[1], Mitra Pashaee[1], Neda Mollakhalili Meybodi[1]

1 .Department of Food Sciences and Technology, School of Public Health, Shahid Sadoughi University of Medical Sciences, Yazd, Iran

Abstract

Atmospheric pressure cold plasma (ACP) is considered as non-thermal treatment with potential microbial inactivation efficiencies. This study is aimed to determine the effect of cold plasma treatment on rheological characteristics of quinoa flour. Regarding, whole quinoa grains were subjected to a dielectric barrier discharge contained plasma reactor for 5min/ 50 kV, 10 min/ 50 kV, 5 min/ 60 kV and 10 min/ 60 kV known S1, S2, S3 and S4 respectively. Untreated sample is named as control sample. Results indicated that ACP treatment could change the rheological properties depending on the treatment exposure time and voltage. As treatment parameter determine the rheological characteristics and consequently the applicability of quinoa flour, an optimization is required.

Keywords: Cold plasma, Quinoa, rheological properties, Non Thermal processing

Introduction

Introduction

Quinoa (*Chenopodium quinoa Willd.*) as gluten-free pseudo cereal with high protein content, balanced amino acid profile, high content of dietary fiber, vitamins, minerals, and bioactive compounds has recently received increased popularity.

considering the potential contamination of quinoa flour with microorganisms through planting, harvesting, and storage, the necessity of using effective antimicrobial treatments and their potential impacts on rheological characteristics needs also be investigated.

Plasma, an equilibrium combination of photons, free electrons and neutral atoms, as the fourth state of matter is electrically neutral despite its chemical activity(1).

Considering the ever growing importance of quinoa as a gluten-free pseudo cereal in formulation of functional foods and the necessity of being properly stored, using atmospheric pressure cold plasma treatment is recommended. this study is aimed to investigate the effect of ACP treatments parameter (voltage, time of exposure) on rheological characteristics of quinoa flour (2).

Materials and methods

Materials

Quinoa grains (*Titicaca*) were purchased from a local retailer and were of Persian origin.

Atmospheric pressure cold plasma (ACP) treatment

Samples obtained by ACP treated whole quinoa grain at 5 min-50 kV, 10 min-50 kV, 5 min-60 kV, and 10 min-60 KV were termed as S1, S2, S3, and S4 respectively.

Fundamental rheological measurement

frequency sweep test was carried out in a frequency range of 0.1 -100 Hz at 30 °C using parallel plate geometry by Physica MCR 301 rotational rheometer. The rheological properties (storage modulus (G') & loss modulus (G")) were reported.

Results and Discussion

The storage (G') and loss modulus (G") indicate the elastic and viscose behavior of materials respectively. As shown in fig 1a and b, elastic modulus for all samples is higher than the viscous modulus (G'>G"), indicating the solid behavior of quinoa gel. As depicted, the elastic moduli of the control sample were higher than the ACP treated samples at different times and voltages. Changes in protein structure induced by active species of ACP treatment may also affect the rheological characteristics of quinoa flour. At constant treatment time of 5 min, increasing the treatment voltage increased the viscosity modulus (S3 compared to S1). Also, at constant treatment time of 10 min, the viscose and elastic moduli has been increased with increasing the treatment voltage (S4 compared to S2). The higher the amount of protein in network, the greater the strength, elastic and viscous properties will be. Also, the cross-links created between starch-starch, protein-protein, or protein-starch molecules by plasma treatment improve the systems rheological properties. This improvement may be due to the partial gelatinization of starch and the interaction between other components. In S1 sample which ACP treated at shortest exposure time and voltage (5 minutes, 50 kV), the rheological properties (G' and G" moduli) had been decreased compared to control sample. This decrease may be due to starch depolymerization (3, 4).

Conclusion

Results indicated that rheological characteristics of quinoa flour can remarkably be influenced by atmospheric pressure cold plasma treatment depending on its voltage and exposure time. Plasma treatment can significantly influence the protein and starch structure. Intermolecular connection like starch-starch, starch-protein or protein-protein may also be formed in quinoa flour through cold plasma treatment. The present study shows that the plasma parameters play a significant role on rheological applicability determination of quinoa flour. Applied voltage and treatment time are factors influenced the functional characteristics of food components.

References

1. Mollakhalili-Meybodi N, Yousefi M, Nematollahi A, Khorshidian N. Effect of atmospheric cold plasma treatment on technological and nutrition functionality of protein in foods. European Food Research and Technology. 2021:1-16.
2. Bußler S, Rumpold BA, Fröhling A, Jander E, Rawel HM, Schlüter OK. Cold atmospheric pressure plasma processing of insect flour from Tenebrio molitor: Impact on microbial load and quality attributes in comparison to dry heat treatment. Innovative Food Science & Emerging Technologies. 2016;36:277-86.
3. Hertwig C, Reineke K, Ehlbeck J, Knorr D, Schlüter O. Decontamination of whole black pepper using different cold atmospheric pressure plasma applications. Food Control. 2015;55:221-9.
4. Hertwig C, Leslie A, Meneses N, Reineke K, Rauh C, Schlüter O. Inactivation of Salmonella Enteritidis PT30 on the surface of unpeeled almonds by cold plasma. Innovative food science & emerging technologies. 2017;44:242-8.

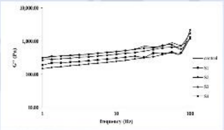

Fig1.a rheological properties (loss modulus) of untreated sample (control) and plasma treated quinoa flour.

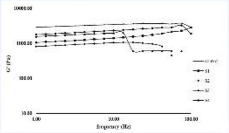

Fig1.b rheological properties (storage modulus) of untreated sample (control) and plasma treated quinoa flour.

Article code: A-10-271-1

2nd International Conference on Rheology

14 & 15 December 2021, Tehran, Iran

Rheological characteristics of wheat dough in the presence of potassium chloride and different fermentation type

Mitra Pashaei[1], Leila Zare[1], Sara Sanaei-Nasab[1], Neda Mollakhalili-Meybodi[2*]

1. MSc. Student, Department of Food Sciences and Technology, School of Public Health, Shahid Sadoughi University of Medical Sciences, Yazd, Iran

2. Assistant professor, Department of Food Sciences and Technology, School of Public Health, Shahid Sadoughi University of Medical Sciences, Yazd, Iran

Abstract: Overconsumption of bread as the main contributors of sodium intake plays an important role in heart disease occurrence. Regarding, its sodium chloride content is recommended to be decreased by different strategies e.g. salt substitution by sodium free mineral salts. Considering the importance of sodium chloride on technological characteristics and fermentation efficiency of wheat bread, this study is aimed to investigate of the impacts of potassium chloride (KCl) substitution level (10, 20, 30, 40, 50%) and fermentation types (yeast and sourdough) on rheological characteristics of wheat dough, using rheometer and parallel plate geometer. Results indicated that despite the prevalence of elastic modulus (G') on viscose modulus (G") at all formulations, KCl replacement can significantly influence the rheological characteristics by decreasing the storage modulus (G'), loss modulus (G"), complex modulus (G*) parameters. Substitution of KCl up to 20% w/w in the presence yeast provide the formulations similar to 100 % w/w NaCl containing sample.

Keywords: Salt reduction-Potassium chloride (KCl) - Rheology- Sourdough (MFSD) - Yeast

Introduction

Wheat bread is a staple food product (1). NaCl considered as a common salt in bread making that influences the technological properties such as dough development time, extensibility, yeast activity and etc. (2). Sodium is considered as an essential nutrient for maintaining the fluid balance, cell functionality and nerve impulses in human body (3). High sodium intake is related to cardiovascular disease (4). Partial substitution of sodium with potassium is a popular strategy in production of low sodium foods (5). Adequate daily intake of potassium has positive effects on decreasing the risk of cardiovascular diseases (6). Despite the positive health effects of KCl, high usage of KCl in food products creates off flavor (bitterness and metal flavor). Adding food permissible flavor enhancers, such as yeast extracts, considered as a recommended strategy for masking the unpleasing tastes (7). In addition to the ingredients, fermentation is also considered as a key step in bread baking that influences the technological and sensory characteristics of final products. Fermentation with yeast and/or MFSD is commonly used in bread making that produced different types of aroma and flavoring agents. The purpose of this work was developing the wheat bread with different ratio of NaCl/KCl and yeast and/or MFSD and evaluating the rheological characteristics of the final products.

Experimental

Materials: Potassium chloride produced by Merk Company were purchased from scientific retail and other materials were also purchased from the local market.

Rheological measurement: Controlled shear/stress rheometer (Anton Paar MCR301, GmbH, Germany) with parallel plate geometry was used for rheological measurement.

The Oscillatory Rheological analysis: Dynamic viscoelastic characteristics of wheat bread were determined by frequency sweep test at frequency range of 0.01-10 Hz and the storage modulus (G') & loss modulus (G") were reported. Parameter damping factor (tan δ) and complex modulus (G*) were calculated respectively using the following formula:

$$Tan\delta = G''/G' \qquad G^* = \sqrt{G'^2 + G''^2}$$

Results and Discussion

Viscoelastic characteristics were determined to investigate the impacts of KCl substitution level and fermentation types on technological characteristics of wheat bread. The frequency sweep curves of wheat dough containing different KCl: NaCl ratio and fermented differently are presented in figure 1 a, b, c and d as G', G", G* and tan δ respectively. All formulations were frequency dependent with storage modulus greater than loss modulus (G'>G") at whole range of angular frequencies as an indicator of elastic-like gel formation of wheat bread as demonstrated by (11). Elastic and viscose moduli are generally monitored as quality determining factors as high quality bread should be more elastic than viscose (11). Alongside, the complex modulus and damping factor also provide valuable information about dough strength. Considering both elastic and viscose modulus, complex modulus should be optimized as formulations with high complex modulus are generally too rigid to facilitate the growth of air bubble and those having low G* are unable to restore gases. In yeast fermented samples, increasing the KCl incorporation level decrease G', G" and G* and increase tan δ. In other words, despite decrease observed in both elastic and viscose moduli, the G' modulus decreased more sharply in yeast fermented samples via increasing the KCl incorporation level. In MFSD fermented samples, increasing the ratio of KCl incorporation level enhance the degradation activity of lactic acid bacteria in a way that lowest G', G" and G* is found in F11 containing 50% w/w KCl in the presence of MFSD. Furthermore, highest G', G" and G* is found in F9 containing KCl: NaCl at 30: 70 ratios. The lowest frequency dependency of G* is also found in F8 confirming the formation of strong gel structure (13).

Conclusion

Results showed that although increasing the KCl incorporation level and added sourdough by inhibiting yeast activity and weakening the gluten network respectively, decreased G', G" and G*, and increased tan δ, decreasing the KCl substitution ratio, Due to the increase in glutenin level, decreased G" and increased G', which is a desirable behavior in dough products. Samples with 20% KCl with the highest elasticity and cohesion were optimal samples and in rheological evaluation were slightly different from the control sample.

References

1 Weegels PL. The future of bread in view of its contribution to nutrient intake as a starchy staple food. Plant Foods for Human Nutrition. 2019;74(1):1-9.
2 Pasqualone A, Caponio F, Pagani MA, Summo C, Paradiso VM. Effect of salt reduction on quality and acceptability of durum wheat bread. Food chemistry. 2019;289:575-81.
3 Cepanec K, Vugrinec S, Cvetkovic T, Ranilovic J. Potassium chloride-based salt substitutes: A critical review with a focus on the patent literature. Comprehensive Reviews in Food Science and Food Safety. 2017;16(5):881-94.
4 He FJ, MacGregor GA. Role of salt intake in prevention of cardiovascular disease: controversies and challenges. Nature Reviews Cardiology. 2018;15(6):371-7.
5 Arab M, Sohrabvandi S, Khorshidian N, Mortazavian AM. Combined effects of salt-related variables on qualitative characteristics of probiotic fermented milk. Current Nutrition & Food Science. 2019;15(3):234-42.
6 Engberink RHO, van den Born B JH, Peters Sengers H, Vogt L. Long term potassium intake and associated renal and cardiovascular outcomes in the clinical setting. Clinical Nutrition. 2020;39(12):3671-6.
7 Sinesio F, Raffo A, Peparaio M, Moneta E, Civitelli ES, Narducci V, et al. Impact of sodium reduction strategies on volatile compounds, sensory properties and consumer perception in commercial wheat bread. Food chemistry. 2019;301:125252.
8 Meybodi NM, Mortazavian AM, Mirmoghtadaie L, Hosseini SM, Yasini SA, Azizi MH, et al. Effects of microbial transglutaminase and fermentation type on improvement of lysine availability in wheat bread: a response surface methodology. Applied Food Biotechnology. 2019;6(3):151-64.
9 Demirkesen I, Mert B, Sumnu G, Sahin S. Rheological properties of gluten free bread formulations. Journal of Food Engineering. 2010;96(2):295-303.

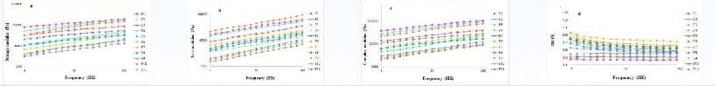

Fig.1.Effect of yeast and MFSD on Rheological characteristics of wheat bread samples. a . Storage modulus of wheat bread samples. b . Loss modulus of wheat bread samples. c . Complex modulus of wheat bread samples. d . tan δ of wheat bread samples

Article code: A-10-275-1

2nd International Conference on Rheology
14 & 15 December 2021, Tehran, Iran

The role of EVA level on melt viscoelasticity, rate of crosslinking and morphology development in cross-linked Ethylene-Vinyl Acetate/ Low-Density Polyethylene/ (EVA/LDPE) blend Foam

Narges Asghari, Azizeh Javadi*, Ali Asghar Katbab
Department of Polymer & Color Engineering, Amirkabir University of Technology, Tehran, Iran

Abstract

Ethylene-vinyl acetate copolymer/Low-density polyethylene (EVA/LDPE) blend foams are prepared by simultaneous crosslinking and foaming via compression molding. Effects of EVA weight fraction on gel content, melt viscosity, and morphology of foams are studied. Cell density increased with reducing cell size by EVA level due to a higher rate of EVA crosslinking, leading to the enhancement of melt viscosity. This is evidenced by an increase in gel content of the foams with the EVA weight fraction.

Keywords: EVA/LD Blend – Foam – Crosslinking – Gel Content – Morphology

Introduction

Foams or cellular structure materials retain the advantages of bulk materials with low-density structures, relatively high stiffness, and flexible cell structure. Due to their properties such as thermal and acoustic insulation, buoyancy, low density, high impact absorbance, long durability, and stress-cracking resistance, polymeric foams are widely used in several engineering applications, including impact energy absorption systems, sound absorbers, electrical and thermal insulators, electromagnetic wave shields [1]. The application of polymeric foam is determined by its structure, e.g., cell type, cell size, cell size distribution, and cell density. Using a Foaming agent as a gas source requires crosslinking to stabilize bubbles growth during expansion and enhance the resistance of the cellular material to thermal collapse, which is necessary for some applications [2]. Low-density polyethylene (LDPE) and ethylene-vinyl acetate copolymer (EVA) are popularly used to manufacture polymeric foams; in particular, the LDPE/EVA foam possesses higher flexibility, toughness, and impact resistance. Cross-linked EVA usually shows a better control of nucleation and formation of cells with uniform size in the foaming of EVA [3, 4].
This study aims to investigate chemical crosslink and EVA content's effect on the cell morphology of the cross-linked EVA/LDPE foams.

Experimental

LDPE L2102TX00 (MFI=1.9 g/10 min) from Laleh Petrochemical Company, Iran, and EVA VS430 (MFI=2.5 g/10 min; 18 wt% vinyl acetate content) from Lotte Company, South Korea, were supplied. Azodicarbonamide (ADC, Anhui Huishang Group, China) as a chemical blowing agent, zinc oxide (ZnO, Rangine Pars, Iran) as ADC activator, dicumyl peroxide (DCP, Di-Cup 98, Hercules) as a cross-linking agent, and stearic acid (Palmac, Malaysia) as an external lubricant were also used. EVA/LDPE blends containing compositions (100:0, 90:10, 70:30, 50:50) were prepared by melt compounding method using a laboratory batch internal mixer (Brabender Plasticorder) at starting temperature of 110 °C and with a rotor speed of 60 rpm. This temperature was chosen to avoid activation and decomposition of ADC and DCP during mixing. First, polymers including EVA and LDPE were added into the mixer and allowed to melt and mixed for 3 minutes. Then, ADC and ZnO were incorporated into the mixture, and mixing was continued for up to 10 minutes. Finally, DCP was added to the mixing chamber, and compounding was completed at 15 minutes. Samples were foamed in a hot-press machine at 155 °C and a pressure of 50 bar. After 25 minutes, the pressure was removed, and the samples were allowed to expand.

Results and Discussions

The gel content was determined by a 24 h Soxhlet extraction cycle using xylene as the solvent at a temperature of 140 °C according to ASTM D-2765. After the extraction cycle, the remaining insoluble sample was dried in a vacuum oven at 60 °C to a constant weight. The gel fraction was calculated from the ratio of the final weight, w_1, of the sample to its initial weight, w_0, as follows:

$$\text{gel content} = \frac{w_1}{w_0} \times 100 \qquad (1)$$

As shown in Table 1, at the same DCP fraction, the gel content increased with EVA content. This indicated that the presence of EVA was favorable to the crosslinking of polymer blends.
Furthermore, according to Figure 1, the Temp-Sweep mode of the RMS result indicates that EVA starts to crosslink in fewer temperatures with a higher rate (higher fitting slope). This can lead to an increase in the gel content and melt strength with increasing EVA content.
The average cell size was obtained by analyzing the SEM photographs (Figure 2) by the software ImageJ. The cell density N_f, was defined as the number of cells per unit volume of the foam, was calculated by:

$$N_f = \left(\frac{nM^2}{A}\right)^{3/2} \qquad (2)$$

Where n, M, and A are the number of cells in the micrograph, the magnification number of the micrograph, and the area of micrograph (cm^2), respectively. According to the results of SEM analysis, For the cross-linked foams, as shown in Table 2, the average cell diameter decreases, and cell density increases with the increasing of EVA content. Wang et al. [4] reported that EVA has lower melt viscosity and melt strength, leading to larger cells and decreased cell density in non-cross-linked foams. Still, we observed that after crosslinking EVA/LDPE blends, due to the EVA higher gel content, melt viscosity and strength of the blends are enhanced by the crosslinking network in the polymer blends. The fusion and break of the cells can be restrained, and the cells can also become smaller.

Conclusion

The crosslinking in the EVA/LDPE matrix with EVA major phase improves the melt viscosity and strength, leading to a higher resistance to cell expansion and a barrier to the coalescence of the neighboring cells. Thus, the smaller cell size and a higher cell density of the foams could be obtained.

References

[1] Soriano-Corral F, Hernández-Gámez JF, Durón-Sánchez LH, Ramos de Valle LF, Lozano-Estrada M, and Soto-Lara YA., Key Engineering Materials, 779, 64-70, 2018 .
[2] Liu, H., Wu, S., Tian, N., Yan, F., You, C., and Yang, Y., Journal of Materials Chemistry A, 8(45), 23699-23723,2020.
[3] Pham TH, Le TM, and Zhang XW., Applied Mechanics and Materials, 889, 223-230, 2019.
[4] Wang, B., Wang, M., Xing, Z., Zeng, H., and Wu, G., Journal of applied polymer science, 127(2), 912-918, 2013.

Table 1. Gel content of EVA/LD foams.

Sample	Gel Content (%)
EVA/LD 50/50	76.27
EVA/LD 70/30	78.86
EVA/LD 90/10	84.15
EVA/LD 100/0	89.13

Table 2. Average cell diameter and cell density of foams.

Sample	Cell diameter (μm)	Cell density ($\times 10^8$ Cells/cm^3)
EVA/LD 50/50	232.52	51.37
EVA/LD 70/30	230.56	59.34
EVA/LD 90/10	187.58	95.64
EVA/LD 100/0	183.45	98.21

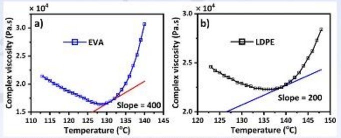

Figure 1. Temp-Sweep test of a) EVA, b) LDPE cross-linked with DCP.

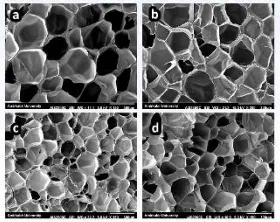

Figure 2. SEM micrographs of EVA/LD foams: a) 50/50, b) 70/30, c) 90/10, d) 100/0.

Article code: A-10-277-1

2nd International Conference on Rheology
14 & 15 December 2021, Tehran, Iran

Evaluation of tribological and rheological characteristics of cress seed gum-xanthan thickened liquids applicable for dysphagia diet

Parisa Poursani, Seyed M.A. Razavi*
Center of Excellence in Native Natural Hydrocolloids of Iran, Ferdowsi University of Mashhad, PO Box: 91775-1163, Mashhad, Iran

Abstract
The physical properties of a bolus (tribology and rheology) affect the bolus transmission behavior in the pharynx, which is important for predicting the swallowing behavior of dysphagia. The tribological (coefficient of friction-COF) and rheological (hardness, adhesiveness, cohesiveness) properties of xanthan gum-cress seed gum thickened fluids at the concentrations of 0, 0.5, and 1%. It was found that the high lubricating capacity of the selected thickeners can help in the management of dysphagia and prevent the feeling of the unpleasantness of the network's stickiness. The results confirmed that increasing the thickeners' concentration lead to increasing cohesiveness from 0.11 to 0.38 as well as aspiration risk reduction.

Keywords: Cress seed gum (CSG), Dysphagia, Texture, Tribology, Xanthan gum (XG)

Introduction

Dysphasia, the difficulty of swallowing, is one of the challenging problems after stroke. According to the statistics, about 8% of the world's people have dysphasia (1). In summary, one of the major challenges in addressing dysphagia diet management is the tribological-rheological characteristics of the product (2). The purpose of this study was to classify the concentration levels of hydrocolloids in the presence of artificial saliva based on tribological and rheological properties.

Experimental

Tribological measurements were conducted on a Physica MCR 301 tribometer (Anton Paar, Graz, Austria) at 37°C using a ball-on-three-pins test configuration.
The solid rheological properties of the samples was evaluated by using a texture analyzer (CT3 Texture Analyzer, Brookfield, USA).

Results and Discussion

Tribological properties

For all samples, there is an increase in the COF at low speeds, and then the coefficient of friction seems to reach a sort of plateau. It can be seen that for most samples the COF did not changed with increasing speed in the mixed regime, then it decreased at increasing values of the sliding speed in the hydrodynamic regime. The 0.0XG-0.0CSG and 0.0XG-0.5CSG samples showed the least lubricating and the highest frictional resistance in the intermediate sliding velocity range (mixed regime).

Rheological properties

The hardness of hydrocolloid solutions depends on their macromolecular structure. Since with increasing amount of gum, the amount of absorbed water and consequently the fluid viscosity also increases. Increased adhesion of the bolus during the swallowing process can increase the residual risk in the esophagus (8). The easy swallowing has been reported for foods with connective texture in the range of 0.2 to 0.9 (10).

K-Mean Clustering

This method is the most efficient method for grouping data points into groups, even in relevant cases with insufficient data and each data point belonging to the cluster with the closest mean. This statistical method was assumed to be useful for classifying variables based on rheological and tribological properties. As a result, the output clusters reflected a group of samples that followed the same dietary pattern.

Conclusion

The rheological and tribological results demonstrated that 1% CSG, as an emerging gum, could be used as a potential food thickener for dysphagia patients combined with commercial 0.5 and 1% xanthan gum (XG).

References
1.Cichero JA, Steele C, Duivestein J, Clavé P, Chen J, Kayashita J, et al. CPMRR.1,280-91, 2013.
2.Munialo CD, Kontogiorgos V, Euston SR, Nyambayo I. IJFST.55,1862-71, 2020.
3.Miller JL, Watkin KL.Dysphagia. 11,117-24,1996.
8.Yakubov G, Branfield T, Bongaerts J, Stokes JJB. 3,1-10, 2015.
10.Nakagawa K, Matsuo K, Shibata S, Inamoto Y, Ito Y, Abe K, et al.5,72-8, 2014.

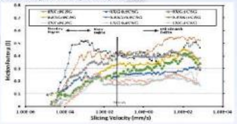

Treatments	Cluster
0.0XG-0.0CSG	1
0.0XG-0.5CSG	1
0.0XG-1.0CSG	2
0.5XG-0.0CSG	2
0.5XG-0.5CSG	3
0.5XG-1.0CSG	3
1.0XG-0.0CSG	4
1.0XG-0.5CSG	4
1.0XG-1.0CSG	5

XG, xanthan gum; CSG, cress seed gum

Fig 1. The Stribeck curves of the xanthan-cress seed gum thickened fluids at T=37°C

Table 1. Rheological characteristics of xanthan-cress seed gum thickened fluids

Treatments	Hardness (g)	Adhesiveness (g.s)	Cohesiveness (g.s)
0.0XG-0.0CSG	1.44[h]±0.37	0.02[h]±0.01	0.11[g]±0.01
0.0XG-0.5CSG	3.68[g]±0.10	0.18[g]±0.01	0.12[g]±0.01
0.0XG-1.0CSG	7.24[f]±0.93	0.24[f]±0.02	0.19[f]±0.02
0.5XG-0.0CSG	12.11[e]±0.33	0.31[e]±0.01	0.28[e]±0.02
0.5XG-0.5CSG	15.24[d]±0.23	0.40[d]±0.02	0.30[d]±0.04
0.5XG-1.0CSG	20.34[c]±0.53	0.47[c]±0.01	0.33[c]±0.03
1.0XG-0.0CSG	17.11[d]±1.93	0.46[c]±0.03	0.32[c]±0.01
1.0XG-0.5CSG	21.15[b]±2.50	0.51[b]±0.02	0.35[b]±0.03
1.0XG-1.0CSG	24.05[a]±3.13	0.54[a]±0.01	0.38[a]±0.03

Article code: A-10-279-1

2nd International Conference on Rheology

14 & 15 December 2021, Tehran, Iran

Effect of Carbon Black Levels on Magic Triangle of Tire Treads Based on SSBR/BR/Silica

Mohammad Barghamadi, Mohammad Karrabi, Mir Hamid Reza Ghoreishy, Ghasem Naderi

Iran Polymer and Petrochemical Institute, Tehran, Iran, P. O. Box. 14965-115

Abstract

In this study, the effects of carbon black on the wet grip, rolling resistance and abrasion resistance behavior of compounds based on SSBR/BR/silica were investigated. By increasing the CB in the compounds, the damping factor in 0 °C (tan $\delta_{0°C}$) and 60 °C (tan $\delta_{60°C}$) were decreased and increased, respectively. Another effective parameter in the tread compounds of green tires is the abrasion resistance, which was studied for different samples containing 10, 20 and 30 phr of carbon black contents. The results showed that adding 10 phr of carbon black improved this criterion.

Introduction

In recent years, with the stricter requirements for tire performance, shortage of petroleum resources, and people's attention to environmental protection, better wet grip property as well as lower rolling resistance are demanded when rubber is applied to tire tread [1–3]. A well-known industrial and practical method for achieving optimum properties is the use of SSBR with silica and CB and also the use of BR with a high cis percentage. Recently, the concept of hybrid fillers has been considered by many researchers. It has been shown that multi-phase hybrid fillers is able to maintain the properties of each filler and also has shown a synergistic effect on processability due to compatibility and effective interactions [4]. The most stubborn problem in the research and development of high-performance tires is that there are contradictions among the abrasion resistance, rolling resistance and wet traction of rubber materials, which is called "magic triangle" in industry [5].

In the present study, rolling resistance, wet grip and abrasion for tread compound with the base of SSBR/BR/Silica/CB were evaluated.

Experimental

100 phr of SSBR with 53% vinyl content, 23% styrene content, 30 phr of BR with a cis content of 97%, 10, 20 and 30 phr of N330 and 60 phr of silica with a BET surface area of 180 m^2 was produced used. Other additives was ZnO and stearic acid, paraffin, CBS, DPG and IPPD as antioxidant and sulfur as curing agent.

Initially, all components except the curing agent and accelerators were fed into Banbury mixer along with half of the silica. Mixing was continued for 3 min at a rotational speed of 80 rpm until a temperature of 100 °C. At this temperature the remaining silica was added to the system and mixing was continued for 3 min until reaching a temperature of 150 °C with a rotational speed of 80 rpm. Sulfur and accelerators were then added to the mixes, and the mixes were rolled for 5 min with the curing system. Curing was performed at a pressure of 150 kg/cm2 and a temperature of 150 °C.

DMTA test and the abrasion resistance were performed according to ASTM D 5026 and DIN 53516, respectively.

Results and discussion

Fig. 1 shows a schematic representation of tan δ versus temperature. The tan δ is the result of dividing the storage modulus (G') by the dissipation modulus (G") at each temperature ($\tan\delta = G'/G''$). The level of the tan δ at 0 °C and 60 °C is a measure of wet grip and rolling resistance, respectively. Therefore, the amount of tan δ at the mentioned temperatures is compared for the rubber compounds filled with hybrid of carbon black and silica, which indicate the two characteristics of green tires, namely wet grip and rolling resistance.

Fig. 2 shows the damping factor at 0 °C (tan $\delta_{0°C}$) of the samples filled with three different amounts of carbon black i.e. 10, 20 and 30 phr. As can be seen, the highest damping factor occurred for the carbon black-free sample. In fact, with the addition of carbon black, the probability of forming a wide filler network increases and the number of rubber chains trapped in the filler networks increases and the effective volume of the rubber chains decreases, leading to a lower amount of dissipation at this temperature. Therefore, increasing the carbon black level to the compounds causes a decrease in wet grip in green tire treads.

It is widely accepted that the loss factor values in 60 °C (tan $\delta_{60°C}$) are a measure of the tread rolling resistance. Compounds with a high dissipation factor at 60 °C show high rolling resistance and therefore require more energy and fuel to drive. Therefore, to achieve low fuel consumption, the ideal tire tread should have a lower loss factor value at 60 ° C. The amount of dissipation factor at 60 °C for compounds containing different amounts of carbon black is shown in Fig. 3. As can be seen, by increasing the amount of carbon black, the rolling resistance increases. It is believed that at high temperatures, the inter-filler frictions causes exothermic and damping raise.

Table 1 shows the abrasion loss of the compounds. Abrasion loss is a function of two mechanisms: energy dissipation and coefficient of friction. Initially, the abrasion resistance improves with increasing energy dissipation, but the coefficient of friction also increases with increasing sample temperature due to the increase in energy dissipation in the form of heat, and finally overcomes the energy dissipation mechanism and reduces abrasion resistance. Therefore, by adding carbon black to the compounds, the abrasion loss is reduced by adding 10 phr, but by adding more carbon black due to high friction, the highest carbon black loss is obtained.

Conclusions

Adding CB to the rubber compounds, resulted in an decrease in tan $\delta_{0°C}$ and increase in tan $\delta_{60°C}$. This means that by the incorporation of CB, the wet grip and rolling resistance characteristics were weakened. But on the other hand, adding 10 phr soot significantly improved abrasion resistance. Therefore, the optimum amount of CB increase of 10 phr was considered.

References

1. Morton M, Rubber technology, Springer Science & Business Media, 2013.
2. Whelan A, Lee KS, Developments in rubber technology-2: synthetic rubbers, Springer Science & Business Media, 2013.
3. Chandra AK, Current Topics in Elastomers Research, 919–933, 2008.
4. Tian Q, Tang Y, Ding T, Li X, Zhang Z, Composites Communications, 10, 190 193, 2018.
5. Dominic M, Joseph R, Begum PMS, Kanoth BP, Chandra J, Thomas S, Carbohydrate Polymers, 230, 115620, 2020.
6. Mao Y, Tian Q, Zhang C, Tang Y, Wang Y, Li X, Ding T, Polymer Engineering & Science, 59, 1270–1278, 2019.

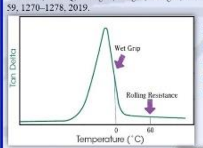

Fig 1. **Schematic representation of determining the wet grip and rolling resistance criteria in green tires.**

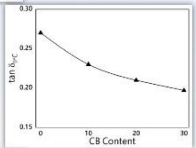

Fig 2. **tan $\delta_{0°C}$ of samples filled with various CB content.**

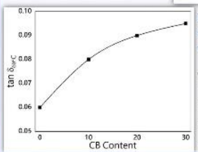

Fig 3. **tan $\delta_{60°C}$ of samples filled with various CB content.**

Table 1. Abrasion loss of compounds.

CB Content	Abrasion loss (mm^3)
0	117.4
10	99.3
20	164.2
30	195.0

Article code: A-10-282-1

A-10-288-1

2nd International Conference on Rheology

14 & 15 December 2021, Tehran, Iran

Investigation of the effect of in-situ microfibril formation on creep-recovery behavior of polypropylene/polyethylene terephthalate polymer composites

Elahe sadat Hejazi[1*], Mahmood Masoomi[2]

1. Chemical Engineering Department (Polymer Group), Isfahan University of Technology, Isfahan, Iran/ es.hejazi@ce.iut.ac.ir
2. Chemical Engineering Department (Polymer Group), Isfahan University of Technology, Isfahan, Iran/ mmasoomi@iut.ac.ir

Abstract

In this study, Microfibrillar Composites (MFCs) based on Polypropylene/Polyethylene terephthalate were prepared in different amounts of dispersed phase, and the effect of in-situ microfibrils formation on creep-recovery behavior was examined. In-situ reinforced microfibrillar composites were prepared during three stages of melt mixing by extrusion, hot drawing immediately after leaving the extruder die and isotropization of the matrix at a temperature lower than the dispersed phase melting temperature using the compression molding method. The fibrillar morphology formed after the hot drawing process was confirmed using scanningelectron microscopy (SEM). Fiber-induced elasticity was investigated as a distinct behavior by creep-recovery test, and it was observed that after formation of mature fibrils, the elasticity of the composites increased significantly. The results of creep-recovery test also showed that the resistance of microfibrillar samples to deformation increases and show stronger recovery after stress removal.

Introduction

Today, the presence of polymers in daily life seems necessary, but these materials are also a major source of environmental pollution. Recyclable polymeric materials have received much attention to reduce pollution caused by polymer waste. A new generation of recyclable polymeric materials are "Micro-Fibrillar Composites (MFC)". In the processing of MFCs by blending two immiscible polymer components, the reinforcing component, which at first appears in the form of spherical elements, takes the fibril form through appropriate thermal and mechanical treatments. Because reinforcing microfibrils are formed in this two-component blend during the process, some researchers call these composites "in-situ microfibrillar composites". By introducing this technique, Fakirov claimed that the problem of aggregation and agglomeration of microfibrils could be solved.

MFCs with a polyolefinic matrix have received a great deal of attention due to their availability, ease of processing, and expansion of the processing window due to their relatively low melting temperature, as well as their low cost. One of the most studied microfibrils in the polyolefin matrices is polyethylene terephthalate (PET) due to the good fibril formation and its availability due to the recycled PET obtained from bottles. For reinforcing polypropylene (PP), which is a hydrophobic thermoplastic with excellent chemical resistance and relatively poor mechanical properties, strong PET seems to be a good choice.

In order to evaluate the viscoelastic behavior, oscillating rheological tests, stress relaxation and creep tests are used. The creep test involves applying a constant shear stress over a period of time and measuring the resulting shear strain. The recovery step includes the removal of applied stress and the monitoring of the strain during relaxation from the stored elastic stresses. Only the elastic deformation of the sample can be fully recovered and its viscous deformation is permanent.

The aim of this study was to investigate the effect of in-situ formation of PET fibrils in PP matrix on creep-recovery behavior of their blend using transient rheological technique. In order to evaluate the formed fibrous morphology and its effect on the final properties, scanning electron microscopy and nonlinear creep-recovery rheological test were used. The results of creep-recovery test showed that with the formation of PET fibrils within the matrix, the composite tends to recover the applied stress more.

Experimental

Polypropylene (grade C30S Maroon Petrochemical Company, with a density of 0.9 g/cc) was used as a matrix, and TG641 grade polyethylene terephthalate, a product of Tondgooyan Petrochemical Company, (with intrinsic viscosity of 0.64 dl/gr) was used as the dispersed phase. Extruded samples of PP/PET blends in a single-screw extruder with a screw speed of 50 rpm in a composition of 7, 10, 13% by weight of PET were prepared by melt mixing. The temperature profile of the extruder was set at 190, 270, 280, and 280 °C from the hopper to the die. To prepare the microfibrillar samples, the output strands of the die was passed through a water bath and entered a take-up device. All samples were subjected to a constant DDR of 8. After the drawing step, the strands were compression molded at 190 °C.

The morphological characteristics of the in-situ formed microfibrils after extraction of the matrix by boiling xylene were performed by the XL30 electron microscope made by Philips Company.

A MCR 502 parallel plate rheometer made by the Anton Paar with plates with a diameter of 25 mm was used for creep-recovery test. Creep recovery test was performed at constant stress (1 and 100 Pa for extruded samples/100 Pa for MFC samples) and after stress removal, strain changes were recorded over time. How the system recovers by removing stress will reflect its viscous and elastic parts.

Results and Discussion

The microscopic images taken from the in-situ formed PET microfibrils, after selective extraction of the PP matrix, are shown in Figure 1. It should be noted that any loss of fibril orientation observed in the micrographs is due to the effect of floating fibrils during the extraction of the PP phase. As shown in Figure 1, the hot drawing step has led to the formation of fibrous morphology in composite samples.

The creep recovery test is used to analyze the material resistance to deformation. By creep-recovery measurements, the contribution of fibrillar structure to the elasticity of PP/PET composite was determined. In addition, the sample recovery response can be considered as a reflection of the evolution of the fibrillar network. Strain changes over time for extruded samples during constant stresses of 1 and 100 Pa (for a duration of 300s) and up to 600s after stress removal are shown in Figures 2-a and 2-b. In order to prevent droplet stretching and fibril formation, the extruded samples were subjected to creep test at 240 °C. In both amounts of stress, it is observed that with increasing the dispersed phase concentration, strain decreases and the recovery after stress removal increases. The extruded sample containing 7 wt.% of PET shows the highest creep, while the sample consisting of 13 wt.% of PET shows the highest resistance to deformation and stronger recovery. In addition, increasing the applied constant stress from 1 to 100 Pa (Figure 2-b) causes a large deformation of the extruded samples due to incompatibility and poor interaction at the interface, and by removing the stress, they show a weak recovery. These results indicate that the spherical regions of the dispersed phase are not able to improve the elasticity of the polymer composite, and polymer composites with matrix-dispersed phase morphology show viscous behavior, especially at high stresses.

The creep-recovery behavior of MFC samples at 200 °C (far below the melting point of the PET) is shown in Figure 2-c. The creep of MFCs under constant stress decreases with increasing dispersed phase content, and samples with a higher amounts of PET microfibrils show higher resistance to deformation. Compared to extruded samples, samples of microfibrillar composites show less deformation and stronger recovery. In addition, the evolution of the physical fibrillar network with increasing the PET content can be considered effective in improving the recovery behavior in microfibrillar composites. This behavior was also observed for PP/PA6 spun blend fibers.

Conclusion

Scanning electron microscopy results showed that by increasing the dispersed phase concentration in MFCs, the fibril diameter increases and samples containing 13 wt.% of PET have fibrils with larger diameter and elongated morphology than other samples. In this study, creep-recovery test was used to determine the contribution of in-situ fibrils on the elasticity of the composite. Samples containing a high amount of PET microfibrils show the lowest creep rate and a sudden recovery, which indicates the high contribution of fibrils to the elasticity of the composite. Increasing the fibrils content increases the interface surface area of these fibrils with the matrix and, as a result, increases the friction at the interface, which results in a higher strength of the composite containing high volume fraction of in-situ microfibrils. In addition, as the fibrils content increases, the interaction of the fibrils dominates, leading to the formation of an interconnected physical network within the matrix. This network distributes the applied force to the composite, resulting in solid-like behavior and stronger recovery by eliminating the applied stress.

References

1. Mishra RK, Thomas S, Kalarikkal N, editors, *Woodhead Publishing is*, 2017.
2. Fakirov S, *Macromolecular Materials and Engineering*, **298**, 9, 2013.
3. Fakirov S, *Composites Science and Technology*, **89**, 211, 2013.
4. McCardle R, Bhattacharyya D and Fakirov S, *Macromolecular Materials and Engineering*, **297.7**, 711-23, 2012.
5. Mezger, T, *Vincentz Network*, 2020.
6. Hajiraissi R, Jahani Y and Hallmann T, *Polymer Engineering & Science*, **58.8**, 1251-60, 2018.
7. Hajiraissi R, *Polymer Bulletin*, **77.5**, 2423-42, 2020.

Fig 1. the SEM images of the MFC samples after extracting the matrix at magnification of 50 micron from left to right at 7, 10 and 13 wt.% PET, respectively.

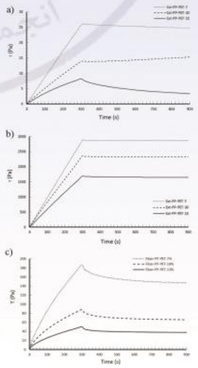

Fig 2. Creep recovery test, a & b) extruded samples experienced stress of 1 and 100 Pa, respectively, at 240 °C. c) MFC samples experienced stress of 100 Pa at 200 °C.

Article code:

www.icor-sor.com

2nd International Conference on Rheology
14 & 15 December 2021, Tehran, Iran

Effect of concentration and temperature on the steady shear flow behavior of Nettle seed (Urtica pilulifera) gum

Zahra Zamani, Seyed M.A. Razavi*
Division of Food Engineering, Department of Food Science and Technology, Ferdowsi University of Mashhad, PO Box: 91775-1163, Mashhad, Iran

Abstract
The steady shear flow behavior of Nettle seed gum (NSG) was investigated between 3% and 5% (w/w) concentration and temperatures of 10–70 ° C. NSG showed shear thinning behavior at all concentrations and temperatures. When the concentration increased from 3% to 5%, the flow behavior index decreased significantly from 0.927±0.021 to 0.686±0.065 with increasing concentration, indicating more thickening, stabilizing, and pseudoplasticity functions at higher concentrations. The dependence of viscosity on temperature was evaluated by applying the Arrhenius-type model. The activation energy for the NSG was calculated as 18.88 kJ/mol at 3% concentration.

Keywords: Hydrocolloid- Pseudoplasticity- Rheology- Shear viscosity- *Urtica pilulifera* seed gum

Introduction
Natural hydrocolloids, as functional biological macromolecules (mainly polysaccharides and proteins), are widely used in food and pharmaceutical products [1]. In our recent research, based on the numerical optimization method, the optimal conditions for extraction of Nettle seed (Urtica pilulifera) gum (NSG) were determined [4]. The purpose of this study was to characterize the steady shear flow properties of NSG solution as well as to study the effect of concentration and temperature on the rheological behavior of NSG solution.

Experimental
Measurement of rheological properties of NSG dispersions was carried out by a rotational viscometer (Visco 88; Bohlin Instruments, UK). Shear rate dependence, Concentration dependence, Temperature dependence was evaluated.

Results and Discussion
Effect of shear rate
Flow behaviors, e.g. the apparent viscosity variation with shear rate, of the NSG dispersions for different concentrations from 3 to 5% (w/w %) at 25°C are shown in Fig. 1 (a).
Effect of concentration
Based on the results of Herschel-Bulkley model, The consistency coefficient and yield stress of NSG increased from 0.009±0.001 to 0.495±0.083 Pa.sn and from 0.148±0.028 to 0.630±0.083 Pa,
Effect of temperature
The effect of temperature on the apparent viscosity of NSG is shown in Fig. 1 (b). The activation energy for the NSG was calculated as 18.88 kJ/mol at 3% concentration.

Conclusion
Time-independent rheological studies showed the Herschel-Bulkley model is the most appropriate model to describe the steady shear flow behavior of the NSG. At all the concentrations and temperatures, NSG indicated a shear-thinning behavior, the rheological properties of NSG were severely affected by concentration and temperature.

References
1. Razavi SMA, Emerging natural hydrocolloids: Rheology and functions, John Wiley & Sons Publisher, Chichester, England, 2020.
4. Zamani Z, Razavi SMA, Amiri MS, Res and Inno in Food Sci and Tech, 9, 143-160, 2020.

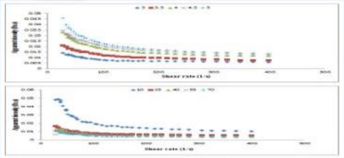

Fig 1. Apparent viscosity of Nettle seed gum; (a) at different concentrations (3%, ♦; 3.5%, ■; 4%, ▲; 4.5%, ×; and 5%, +) and constant temperature (25 °C), (b) at different temperatures (10°C, ♦; 25°C, ■; 40°C, ▲; 55°C, ×; and 70°C, Ж) and constant concentration (3%).

Article code: A-10-290-2

2nd International Conference on Rheology
14 & 15 December 2021, Tehran, Iran

Effect of Gamma Irradiation Treatment on Rheological Characteristics of Quinoa Flour

Sarah Sanaei Nasab[1], Leila Zare[1], Mitra Pashaee[1], Neda Mollakhalili Meybodi[2*]
1. MSc. Student, Department of Food Sciences and Technology, School of Public Health, Shahid Sadoughi University of Medical Sciences, Yazd, Iran
2. Assistant professor, Department of Food Sciences and Technology, School of Public Health, Shahid Sadoughi University of Medical Sciences, Yazd, Iran

Abstract: This study aimed to investigate the effect of gamma irradiation on the rheological properties of quinoa flour using six different doses of irradiation (0.5, 1, 2.5, 5, 7.5 & 10 kGy). The changes in rheological properties using frequency tests were evaluated. Where decreased in the storage modulus (G′), loss modulus (G″), and complex modulus (G*) after the treatment was observed. Results also revealed that there is an increase in damping factor (tan δ) after the treatment. Thus, gamma irradiation treatment can be one of the physical modification methods for changing the rheological properties of quinoa.

Keywords: Gamma irradiation - quinoa - rheological properties - loss modulus - storage modulus.

Introduction

Quinoa (*Chenopodium quinoa*) is a gluten-free grain that has a high protein content (more than 15%) with a balanced combination of essential amino acids as well as significant amounts of lipids, dietary fiber, vitamins, minerals, antioxidants and bioactive compounds (1, 2). Contamination of quinoa with microorganisms such as *Fuma Exigua, Sclerotiumrolphsi*, and *Pythium zingiber* during different stages requires the use of effective antimicrobial treatments (3). Food irradiation is a beneficial, cost effective , and environmentally friendly technology (4) to reduce microbial load, increase shelf life and maintain quality (5). Gamma irradiation alters food carbohydrates and proteins and eventually causes physical, textural, and rheological changes in food. Hence this study aims to investigate the effect of gamma irradiation on the rheological characteristics of quinoa flour.

Experimental

Materials: The white Quinoa seeds (*Titicaca*) were purchased and packed into airtight polyethylene bags.
Gamma Irradiation Treatment: Irradiation treatments of samples using Gamma source Co-60 at doses of 0.5, 1, 2.5, 5, 7.5 & 10 KGy (1.15 Gy/sec, 23–2°c) were done at NSTRI of Iran and un-irradiated sample used as control.
The Oscillatory Rheological analysis: Frequency sweep test (0.1-100 Hz, 30 °C) was carried out using Physica MCR 301 rotational rheometer and the storage modulus (G') & loss modulus (G") were reported. Parameter damping factor (tan δ) and complex modulus (G*) were calculated respectively using the following formula:

$$Tan\delta = G''/G' \qquad G^* = \sqrt{G'^2 + G''^2}$$

Results and Discussion

In frequency sweep tests the values of storage modulus (G′; elasticity) were higher than loss modulus (G″; plasticity) for all samples (Fig. 1); which shows a gel-like viscoelastic behavior of quinoa flour. Similar results have been reported by Ye et al. (2016) and Bashir et al. (2017). Higher values of both moduli (G′ and G″) were found in un-irradiated flour, whereas the lowest values were found in the 10 kGy (G6) irradiated flour as similar as Zhu (2016). The decreasing trend of G′ and G″ as increasing the irradiation dose can be attributed to interaction between particles in quinoa flour and starch, degradation of the starch molecules and the structural breakdown of the polymers at higher doses which lead to the formation of weaker gel network of quinoa flour (6-8). Also Higher frequencies led to an increase in the patterns of storage and loss modulus as in Kong et al. (2009). The complex modulus (G*) and damping factor (tan δ) of samples at constant frequency of 10 Hz (table 1.) shows significant reduction in complex modulus of irradiated samples compared to control sample indicating the formation of weaker gel in irradiated quinoa flour (6). Gel formation with higher complex modulus may be due to the polymerization of proteins and the formation of disulfide bonds (9). Damping factor (tan δ) significantly increased in irradiated sample compared to control. validating the predominant solid-like character of quinoa flour structure (7). The rheological characteristics results, thus, might be due to the cleavage and rearrangement of the starch granules after irradiation (10).

Conclusion

Gamma irradiation treatment of quinoa resulted in decreasing the viscoelastic nature of its gel (G′ and G″) as well as complex modulus (G*) and increasing damping factor (tan δ) significantly and induced changes in the rheological properties of quinoa flour. Results indicated that this treatment can cause the degradation of starch molecules and the structural breakdown besides changing gel network. Therefore, can be used to change rheological properties of quinoa.

References

1. El Sohaimy S, Mohamed S, Shehata M, Mehany T, Zaitoun M. Compositional analysis and functional characteristics of quinoa flour. Annual Research & Review in Biology. 2018:1-11. 2. Wang S, Zhu F. Formulation and quality attributes of quinoa food products. Food and bioprocess technology. 2016;9(1):49-68. 3. Danielsen S, Bonifacio A, Ames T. Diseases of quinoa (Chenopodium quinoa). Food Reviews International. 2003;19(1-2):43-59. 4. Sá AGA, Moreno YMF, Carciofi BAM. Food processing for the improvement of plant proteins digestibility. Critical reviews in food science and nutrition. 2019:1-20. 5. Ito VC, Bet CD, Wojeichowski JP, Demiate IM, Spoto MHF, Schnitzler E, et al. Effects of gamma radiation on the thermoanalytical, structural and pasting properties of black rice (Oryza sativa L.) flour. Journal of Thermal Analysis and Calorimetry. 2018;133(1):529-37. 6. Bashir K, Jan K, Aggarwal M. Thermo-rheological and functional properties of gamma irradiated wholewheat flour. International Journal of Food Science & Technology. 2017;52(4):927-35. 7. Kong X, Kasapis S, Bao J, Corke H. Effect of gamma irradiation on the thermal and rheological properties of grain amaranth starch. Radiation Physics and Chemistry. 2009;78(11):954-60. 8. Du Z, Li Y, Luo X, Xing J, Zhang Q, Wang R, et al. Effects of Electron Beam Irradiation on the Physicochemical Properties of Quinoa and Starch Microstructure. Starch‐Stärke.1900178. 9. Thirumdas R, Trimukhe A, Deshmukh R, Annapure U. Functional and rheological properties of cold plasma treated rice starch. Carbohydrate polymers. 2017;157:1723-31. 10. Zhu F. Impact of γ-irradiation on structure, physicochemical properties, and applications of starch. Food Hydrocolloids. 2016;52:201-12.

Table 1. Effect of gamma irradiation on Complex modulus (G*) and Parameter damping factor (tan δ) of quinoa flour in 10 Hz.

Sample	G*	Tan δ
Control	$3.47\times10^{3}\pm0.03$ a	$1.37\times10^{-1}\pm0.02$ f
G1	$3.11\times10^{3}\pm0.01$ b	$1.42\times10^{-1}\pm0.01$ f
G2	$2.72\times10^{3}\pm0.05$ c	$1.56\times10^{-1}\pm0.01$ e
G3	$1.95\times10^{3}\pm0.02$ e	$1.74\times10^{-1}\pm0.02$ d
G4	$2.38\times10^{3}\pm0.02$ d	$1.91\times10^{-1}\pm0.03$ c
G5	$1.13\times10^{3}\pm0.03$ f	$2.25\times10^{-1}\pm0.01$ b
G6	$1.02\times10^{3}\pm0.05$ g	$2.43\times10^{-1}\pm0.05$ a

*Values followed by different letters in each column are significantly different (P <0.05).

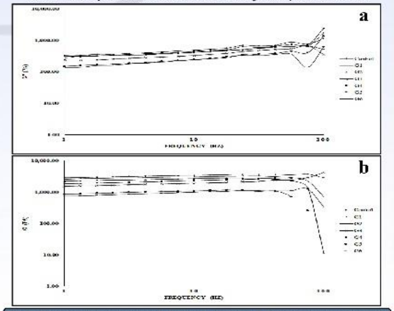

Fig 1. Frequency sweep test (a)-Loss modulus and (b)-Storage modulus of irradiated and un-irradiated (control) quinoa flour.

Article code: A-10-292-1

2nd International Conference on Rheology
14 & 15 December 2021, Tehran, Iran

Rheological properties of bovine serum albumin-cress seed gum complex coacervates

Fatemeh Hamedi, Seyed Mohammad Ali Razavi*
Center of Excellence in Native Natural Hydrocolloids of Iran, Ferdowsi University of Mashhad, Iran

Abstract

The intermolecular interactions between the bovine serum albumin (BSA) and cress seed gum (CSG) were investigated by rheological characterization as a function of pH (7.0- 2.0), and concentrations of BSA (0.1, 0.5 and 1%, w/w) and CSG (0.01, 0.05 and 0.1%, w/w). Dominant storage modulus (G') over loss modulus (G") demonstrated the formation of a weak gel-like structure. Moreover, the complex viscosity (η*) of the complex coacervate decreased linearly in a small range of frequency (0.1-10), implying the shear-thinning behavior of the coacervates. These results reflect that CSG-BSA complex coacervate could be a suitable biopolymer carrier for sensitive and bioactive compounds.

Keywords: Biopolymer- Complex coacervation- Rheology- Protein-Polysaccharide.

Introduction

In the food industry, proteins and polysaccharides are the most important structure-forming ingredients (Tolstoguzov, 1991). Both are important in controlling the stability and rheology of food colloids. Interactions between proteins and polysaccharides are the basis for many important biological processes. In this regard, mixed systems can improve or modify their functional behavior (Dickinson & Galazka, 1991). Protein–polysaccharide complexes have better mechanical, thermal, and emulsifying properties than either of the individual biopolymers with an advantage of modulating electrostatic interactions and in consequence, their complex properties (Ye, 2008). Lepidium sativum, known as garden cress, which belongs to the Brassicaceae family, is a fast-growing annual herb native to Iran, Egypt, and West Asia. When soaked in water, cress seeds swell and get covered with transparent colorless mucilage. Cress seeds contain a significant amount of mucilage (6.5-15 wt.%) with outstanding functional properties comparable to commercial gums such as xanthan, guar, and locust bean gum.

Experimental/Theoretical

Materials

The biopolymers used in this study were bovine serum albumin (BSA) and cress seed gum (CSG). Sodium azide, hydrochloric acid (HCl), and sodium hydroxide (NaOH) were obtained from Merck (Darmstadt, Germany). Deionized water was used in all experiments.

Complexes formation

Binary mixtures of CSG-BSA (0.1-0.1, 0.05-0.1, and 0.1-0.5% w/w) were prepared by adding appropriate proportions of the two biopolymer dispersions then stirred at 300 rpm for about 1h at ambient temperature (25±2 °C). All samples were made in triplicate.

Rheological tests

Dynamic shear rheological properties of the dispersions of complexes and also the BSA and CSG dispersions separately were determined by a Physica MCR 301 rheometer (Anton Paar, GmbH, Graz, Austria) equipped with a coaxial cylinder system (ME21/T200/Q1; bob diameter of 21 mm and cup diameter of 22.158 mm). BSA, CSG, and CSG-BSA complexes at pH=3.5 were analyzed, while each sample was equilibrated at 25°C for at least 5 min before testing. Strain sweep tests were performed over a strain range of 0.01-100% in the controlled rate mode and 1 Hz to determine the linear limit of strain (γL) and the critical strain value (γc). Furthermore, elastic modulus at LVR (G'LVR), loss modulus at LVR (G" LVR), the flow point stress or τf, and loss tangent (tan δ), were extracted from the strain sweep data. Frequency sweep measurements were carried out at a 0.5% strain (which was within the linear viscoelastic region, LVR) over a frequency range of 0.01-10 Hz (Alghooneh, Razavi, 2017). The empirical power-law model was used to describe the frequency dependence of the storage modulus (G′) and loss modulus (G″) (Rao, 1999).

Results and Discussion

Dynamic rheological properties

Rheological properties can be related to structural elements in materials and oscillatory shear measurements monitor structures in weak gels and viscoelastic fluids (Behrouzain et al., 2020). Because of the Newtonian behavior of the BSA solution (0.5%, w/w), the BSA results were omitted here. The obtained results of the strain sweep are represented in Table 1. Within the linear viscoelastic region, the G'LVE dominated over the G"LVE at all samples, showed a solid-like behavior primarily (G'LVE>G"LVE), but after the flow point (crossover point), the samples revealed a liquid-like behavior (G'LVE<G"LVE) and the moduli values reduced at strains greater than the critical strain. The characteristic value of loss tangent (tan δ LVE= G"LVE/G'LVE) is applied for evaluation of the viscoelastic behavior, the low value of tan δ (tan δ < 1) represents a predominantly elastic behavior, while tan δ > 1 shows a predominantly viscous behavior. Also, the Tan δ value lower than 0.1 means that the sample is a true gel while the value between 0.1 and 1 shows the structure is a weak gel (Mandala & Kostaropoulos, 2004). TanδLVE values of the CSG dispersion (0.46) and the CSG-BSA mixtures (0.50-0.54) were lower than 1 but higher than 0.1, which shows the presence of predominant elastic structure in the weak biopolymer gel. Beyond the crossover point, the stress is considered a good indicator of yield stress, while the structure ruptured and the flow behavior started (Rafe et al., 2013). Frequency sweep spectra of the CSG and 0.05CSG-0.1BSA complex coacervate at pH 3.5 are shown in Figure 1. As is seen, a gel-like network structure with mainly elastic behavior was observed for the samples, as both moduli (G′>G") were slightly frequency-dependent without any crossover point in the selected frequency range (0.1-10). Besides, the complex viscosity (η*) decreased almost linearly with increasing frequency, which indicates the general shear-thinning behavior. The dispersions of cress seed gum and its fractions with random coil conformation showed solid-like behavior and were classified as weak gels in the concentrate regime, which might impact the behavior of the CSG-BSA complex coacervates. The gel-like behavior of the CSG-BSA coacervates implies that the BSA molecules and the CSG chains form a more strongly entangled network structure.

Conclusion

The present study showed that interactions between BSA and CSG could produce complex coacervates, depending on the protein or polysaccharide content and the pH level. The dominant G' over G" values in the frequency range of 0.1-10 Hz revealed the highly interconnected gel-like network structure of the complex coacervates, which mainly results from the electrostatic interactions between BSA molecules and CSG chains. Regarding the amorphous structure in the CSG-BSA complex coacervate and also the gel-like network structure, it could be a suitable biopolymer carrier for sensitive and bioactive compounds.

References

1. Tolstoguzov, V. B. (1991). Food Hydrocolloids, 4(6), 429–468.
2. Dickinson& Galazka,V.(1991). Food Hydrocolloids,53), 281–296.
3. Ye, A. (2008). International Journal of Food Science & Technology, 43(3), 406–415.
4. Karazhiyan, H., Razavi, S. M. A., & Phillips, G. O. (2011). Food Hydrocolloids, 25(5), 915–920.
5. Alghooneh, A., Razavi, S. M. A., & Behrouzian, F. (2017). Food Hydrocolloids, 66, 206–215.
6. Behrouzian, F., Razavi, S. M. A., & Alghooneh, A. (2017). Journal of Applied Polymer Science, 134(5).
7. Rao, M. A. (1999). Rheology of Fluid and Semisolid Foods—Principles and Applications Aspen.

Table 1. Strain sweep parameters determined for coacervates at pH 3.5, 25 °C, f=1 Hz

CSG-BSA	G'_{LVE}	G''_{LVE}	Tan δ_{LVE}
0.2 – 0	9.28±0.44c	4.23±0.09c	0.46±0.02c
0.1 - 0.1	123.30±3.11a	62.2±1.52a	0.50±0.05b
0.05 - 0.1	25.69±1.37b	13.24±1.25b	0.51±0.03b
0.1 - 0.5	12.23±0.16c	6.58±0.34c	0.54±0.01a

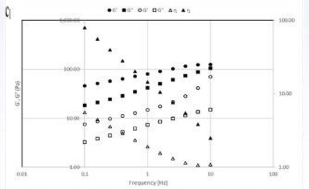

Fig 1. Frequency sweep of the CSG (open symbols) and 0.05%CSG-0.1%BSA (filled symbols) complex coacervate (pH 3.5) at 0.5% strain amplitude and 25 °C.

Article code:

2nd International Conference on Rheology

14 & 15 December 2021, Tehran, Iran

Properties of styrene butadiene rubber (SBR) nanocomposites filled with modified silica

Masoumeh Kalantari, Ali Asghar Katbab, Hossein Nazokdast

Department of polymer Engineer, Amirkabir University of Technology, Tehran, Iran

Abstrac

The traditional method for directly compounding rubber, silica, and bis (3-triethoxysilylpropyl) tetrasulfide (TESPT) by shear force, which we called it One-Step Method (OSM), results in a modification of mechanism: indicated that the TESPT hydrolyzed firstly to generate the silanol (Si–OH), and the silanol reacted with the hydroxyl groups on the surface of silica, which characterized by FTIR. The properties of modified silica were studied. Furthermore, the SBR nanocomposites filled with modified silica by OSM were prepared and the properties comparisons were carried out. The obtained results exhibited the advantages of TESPT.

Keywords: Nanocomposites-Surface Treatment-Nanoparticles-Coupling Agents-SBR

Instruction

Silica is widely used to improve the static and dynamic mechanical properties of rubber, such as wet skid resistance and rolling resistance. Furthermore, silica is also independent of oil resources and environmentally friendly filler used as a replacement for carbon black[1]. Because of the poor compatibility between silica and the rubber matrix and the severe agglomeration resulting from the surface hydroxyl groups of silica, the applications of silica are limited. So the surface modification must be introduced in application of silica and silane coupling agents, such as bis(3 triethoxysilylpropyl)tetrasulfide (TESPT), are most commonly used to modify the silica[2].About the method for the surface modification of the silica. The rubber matrix, silica, and TESPT are compounded in a two-roll mill or an internal mixer. TESPT reacts in situ with the surface hydroxyl of the silica by shear force in the compounding process, and then the sulfur of TESPT reacts with the unsaturated bonds of the rubber matrix during the curing process. Sae-oui et. al [3] used this method to prepare a silica/TESPT/polychloroprene nanocomposite in a Haake Rheomix mixer. They suggested that TESPT improved the processability of the compound, mechanical properties of the vulcanizates, and dispersion of silica in the vulcanizates. However, it is not clear whether the interaction between silica and TESPT is simple physical absorption or the chemical bonding during the condensation reaction of the hydrolyzed hydroxyl of TESPT and surface hydroxyl of silica. As is well known the deep chemical bonding of silica and silane favors the dispersion of silica and interfacial interaction between the rubber and silica during mixing.

Materials

Styrene butadiene rubber was from Lanxess Chemical Industry Co., Ltd. (Germany). Precipitated silica of Tixosil 383 (median diameter is 13.7 nm, DOP oil absorption is 2.66 mL/g, CTAB specific surface area is 163 m^2/g) was produced by Rhodia France (Qingdao, China). Bis (3-triethoxysilylpropyl) tetrasulfide (TESPT) was obtained from Nanjing Shuguang Chemical Group Co., Ltd. (China). The other materials are all commercially available.

Preparation of rubber nanocomposites

The formulation of modified silica filled SBR compounds is shown in Table 1. First, because silica is a fan of silica, we put it in the oven for 24 hours to absorb its moisture.The mixture is first prepared in laboratory rollers at room temperature. In order to reduce the viscosity and to completely wet the reinforcements with the matrix, we masticated the rubber several times and then add the reinforcements with oil. When fully dispersed, add zinc oxide and stearic acid. We should note that if the silane modifying agent was present in the formulation, it should be added directly to the silica in the same second step to perform the in situ correction operation. The optimum cure time (t90) of the compounds was determined by a Disc Vulkameter (Beijing Huanfeng ChemicalMachinery Trial Plant, Beijing, China). The compounds were vulcanized at 160 °C for t90 in a standard mold to form the nanocomposites.

Table 1. The formulation of modified silica filled SBR compounds.

	N35	N15
SBR1500	100	100
N55	35	15
silica	15	35
TESPT(si69)	4	5
Naphtenic oil	10	10
zno	5	5
Stearic acid	1/5	1/5
sulfur	1/7	1/7
TMTD	0/015	0/015
MBTS	1	1

3. Results and discussion

According to the results obtained in Figure 1, it can be seen that: The peaks appearing in the wave numbers 3411 cm^{-1} and 1100 were the main characteristics of silica. And belongs to OH and Si-O-Si groups, respectively. Poor peak for C-H bond tension around 12811 cm^{-1} Approves surface modification of silica with silane. Simultaneously decreasing the peak intensity of the OH group and increasing the peak intensity related to Si-O-Si tension in the modified sample confirms the surface correction reaction. In other words, the amount of hydroxyl groups on the silica surface decreases after activation by Si69, thus destroying the hydrogen bonds on the silica surface as much as possible[4].

The frequency dependence of viscoelasticity of storage modulus for the silica/SBR vulcanizates is shown in Fig. 2. The storage modulus of the vulcanizates in the rubbery state can be used to evaluate filler–filler interaction. The low frequency storage modulus was increased for each sample compared to pure styrene butadiene. Storage modules are similar at higher frequencies. Low frequencies are associated with rolling resistance[5]. Rolling resistance is the energy that is lost when the tire is rotated by the constant deformation of the tire. If desired, the material's ability to return more stored energy reduces the tire's rolling resistance.

Conclusion

The primary objective of this research was to explore polymer and nanoparticle interactions that effect rheological properties related to increasing grip while decreasing rolling resistance in tires.The chemical bond formed after grafting reaction between silica and TESPT was generated, which was confirmed by FTIR experiments.and For vulcanizates, the rheological properties associated with rolling resistance were improved. At low frequencies that correspond with rolling resistance, the storage modulus was significantly improved. Additionally, greater improvements of several orders of magnitude was observed at higher weight percentages of silica.

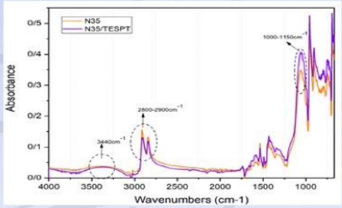

Fig. 1. FT-IR spectra of nanocomposites.

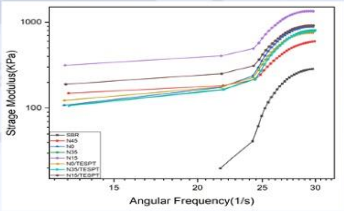

Fig. 2. G' versus frequency for nanocomposites at varying weight percentages.

Reference

[1] M. Gerspacher, C. P. O'Farrell, L. Nikiel, H. H. Yang, and F. Le Méhauté, "High frequency viscoelasticity of carbon black filled compounds," *Rubber Chemistry and Technology*, vol. 69, no. 5. pp. 786–800, 1996.

[2] H. Zou, S. Wu, and J. Shen, "Polymer/Silica Nanocomposites: Preparation, characterization, propertles, and applications," *Chem. Rev.*, vol. 108, no. 9, pp. 3893–3957, 2008.

[3] P. Sae-Oui, C. Sirisinha, U. Thepsuwan, and K. Hatthapanit, "Roles of silane coupling agents on properties of silica-filled polychloroprene," *Eur. Polym. J.*, vol. 42, no. 3, pp. 479–486, 2006.

[4] Q. Tian, Y. Tang, T. Ding, X. Li, and Z. Zhang, "Effect of nano-silica surface-capped by bis[3-(triethoxysilyl)propyl] tetrasulfide on the mechanical properties of styrene-butadiene rubber/butadiene rubber nanocomposites," *Compos. Commun.*, vol. 10, pp. 190 193, 2018.

[5] "Rheology of Polymer Nanocomposites for Advanced Tire Tread," 2016.

Article code: A-10-296-1

2nd International Conference on Rheology

14 & 15 December 2021, Tehran, Iran

Graphene Oxide decoration for enhancement of rheological performance of nanocomposites

Fahimeh Shahsavar[a], Amir Babaei[a*]

presenting author's name: Fahimeh Shahsavar

[a] Department of Polymer Engineering, Faculty of Engineering, Golestan University, Gorgan, Iran.

E-mail addresses: a.babaei@gu.ac.ir, Fahimeh_shahsavar@yahoo.com

Abstract

The present study explores the effect of the incorporation of Graphene Oxide-Chitosan nanohybrid on the rheological properties of the Polycaprolactone matrix. To this end, firstly, covalently functionalized graphene oxide sheets were successfully synthesized by grafting Chitosan. Afterward, the effect of the addition of various amounts of GO-CS nanohybrid on the rheological properties of PCL-based nanocomposites was investigated. The result indicated that GO-CS nanohybrid has an interesting dual role based on the amount of addition. It was found that GO-CS is a candidate for enhancing the processability of polymer matrices.

Keywords: Graphene Oxide, Nano-hybrid, Rheological properties, Nanocomposites.

Introduction

Among numerous kinds of degradable polymers, polycaprolactone (PCL) as a biopolymer is currently one of the popular materials with a bright development prospect and is considered as the 'green' eco-friendly polymer [1]. Nonetheless, despite the unique properties of PCL, its limitations in some of the applications [2]. Graphene Oxide (GO) nanoparticles can dramatically improve the properties of PCL-based composites. However, the high surface energy and relatively low biocompatibility of GO puts some limits on the wide application, especially in the bio-applications, which potentially can be resolved through functionalization. One of the best candidates for this approach is Chitosan (CS). CS, a bio-sourced natural polymer, has generated enormous interest due to several unique physicochemical properties and biological functions[3]. Hence, the formation of organic-inorganic hybrids by a covalent conjugation between GO and CS is an effective approach for improving their valuable properties. In this regard, the performance of PCL/GO and also PCL/GO-CS nanocomposites were investigated in terms of rheological properties. To this aim, firstly GO-CS nanohybrid is synthesized and, subsequently, the effect of the addition of various amounts of GO-CS nanohybrid on the rheological properties of PCL-based nanocomposites was investigated.

Experimental section

GO was prepared by modification the Hummers method [4]. GO-CS nanohybrid was synthesized via the covalent linkage between GO sheets CS chains, according to the previously published method in the presence of catalysts [3]. The films were obtained through the solvent-casting method with various concentrations of nanoparticles.

Result and Discussion

The complex viscosity (η^*) for PCL-based nanocomposites is shown in Fig.1. The results indicate that the presence of 0.5 %wt of GO into the polymer matrix, due to network-like structures of GO sheets in the nanocomposite, the complex viscosity increased[5]. On the other hand, in the case of PCL/GO-CS 0.25% and 0.5% wt, the complex viscosity increased, while in the PCL/GO-CS 1 %wt, the complex viscosity significantly decreased. It can be explained that, after covalently grafted GO with CS, the number of layers increased [7, 8]. Moreover, CS covered the GO layers, thus, the surface chemistry of nanoparticles changed, resulted in the interaction of PCL chains with the functional groups of GO nanosheets is reduced. It can be interpreted that, the GO-CS nanohybrid exhibited a dual role according to the amount of addition: motion-limiting role and the lubricating role. It can be interpreted that a homogenous distribution in the case of PCL/GO-CS 0.25 and 0.5 wt% can be realized, hence, dual roles of nanohybrid are relatively neutralized. On the contrary, the PCL/GO-CS 1 %wt nanocomposite, the quality of distribution changed and the lubrication role is dominated [9, 10]. Fig. 2 gives the storage modulus (G′) for neat PCL and PCL-based nanocomposites. The results imply that the addition of GO to the PCL matrix increased the storage modulus, which can be assigned to 'pseudo-solid'-like behavior and a percolating network. It can be deduced that there is an interconnected GO network and strong interfacial interaction between nanoparticle and PCL chains [11]. In the case of PCL/GO-CS 0.25 %wt and PCL/GO-CS 0.5%wt nanocomposites, the storage modulus increased it can be attributed to the high elasticity. Nevertheless, in the PCL/GO-CS 1%wt the lubricating role of nanohybrid layers is dominant and, a decrease in the elasticity can be observed. The Han plots for the samples are shown in Fig. 3. The results imply that the slopes of the samples are almost close to each other and fairly lower than that of the pure PCL. One can conclude that PCL/GO-CS nanocomposites follow a nearly straight line, indicating a moderate physical network and, subsequently, induced elasticity linked with the added nanohybrids. Alternatively, the Han plot of PCL/GO 0.5 %wt nanocomposite exhibited a remarkable deviation, signifying the formation of nanolayer networks within the PCL. Weighted relaxation spectra of samples can be clearly detected in Fig 4. The results imply that the relaxation spectra of the PCL-GO 0.5%, PCL/GO-CS 0.25%, and PCL/GO-CS 0.5 %wt, are shifted toward higher relaxation times, as compared to a neat PCL system. This confirms that mobility is limited by the nanoparticles or the interaction between the nanoparticles and the matrix [12]. It should be mentioned that the lower relaxation time of the PCL/GO-CS 1%wt chain in comparison to others is due to the lubricating role of nanohybrid, which ultimately facilitates the movement of polymer chains. As was discussed above, the higher solid-like behavior of nanocomposites is assigned to the formed nanoparticles and nanohybrid network in the nanocomposites. Therefore, GO sheets and GO-CS nanohybrid have a different effects on the nanocomposite microstructure and properties.

Conclusion

This work aimed to investigate the effect of GO-CS nanohybrid as a nanofiller on the rheological properties of the PCL matrix. The GO-CS nanohybrid has a lubricant role and motion limiting the role. It was found that GO-CS is a candidate for enhancing the processability of polymer matrices.

References

1. Mohamed, R. M.; Yusoh, K. In *A review on the recent research of polycaprolactone (PCL)*, Advanced Materials Research, Trans Tech Publ: 2016; pp 249-255.
2. Ahmed, J.; Luciano, G.; Schizzi, I.; Arfat, Y. A.; Maggiore, S.; Thai, T. L. A., Non-isothermal crystallization behavior, rheological properties and morphology of poly (ε-caprolactone)/graphene oxide nanosheets composite films. *Thermochimica Acta* **2018,** *659*, 96-104.
3. Hu, H.; Wang, X.; Wang, J.; Liu, F.; Zhang, M.; Xu, C., Microwave-assisted covalent modification of graphene nanosheets with chitosan and its electrorheological characteristics. *Applied Surface Science* **2011,** *257* (7), 2637-2642.
4. Hummers Jr, W. S.; Offeman, R. E., Preparation of graphitic oxide. *Journal of the american chemical society* **1958,** *80* (6), 1339-1339.
5. Zuo, P.-P.; Feng, H.-F.; Xu, Z.-Z.; Zhang, L.-F.; Zhang, Y.-L.; Xia, W.; Zhang, W.-Q., Fabrication of biocompatible and mechanically reinforced graphene oxide-chitosan nanocomposite films. *Chemistry Central Journal* **2013,** *7* (1), 39.
6. Kim, J. Y.; Kim, D. K.; Kim, S. H., Effect of modified carbon nanotube on physical properties of thermotropic liquid crystal polyester nanocomposites. *European polymer journal* **2009,** *45* (2), 316-324.
7. Emadi, F.; Amini, A.; Gholami, A.; Ghasemi, Y., Functionalized graphene oxide with chitosan for protein nanocarriers to protect against enzymatic cleavage and retain collagenase activity. *Scientific Reports* **2017,** *7*, 42258.
8. Bao, H.; Pan, Y.; Ping, Y.; Sahoo, N. G.; Wu, T.; Li, L.; Li, J.; Gan, L. H., Chitosan-functionalized graphene oxide as a nanocarrier for drug and gene delivery. *Small* **2011,** *7* (11), 1569-1578.
9. Alzari, V.; Nuvoli, D.; Scognamillo, S.; Piccinini, M.; Gioffredi, E.; Malucelli, G.; Marceddu, S.; Sechi, M.; Sanna, V.; Mariani, A., Graphene-containing thermoresponsive nanocomposite hydrogels of poly (N-isopropylacrylamide) prepared by frontal polymerization. *Journal of Materials Chemistry* **2011,** *21* (24), 8727-8733.
10. Kinoshita, H.; Nishina, Y.; Alias, A. A.; Fujii, M., Tribological properties of monolayer graphene oxide sheets as water-based lubricant additives. *Carbon* **2014,** *66*, 720-723.
11. Wu, D.; Wu, L.; Sun, Y.; Zhang, M., Rheological properties and crystallization behavior of multi-walled carbon nanotube/poly (ε-caprolactone) composites. *Journal of Polymer Science Part B: Polymer Physics* **2007,** *45* (23), 3137-3147.
12. Sodeifian, G.; Nikooamal, H. R.; Yousefi, A. A., Molecular dynamics study of epoxy/clay nanocomposites: rheology and molecular confinement. *Journal of Polymer Research* **2012,** *19* (6), 9897.

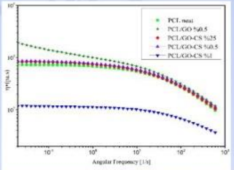

Fig 1. Complex viscosity of PCL neat and PCL based nanocomposites with frequency sweep

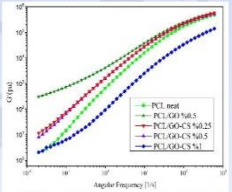

Fig 2. The storage modulus of PCL neat and PCL based nanocomposites with frequency sweep.

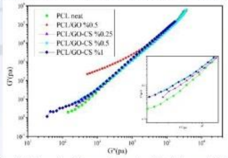

Fig 3. Han plot of loss modulus (G″) versus storage modulus (G′) for PCL neat and PCL based nanocomposites.

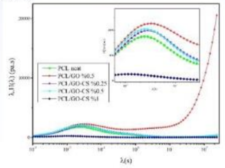

Fig 4. Weighted relaxation spectrums of the pure PCL and their nanocomposites

Article code: A-10-298-1

2nd International Conference on Rheology
14 & 15 December 2021, Tehran, Iran

Magnetically superhydrophobic sawdust powder for removal of oil from water surface

Rezaei Fateme[1], **Hassanajili Shadi[1 *]**
1. School of Chemical and Petroleum Engineering, Shiraz University, Shiraz, Iran
* corresponding author, Email: ajili@shirazu.ac.ir

Abstract

Because of frequent oil spill pollution and resulting immeasurable harm to the environment and human health, it has attracted a wide concern in recent years. Magnetic bio-sorbents are effective materials for collecting and removing oil from the surface of water. In this work magnetically superhydrophobic green oil sorbent was fabricated through precipitating of $CoFe_2O_4$ magnetic nanoparticles on the surface of sawdust and subsequently chemically modification with low surface energy fluorosiloxane. This prepared sorbent shows a great superhydrophobicity (water contact angle of 156°), and acceptable oil sorption capacity (4.2 g/g). Scanning electron microscope (SEM) and Fourier transform infrared (FT-IR) were employed to characterize this composite sorbent. This magnetic bio-sorbent can be dispersed in oil as carrier fluid and magnetize the oil which could effectively remove the oil slicks under magnetic field. In this regard rheological properties of this fluid have been investigated. The results show that in the presence of magnetic field, increasing magnetic strength, viscosity increased and MR fluid exhibits solid-like behavior.

Keywords: oil-water separation- $CoFe_2O_4$ magnetic nanoparticles – magnetorheological – superhydrophobicity

Introduction

Due to the importance of oil spill pollutions and their serious problems, more attention has been paid to effective and efficient ways to remove the oil slicks. In some cases, preference is magnetic bio sorbents because of eco-friendly and low-cost properties. Also, magnetic separation is another advantage of magnetic bio sorbent [1]. Inherently, bio-sorbents are low hydrophobicity materials, so different kind of modification can be applied in order to enhance this feature. Modification of magnetic bio sorbent with low surface chemicals improves their adsorptive capabilities [2]. In the present work, environmentally-friendly, economical and recyclable bio material was employed in order to fabricate versatile magnetic superhydrophobic $CoFe_2O_4$/sawdust oil sorbent.

Experimental

The reduced size sawdust was washed with abundant water and ethanol and dried in an oven for 24 h. First, 1 g pretreated sawdust was added to $CoCl_2.4H_2O$ and $FeCl_2.6H_2O$ solution at 80 °C for 1h. Then, NaOH as the precipitation agent and KNO_3 added to the mixture until pH 12 and stirred for 3h at 80 °C. The black precipitate was collected by a magnet and washed with DI water and dried. To modify $CoFe_2O_4$/sawdust composite, it was immersed in FAS, ammonia and ethanol solution under magnet stirring for 12h at ambient temperature. After passing through filter paper and washing with distilled water, it was dried at 60 °C for 6h, superhydrophobic sawdust powder was successfully obtained. The surface morphology and chemical structure of magnetic bio-sorbent was examined by scanning electron microscopy (SEM) and Fourier transform infrared (FTIR), respectively. To analyze the MR behavior of the fabricated magnetic bio-sorbent with the weight percent of 10% was dispersed in N-500 oil as carrier fluid. Rotation rheometer equipped with a magnetic field generator was employed to determine the MR properties.

Results and Discussion

SEM images of raw and modified sawdust are shown in Fig. 1. It is obvious that the surface of pristine sawdust is smooth and clear. After chemical modification a layer of aggregate magnetic particles precipitated on the surface of the sawdust. This modification results a rough morphology on the surface. Finally, superhydrophobic surface was obtained by roughening and modifying with low surface energy fluorosiloxane [3].

In order to show the successful modification of sawdust surface with $CoFe_2O_4$/FAS the FTIR spectra of raw and modified sawdust are presented in Fig. 2. By comparing, adsorption peaks were observed at 559 and 467 cm^{-1} in modified spectra attributed to Fe-O bond which indicate favored coating of $CoFe_2O_4$. The strong peaks at 935 and 848 cm^{-1} conform the existence of CF_2 and CF_3 in modified sawdust. Also, the adsorption peak at 1219 cm^{-1} indicated C-F stretching bond.

The variation of viscosity versus shear rate for the prepared MR fluids under different magnetic fields is shown in Fig. 3. According to the results at low shear rates the MR fluid shows a non-Newtonian behavior. Under magnetic field, MR fluid exhibited Bingham- like behavior. By increasing magnetic strength, viscosity increased which is due to the formation of strong chain-like structure of magnetic particles along the direction of magnetic field [4]. The orientation of MR fluid under magnetic field results the oil movement along the direction of field. This property causes to better oil sorption of the prepared magnetic sawdust.

Conclusion

In the present study magnetically superhydrophobic green oil sorbent was fabricated through precipitating of $CoFe_2O_4$ magnetic nanoparticles on the surface of sawdust and subsequent chemically modification with low surface energy fluorosiloxane. Magnetic nanoparticles and subsequent modification result a rough morphology and superhydrophobic magnetic bio-sorbent. This magnetic bio-sorbent can be dispersed in oil as carrier fluid and magnetize the oil which could effectively remove the oil slicks under magnetic field.

References

1. Soares, S. F., Fernandes, T., Trindade, T., & Daniel-da-Silva, A. L., Recent advances on magnetic biosorbents and their applications for water treatment. *Environmental Chemistry Letters*, **18**, 151-164, 2020.
2. Fan, S., Pei, S., Shen, T., Xu, G., Li, Y., & Fan, W. Fabrication of Superhydrophobic Magnetic Sawdust as Effective and Recyclable Oil Sorbents. *Materials*, **12**, 3432, 2019.
3. Ma, M. and Hill, R.M., Superhydrophobic surfaces. *Current opinion in colloid & interface science*, **11**, 193-202,2006.
4. Kamgar, A., Hassanajili, S. and Unbehaun, H., Oil spill remediation from water surface using induction of magnetorheological behavior in oil by functionalized sawdust. *Chemical Engineering Research and Design*, **160**, 119-128, 2020.

Figures

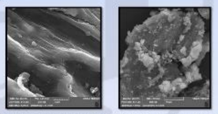

Fig 1. Scanning electron microscopy images of (a) raw sawdust powder (b) modified sawdust powder.

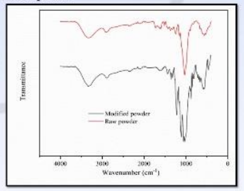

Fig 2. FT-IR spectra of the raw corn cob powder and modified powder.

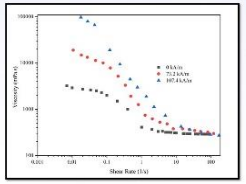

Fig 3. The MR behavior of modified bio sorbent at different magnetic fields.

Article code: A-10-300-1

2nd International Conference on Rheology
14 & 15 December 2021, Tehran, Iran

The effect of activator on rheological properties of inorganic polymers used for 3D printing

Mahdi Madelatparvar
Department of Material Science and Engineering, School of Civil Engineering, Qingdao University of Technology, Qingdao 266033, China

Chunwei Zhang
Center for Infrastructure Engineering Kingswood Campus University of Western Sydney University Australia Locked Bag 1797 Penrith NSW Australia

corresponding author: Mahdi@qut.edu.cn

Abstract

Designing the rheological properties of alkali-activated materials (AAM) used for 3D printing are of important challenge for material designers. During the process, AAM are pumped, extruded and placed layer by layer to form a structure without any mold as supporter. The lower viscosity and pumpability are required before extruding materials. In contrast, higher thixotropic properties are desirable after placing the material to tolerate the own weight and the next layer weight. This characteristic is compatible to Bingham model. The sustainability of materials after printing is mainly related to the static yield stress. This parameter can be calculated through multiplying the critical shear strength and extrapolation storage modulus against time. Static yield stress then compared with the weight of layers to investigate the sustainability of the products against gravitational forces. None of the specimens could resist the own weight in this study.

Keywords: Inorganic polymer, Alkali activated materials, 3D printing, Rheology,

Introduction

Alkali activated materials (AAM) are inorganic polymers made from the chemical activation of silicate materials and alkaline activators. The consumption of geopolymers including alkali activated materials instead of common cementitious concrete has been raised due to reducing the carbon dioxide emission and other green construction activity. Every day new types of geopolymers are being developed from waste materials with different properties. On the other hand, 3D printing of building has gained many attentions and is projected to replace the common labor and time-consuming construction method in the near future. Indeed, 3D concrete printing uses minimum material wastage, and there is no need for molds and frameworks. The process of concrete 3D printing contains pumping, extruding and positioning materials at the certain place based on CAD file, layer by layer. Materials are used for 3D printing should meet certain mechanical and rheological properties in each process level. The shear stress required for concrete flowing called dynamic yield stress and plastic viscosity are the key properties of the materials in the pumping and extrusion stages. Also, at the positioning state, static yield stress which increases after positioning play an important role in material design for printability[1]. Stress growth test and flow curve test have been used for static yield stress and dynamic yield stress measurement respectively. The appropriate material has to own low viscosity at the time of pumping and high viscosity and high thixotropy during the printing. Hence, the rheological properties of material before and after extrusion is in contrast. The aim of this study is to find a relationship between the type of AAM and those rheological properties of the specimens which are related to printing.

Experimental/Theoretical

The components of the material consisted of granulated blast furnace slag (GBFS), the commercial by-product of Isfahan Steel Company Sodium hydroxide was purchased from Bandar Imam Petrochemical Company and diluted to two different molarities with tap water. Silica sand with mesh size of 0-0.3 mm was purchased from Taban powder Malayer Company located in Hamedan, Iran. Chemical analysis through XRF is shown in Table 1. Anton paar 300 was employed for determination the rheological behavior of the AAM. The samples properties were also shown in Table 2. The relationship for calculation static yield stress is $\tau_s = G'_s \times \gamma_c$ where τ_s is static yield stress, G'_s is storage modulus which is gained through extrapolation of storage modulus against time, and γ_c is the critical shear strain. Samples mixed 10 min with hand and rested for 10 min then tested.

Results and Discussion

In order to investigate the printability of the material static shear strength has been calculated for 3 samples and have been shown in the Table 2.

The loss modulus and storage modulus of two samples with two different activator molarities were measured and were depicted against shear strain in Figure 1. The critical shear strain γ_c was obtained from the interaction of two fitted line on storage modulus plot. The first line is the tangential of linear elastic stage whereas the second line is fitted to the viscoelastic phase. The critical shear strain was approximately 0.03% for those two samples. Figure1 also shows that the storage modulus of AAM decreased with increasing the molarity of the activator. The differences between critical shear strain of other samples can be neglected. Results show that by increasing the molarity of activator to slag ratio, the storage and loss modulus of the printed inorganic polymer is decreased. This is mainly because of the interaction forces between particles which leads to formation and cessation of 3D gel of C-S-H bonds inside the AAM. Table 3 shows the increase in molarity of activator led to decrease the storage modulus of samples. As the critical shear strength in two samples with different molarity was approximately the same, the static yield stress of high activator molarity sample is lower than low activator sample. Addition of silica sand also increased the storage modulus of the AAM to more than 1 order of magnitude. The result of static yield stress was lower than the stress level of the printed layer which is calculated through the ρgh where ρ is 1800 Kg/m3, g is 9.8m/s2 and h is 0.01 m. print (176.4 Pa >> τ_0 = 0.597 Pa). Although addition of silica sand increased the storage modulus to a considerable amount, it is still lower than being sustainable to print.

Conclusion

Static yield stress was calculated as the main parameter of the material printability. Results show that by decreasing the molarity of the activator and adding silica sand, the static yield stress has been increased. In this case the very low static yield stress shows that this material is not printable.

References

1. Ranjbar, N., Mehrali, M., Kuenzel, C., Gundlach, C., Pedersen, D. B., Dolatshahi-Pirouz, A., & Spangenberg, J. (2021). *Cement and Concrete Research*, 147, 106498.
2. Panda, Biranchi, Cise Unluer, and Ming jen Tan. *Composites Part B: Engineering* 176 (2019): 107290. Design 108 (2016): 551-559.

Table 1. Raw materials analysis

Material	SiO_2	CaO	Al_2O_3	MgO	MnO	FeO
GBFS	37.5	36.4	9.3	7.3	1.9	0.
Silica Sand	99.51	0.3	0.1	0	0	0.01>
Material	**TiO_2**	**V_2O_5**	**Na_2O**	**LOI**		
GBFS	3.2	1.9	4.2	0.01>		
Silica Sand	0.01>	0	0.01>	0.01>		

Table 2. AAM samples components and G'_0

	NaOH/Slag	Silica Sand	Activator Molarity	Storage Modulus Pa
M35	0.35	0	3.5	163
M85	0.35	0	8.5	127
M85S	0.35	20	8.5	1990

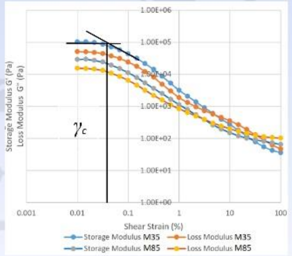

Figure 1. Storage and loss modulus of samples with different activators molarity.

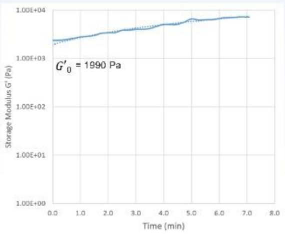

Figure 2. The evolution of the storage modulus of M85s after printing and extrapolation.

Article code: A-10-305-1

A-10-306-1

2nd International Conference on Rheology
14 & 15 December 2021, Tehran, Iran

Study of uniformity and diameter variation of electrospun PVDF/CNC fibers by rheology

Zohreh Solouki[a] , Fatemeh Goharpey[a]
a. Department of Polymer Engineering & Color Technology, Amirkabir University of Technology, No. 242, Hafez St. Tehran, Iran

Abstract
We prepared poly (vinylidene fluoride) (PVDF)/cellulose nanocrystals (CNC) nanocomposites using the electrospinning process and investigated the effects of PVDF concentration and varying the CNC content on the rheological behavior, uniformity and diameter of the fibers obtained. The diameter and uniformity of the nanofibers were evaluated by scanning electron microscopy. By using rheometry technique, complex viscosity and storage modulus were measured and it was found by CNC increasing, storage modulus increases monotonically up to 3 wt%, while complex viscosity hasn't specific trend.

Keywords: electrospinning- Polyvinylidene fluoride (PVDF)- cellulose nanocrystals (CNC)-nanocomposite- rheological behavior

Introduction

Factors affecting the formation of fibers resulting from the electrospinning process are solution properties such as concentration, polymer molecular weight, viscosity and conductivity. A minimum concentration is required to form fibers in polymer solutions, below which electrospinning is converted to electrospraying [1]. For a polymer solution, the higher polymer concentration, the higher entanglement density, resulting in an increase in apparent viscosity and an increase in fiber diameter. Addition of nanoparticles to the polymer solution, due to the interaction of nanoparticles with polymer chains and nanoparticles network formation; the viscosity and storage modulus increase [2].
In this work, the changes in fiber diameters resulting from the electrospinning of PVDF/CNC solution in different content of CNC are investigated.

Experimental

Materials: Poly (vinylidene fluoride) (PVDF) (Kaynar 720 molecular weight 250,000 g / mol), DMF, acetone and cellulose nanocrystals (length range of 200-300 nm and a diameter of 20-30 nm) was used.

Preparing the electrospun PVDF/CNC fiber: PVDF/CNC solution (23%) with different percentages of CNC (0, 1, 3 and 5% by weight of the polymer) and DMF/acetone ratio of 50.50 was prepared. The CNC and PVDF granules were added in to the solvent and magnetized for two hours at 60 ° C. The solutions were exposed to 15 KV at 25 ° C, feed rate of 1 ml/h and a distance of 18 cm from the nozzle tip to the collector plate

Characterization: By Using the abeload viscometer, Intrinsic viscosity was obtained. Morphology and mean diameter of electrospun nanofibers were analyzed by scanning electron microscopy (SEM). The complex viscosity and storage modulus of PVDF/CNC have been measured by using RMS.

Results and Discussion

Minimum concentration required for uniform fiber formation is 2-2.5 Ce. Also, considering that Ce = 10 C * and C * = 0.77 / [η] [3]. Intrinsic viscosity calculated from the extrapolation of the Kramer-Huggins equations obtained from abeload, which is equal to 0.79 dl/gr. According to this result, 23 wt% solution of PVDF/acetone/DMF was obtained from uniform polymer fibers. Also, with increasing PVDF, due to the increase of entanglement, the diameter of the fibers increases (Fig. 1)[4]. Fig. 2 shows the SEM images of electrospun nanocomposites. The mean diameters of fibers with different CNC content are measured and are tabulated in Table 1. By increasing CNC, the fiber diameter increases up to 3 wt%, but at 5 wt%, in addition to decreasing the diameter, heterogeneity is also observed. In Fig .3, it was observed that by adding 1 wt% CNC, complex viscosity decreases and then by adding 3% CNC, increases. Therefore, viscosity cannot be responsible for the increase in diameter. The storage modulus was shown in fig. 3. By addition CNCs up to 3 wt%, the storage modulus increases at low frequencies and decreases at 5 wt% due to agglomeration formation. Adding 1 wt% CNC may increase the free volume, which facilitates movement and thus reduces viscosity. Another possibility is that the long chains interacted with the CNCs, which reduced the bulk viscosity. The reason of modulus increasing is formation of nanoparticles network [2]. Therefore, it is possible that increasing the storage modulus in the lower regions, because of the solid-like of the jet during the electrospinning process, could be responsible for diameter increase. Extensional viscosity of PVDF and 1 and 3 wt% PVDF/CNC samples is shown in Figure 4. By adding CNC, the Extensional viscosity increases and strain hardening occurs earlier.

Conclusion

The optimum concentration for uniform fiber formation was 23% wt PVDF. The fiber diameter also increased with increasing polymer concentration. The addition of nanoparticles increases the fiber diameter by up to 3% wt. The viscosity of the complex does not increase monotonically with adding CNC. While increasing the modulus and extensional viscosity by adding nanoparticles has a trend similar to increasing diameter.

References

1. S. Li et al., "Uniform high-molecular-weight polylactide nanofibers electrospun from a solution below its entanglement concentration," vol. 44853, pp. 1–7, 2017
2. Y. Chee et al., "Rheological properties of cellulose nanocrystal-embedded polymer composites : a review," *Cellulose*, 2016.
3. C. Wang and Y. Wang, "Impact of entanglement density on solution electrospinning : a phenomenological model for fiber diameter," pp. 1–7.
4. B. Bera, "Literature Review on Electrospinning Process (A Fascinating Fiber Fabrication Technique)," no. 8, pp. 972–984, 2016.
5. A. Zell, S. Gier, S. Rafaï, and C. Wagner, "Journal of Non-Newtonian Fluid Mechanics Is there a relation between the relaxation time measured in CaBER experiments and the first normal stress coefficient ?," *J. Nonnewton. Fluid Mech.*, 2010.

Table 1. Mean diameters of PVDF/CNC electrospun fibers with different CNC loadings

PVDF/CNC nanocomposit	CNC 0	CNC 1	CNC 3	CNC 5
Mean diameter (µm)	0.206	0.250	0.310	0.149

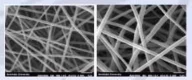

Fig 1. SEM images of nanofibers produced from solutions with a) 23 wt% b) 27 wt% of PVDF

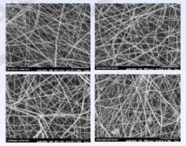

Fig 2. SEM images captured from PVDF/CNC electrospun nanocomposites with different CNC contents with respect to PVDF weight: a) 0 % CNC, b) 1 %, CNC c) 3% CNC and d) 5 % CNC.

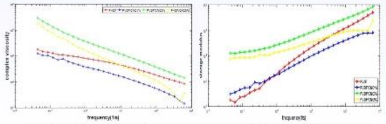

Fig 3. complex viscosity and storage modulus of samples with different CNC contents

Article code: A-10-306-1

2nd International Conference on Rheology
14 & 15 December 2021, Tehran, Iran

An experimental study on the rheological effect of silica and modified silica-IL in PU nanocomposites

Hasansanjili Shadi[1*], Khavand Abed[1], Azangou Ghazal[1], Omraninasab Fatemeh[1]

1. School of Chemical and Petroleum Engineering, Shiraz University, Shiraz, Iran

*corresponding author, Email: ajili@shirazu.ac.ir

Abstract

The rheological behavior of polymer melt has a significant role in polymer processing as it describes the deformation and flow behavior of the material. In this work, the rheological and viscoelastic properties of three Polyurethane (PU) based nanocomposite samples were investigated in oscillatory rheometer in molten state. The samples are 1. pure PU 2. PU/silica nanocomposite and 3. PU/silica-IL nanocomposite. The effect of silica nanoparticles on rheological properties of PU/silica nanocomposite has been investigated. The second sample has a larger cross over in modulus compared to the other two samples, in fact, the crossover is shifted to lower frequency. The parameters for shear viscosity models obtained and the effect of nano particles on viscosity models are described. In addition, the twin Maxwell elements model has been used to describe the stress relaxation behavior in linear viscoelastic region approximately for these three samples.

Keywords: Polyurethane/silica-IL – Viscosity model – non-Newtonian fluid – Linear viscoelastic_–Twin Maxwell elements model

Introduction

Rheological investigation on polymer melts is widely used for quality control and the optimization of processing. Polyurethanes (PU) have a wide range of chemical and rheological properties. Polyurethane composites (PUC) have attracted much attention because of their high potential to achieve great improvement in properties including good processability, mechanical and physical properties by adding a small amount of nanoparticles in the polymer matrixes. [1,2] In this study Polyurethane nanocomposite with silica and silica/IL have been studied. Silica is hydrophilic due to the presence of the silanol (Si-OH) group on the surface of the particle and does not show a tendency to non-polar polymers, for this reason, adding silica nanoparticles have no positive effect on properties and do not disperse homogeneously [2]; so, we modified silica nanoparticles with IL that is increase their compatibility with polymeric matrix.[2]

Experimental

I. Preparation of samples:

Pure PU sample was made by 10% wt. of polyether urethane in dimethylformamide (DMF) as a solvent. For composite samples, at first modified commercial silica with [BMIM][PF6] and non-modified silica should disperse for an hour in DMF at 70°C then PU granules added to the solution and mixed enough for better dispersion. Three samples were made from pure PU and two different silica nano particles (modified and non-modified). The silica nanoparticles concentration in 2 samples are 5% (wt./wt.). Ultrasonication must be done to prevent nanoparticles agglomeration. [3,4]

II. FTIR analysis of samples:

Molecular interaction identification can be observable in FTIR spectra.

III. Viscosity analysis of samples:

An oscillatory rheometer has been used in molten state of samples (185°C). The cone and plate disks with 2.5cm diameter and 0.034 mm height were applied on rheometer [4].

IV. Frequency sweep test of samples:

The same device in the last experience has been used for frequency sweep tests in molten states. To study on the viscoelastic region. 1% of shear strain was applied in all points of 3 tests [4].

Results and discussion

I. FTIR analysis of samples:

In Fig 1, FTIR peaks shows N-H bonds in the range of 3200-3500 cm^{-1}. C=O in 1600-1800 cm^{-1} and C-O-C between 1000-1200 cm^{-1}. Stretching Si-O-Si peaks can be observed between 1010-1190 cm^{-1} in samples no.1 and no.2. Around 850 cm^{-1} in sample no.3 we have P-F peaks to prove the presence of IL in PU/silica-IL.

II. Viscosity analysis of samples:

The Power-low (Eq. 1) and Carreau viscosity equations (Eq. 2) have been used to find the viscosity behavior of samples. All the samples behave like pseudoplastic fluid (Fig. 2) and viscoplastic fluid behavior not seen, so the Herschel-Bulkley and other same equations did not used [6,7]. The viscosity parameters are reported in Table 1

$$\tau_{yx} = m.\dot{\gamma}_{yx}^{\ n} \quad (1) \qquad \frac{\mu-\mu_\infty}{\mu_0-\mu_\infty} = (1-(\lambda\dot{\gamma}_{yx})^2)^{\frac{n-1}{2}} \quad (2)$$

III. Frequency sweep test of samples:

The storage modulus of the samples versus frequency are reported in Fig. 4. As it is obvious adding unmodified silica into PU increase G' at low frequencies due to solid-like network structure and filler aggregation. But adding IL modified silica with the same percent has reduced storage G' in this region due to better silica dispersion. The frequency sweep data used to obtain a linear viscoelastic model. The Maxwell parameters reported in Table 2. For better calculations we are able to use more elements, so the modeling gets closer to better fitting on experimental data, but it can be more difficult and time consuming.

Conclusion

Nanoparticles and modifier have a negative effect on functionality of viscosity specially in high shear rates, the Carreau model is able to use in nanocomposites. The silica nanoparticles caused the viscosity shifted to high values, but the modified silica had inverse effect and intensified the pseudoplastic behavior. In low frequency, PU and PU/silica nanocomposite are closer in complex viscosity (Fig. 3), storage modulus (Fig. 4) and loss modulus compared to modified nanocomposite, but in high frequency both of nano composites (modified and non-modified) get closer to each other, and PU modulus make a difference with other samples.

References

1. Vaithylingam R, Ansari M. N. M., Shanks R.A., Recent Advances in Polyurethane-Based Nanocomposites: A Review. Polymer-Plastics Technology and Engineer J.56, .2017.
2. Hassanajili S. Sajedi T. Fumed silica/polyurethane nanocomposites: effect of silica concentration and its surface modification on rheology and mechanical properties. *Iran Polym J.25, .2016*
3. Sasikumar B, Arthanareeswaran G, Ismail A. F. Recent progress in ionic liquid membranes for gas separation, *Journal of Molecular Liquids*, 226. 2018, 330-341
4. Hassanajili S, E Masoudi E, Karimi G. Mixed matrix membranes based on polyether urethane and polyester urethane containing silica nanoparticles for separation of CO2/CH4 gases, *Separation and Purification Technology*, 116, 2013, 1-12.
5. Dealy J. M., Wissbrun. K. F. (2012). Melt rheology and its role in plastics processing: theory and application. Springer science & Business Media.
6. R. P. Chhabra, J. F. Richardson (2008) , Non-Newtonian flow and applied rheology. *Elsevier*
7. R.J. Crawford (1998). Plastic engineering

Tables and figures

Table 1. Viscosity parameters.

Sample	Eq.	Parameter	Value
Pure PU	1	m	1229
		n	0.3979
		R^2	0.9656
	2	λ	5.18
		n	0.3608
		R^2	0.9951
PU / silica	1	m	3786
		n	0.2267
		R^2	0.7968
	2	λ	6.046
		n	0.08246
		R^2	0.9823
PU / silica – IL	1 (γ =0.0998 - 25.1 1/s)	m	391.5
		n	0.4029
		R^2	0.9521
	2	λ	9.259
		n	0.0265
		R^2	0.9135

Table 2. Maxwell model parameters.

Sample	i	G_i	λ_i	R^2
1. Pure PU	1	4236.65	0.052	0.9996
	2	1.112e5	0.0021	
2. PU / silica	1	1.23e4	0.080	0.9964
	2	8.956e4	0.029	
3. PU / silica - IL	1	3.5e4	0.012	0.9997
	2	8.809e4	0.003	

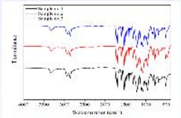

Fig 1. FTIR spectra of samples.
1. PU, 2. PU/Silica, 3. PU/silica-IL.

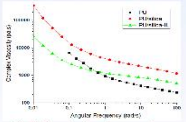

Fig 3. Complex viscosity comparison

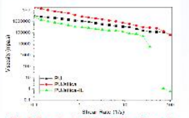

Fig 2. Pseudoplastic behavior of samples

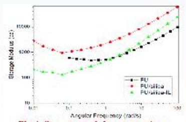

Fig 4. Storage modulus comparison

Article code: A-10-312-1

www.icor-sor.com

2nd International Conference on Rheology
14 & 15 December 2021, Tehran, Iran

Investigation of cure characteristics of silicon rubber / SEBS blends by moving die rheometer

Ehsan Alikhani, Mohsen Mohammadi*

Department of Polymer Engineering, Faculty of Engineering, Qom University of Technology, Qom, Iran, Box: 37195-1519

Abstract
In this study, silicon rubber (SR) / styrene-ethylene butylene-styrene (SEBS) blends with different ratios were prepared for the first time. Then, cure characteristics of SR / SEBS blends by moving die rheometer (MDR) were investigated. The results showed that the curing time of SEBS is longer than SR. In addition, the cross-link density of SEBS is significantly lower than SR. Mixing was evaluated and performed through a lab torque rheometer as internal mixer and the obtained diagrams of torque and melt temperature were analyzed. Steady trend in torque over time confirmed that the blends were not cross-linked during mixing with peroxide.

Keywords: Silicone rubber, SEBS, Rheometer, Curing, Mixing

Introduction
Because of higher properties of silicone rubber (SR) in biomedical and industrial issues, it has been interested extensively [1]. Styrene-ethylene butylene-styrene copolymer (SEBS) is one of the most important TPEs that has thermal stability, aging resistance and good electrical properties [2]. In the past, SR blends systems with polyolefins have been investigated [1, 3]. However, the SR / SEBS blend system and its properties have not been studied, so far. SEBS has an olefin component in its chain, which usually contains more than 50% of each chain. So that, the study of the SR / SEBS blend system seems to be an interesting research topic.

Experimental
Commercial Silicone rubber (NE-5280) with a hardness of 80 (Shore A) having density 1.25 g/cm^3 was obtained from Djsilicone Co., Ltd. (China). Commercial Tri-block copolymer SEBS (Globalprene-7550U), with 30 wt% styrene units and density 0.91 g/cm^3, was supplied by LCY Co., Ltd (Taiwan), Peroxide curing agent BIPB (Bis (tert- butylproxy isopropyl) benzene) was purchased from Rhein Chemie Co., Ltd. (China).

Silicone rubber and SEBS were melt mixed into a Rheosens Lab Torque Rheometer, IPPI Co., Ltd (Iran) as internal mixer. The mixing was performed at 190°C at a rotor speed of 60 rpm for 8 min. First SEBS was added, and it was melted for 2 min. Silicone rubber was then added and mixed for 6 min. Then the obtained blend was mixed with the peroxide agent for 5 min at 70 °C and 60 rpm using the internal mixer. The given low mixing temperature for adding peroxide was chosen to ensure that the peroxide was not degraded. The samples were then compression molded for T90 + 2 min at 175 °C under 30 tones in an electrically heated hydraulic press (SPH-300, Santam Co., Ltd. Iran). Samples were designated as B1, B2, B3, B4, B5 and B6 containing 0, 10, 25, 75, 90 and 100 wt% of silicone rubber, respectively.

The cure characteristics of the samples were studied by a moving disk rheometer (MDR) (SMD-200, Santam Co., Ltd., Iran). About 5 cm^3 of samples were used to perform the tests. This test was performed at a frequency of 1.68 Hz, a temperature of 175 °C and amplitude of 0.5° for 20 minutes.

Results and Discussion
The samples rheograms are shown in Fig 1. The rheograms of all the samples show an initial decrease in their torque. The initial reduction in torque is due to the softening of the polymer as it heats up, which reduces the viscosity and thus the torque required to move the rheometer disc. Then, with the activation of the curing agent and the generation of the first cross-links, the resistance of the chains to movement increases and then the torque increases until it finally reaches a constant value. According to Fig 1, and the information in Table 1, the following results are inferred:

I. As the amount of SEBS increases, the scorch time (Ts2) increases. As a result, scorch safety is improved.
II. As the SR content increases, the cure time (T90) of the blends decreases.
III. Increasing the content of SR increases the cure rate.
IV. Increasing the content of SR increases the ΔM of blends. Since this difference is directly related to the cross-link density, increasing the SR content increases the cross-link density of the blends.
V. There is a significant difference between the cure characteristics of SR and SEBS.

The same behavior was observed in the SR blend with EVA [1] and the SR blend with polyurethane rubber [4]. In those blends, increasing the content of SR reduced the scorch time and curing time. Also, increasing the content of SR increased the cure rate and ΔM. It should be noted that the difference in solubility of the curing agent in elastomers can cause significant differences in their curing speed and the amount of their crosslinking [1]. In addition, it should be noted that the nature of each polymer, the energy of the chains and the type of chemical bonds in each polymer, cause differences in its cure characteristics. But there are other reasons for the difference in SR and SEBS cure characteristics. In the present study, the mixing temperature of the samples with peroxide was set at 70°C. When polymers are mixed inside the internal mixer, the friction caused by the polymer chains with each other as well as with the wall of the internal mixer generates additional heat. The excess heat generated also causes the temperature of the polymer in the internal mixer to be slightly higher than the set temperature. Fig 2 shows the changes in torque, middle zone temperature (set temperature) and melt temperature of the polymer while mixing with peroxide (melt temperature refers to the temperature of the polymer in the internal mixer). This diagram is obtained from the Rheosens Lab Torque Rheometer, for B1. Mixing diagrams of other samples follow a similar procedure.

Changes in torque over time (Fig 2) confirm that the presence of peroxide and mixing with SEBS for 5 minutes did not cause the polymer to cure, as torque did not increase during SEBS mixing with peroxide. Therefore, at the mixing temperature and time most of peroxide was not activated. It should be noted that peroxide was added to SEBS after 1.5 minutes. A comparison of the middle zone temperature and the melt temperature shows that the middle zone temperature, which was considered as the mixing temperature, remained almost unchanged at about 70 °C. The melt temperature has risen from 70 °C to 97 °C. Therefore, the PS blocks were close to their glass transition temperature when mixing with the peroxide. In this case, there is weak possibility of penetrating peroxide into the PS blocks. Because PS blocks are still solid, while EB blocks are very soft and fluid at this temperature.

Conclusion
The rheograms revealed that as the SR content increases, the cure time (T90) of the blends decreased and ΔM and cross-link density of the blends increased. There was a significant difference between the cure characteristics of SR and SEBS. When the blends prepared, after adding peroxide into the internal mixer, because of friction the melt temperature rose from 70 °C to 97 °C, but torque was steady, which confirms no curing occurred during the mixing time.

References
1. Ganesh, B., & Unnikrishnan, G. *Journal of applied polymer science*, 99(3), 1069-1082, 2006.
2. Wu, Y., Shentu, B., & Weng, Z. *Journal of Applied Polymer Science*, 134(5), 1-7, 2017.
3. Serenko, O. A., Pryakhina, T. A., Vasil'ev, V. G., Buzin, M. I., Volkov, I. O., Kotov, V. M., & Muzafarov, A. M. *Russian Chemical Bulletin*, 70(5), 960-966, 2021.
4. Gan, L. M., Ni, H. Y., Zhou, Y. J., & Chen, J. Journal of Macromolecular Science, Part B, 50(8), 1491-1499, 2011.

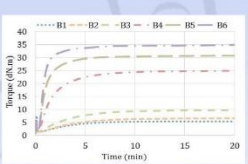

Fig 1. Rheograms of the SR / SEBS blends.

Table 1. Cure paprameters of the samples

Name	Ts2 (min)	T90 (min)	ML (dN.m)	ΔM (dN.m)	Rate of Cure (dN.m/min)
B1	2.50	8.01	1.35	4.18	0.35
B2	2.23	7.95	1.35	5.30	0.48
B3	1.42	7.78	1.54	8.23	0.93
B4	0.53	5.15	1.77	23.19	4.07
B5	0.38	3.03	1.61	29.13	9.18
B6	0.38	2.22	1.25	33.66	15.43

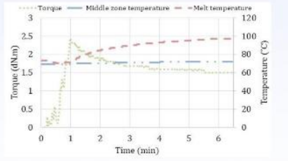

Fig 2. The mixing diagrams of B1, obtained from the Rheosens Lab Torque Rheometer.

* mohammadi@qut.ac.ir

Article code:

2nd International Conference on Rheology
14 & 15 December 2021, Tehran, Iran

Rheological Hysteresis in complex fluids

Zahra Daneshfar*
Department of Chemical and Polymer Engineering, Faculty of Engineering, Yazd University, Yazd, Iran

Abstract
Rheological hysteresis has been studied combining global flow curve and local velocity profiles measurements. This behavior is not unique to thixotropic materials either. it also occurs in other complex fluids. The surface area of the hysteresis loop depends on several parameters; such as the shear history prior to the test, the sweep time and the maximum value of shear rate. Indeed, transient and time-dependent shear band affected the loop area and the range of hysteresis. This review summarizes the most important aspects covered in the rheological hysteresis in different complex fluids.

Keywords: Rheological hysteresis, thixotropy, shear banding, Complex fluids,

Introduction
In the rheological literature, the first mention of hysteresis loops reported by F. L. McMillen in paints [1]. The rheological hysteresis in different complex fluid [2-8] can be studied from apparent flow curve measurements by applying ascending and descending shear rate (stress) sweep. For a given material, the hysteresis loop will depend on test conditions such as the shear history prior to the start of the experiment, the maximum shear rate and the sweep rate [9]. In addition, hysteresis appears in the measured velocity profiles, with profiles at any given shear rate differing between the descending and ascending sweeps. The experimental and simulation studies reported that hysteresis is often also accompanied by the spatial heterogeneous flows such as shear banded or plug flows [10, 11]. This review summarizes the most important aspects covered in the rheological hysteresis in different fluid complex.

Hysteresis in thixotropic systems
Thixotropy defines as the continuous decrease of viscosity with time when flow is applied to a sample that has been previously at rest, and the subsequent recovery of viscosity when flow is discontinued. The excellent reviews of thixotropy are already available; namely, those of Mewis [9], Larson et al [12]. The observed hysteresis often demonstrate the existence and extent of the thixotropic behavior in complex fluids. The shape and area of the hysteresis loops have been used to evaluate the thixotropic degree i.e., larger area means larger thixotropic degree. However, due to the simultaneous change of two variables of shear rate and time during the experiment, hysteresis in flow curves represents nonequilibrium behavior. The shapes of the hysteresis loop in the flow curve of the complex fluid are shown in Figure 1. In ordinary thixotropic fluids, stress in ascending sweep is higher compared to descending ones (fig 1a). Fig 1b illustrates a system where breakdown of the initial structure after starting up dominates the time evolution of the stress, resulting in a stress overshoot. In ascending sweep measurements, a reduction of stress can cause shear banding and heterogeneous shear rate distributions in the sample. When shear at relatively low shear rates induces structure formation the hysteresis loop can take a shape as the one in Fig. 1c [13]. Zhu et al. [14] observed flow hysteresis loop in Al_2O_3 colloidal gels, and suggested that the rates of agglomeration and breakdown of flocs which determined by the rate of collision of them lead to the time-dependent colloidal structure and thixotropy. In literature, the area of the hysteresis loop from flow curve ($A\sigma$) and velocity profiles (Av), defined as follows:

$$A_\sigma = \int_{\dot\gamma_{min}}^{\dot\gamma_{max}} \left| \Delta \left\langle \overline{\sigma} \right\rangle (\dot\gamma) \right| d(\log(\dot\gamma)) \qquad (1)$$

$$A_v = \int_{\dot\gamma_{min}}^{\dot\gamma_{max}} \int_0^1 \left| \Delta v(\dot\gamma, y) \right| dy\, d(\log(\dot\gamma)) \qquad (2)$$

Di. [11] demonstrated that the A_σ and A_v depend on the sweep time, δt. For thixotropic materials such as mayonnaise, laponite and carbon black suspensions exhibit a robustly reproducible bell-shape dependence hysteresis loop area on the sweep time δt. In simple yield stress fluids such as carbopol microgel, this time scale is very small, and thus, A_σ and A_v decrease monotonically as δt increases. Recently, Radhakrishnan et al. [15] showed that the fluidity models and the soft glassy rheology model can reproduce such hysteresis loops. According to the simulation results, different tendencies to form shear bands in simple and time-dependent yield stress fluids during the sweeps cause to two different form of dependence hysteresis loop on sweep time. Simple yield stress fluid exhibit the homogenous flow response during the descending sweep in shear rate, followed by shear banding triggered by stress overshoot in the ascending sweep. While in time-dependent yield stress fluids, shear banding formed during descending weeps. In particular, Puisto et al.[16] suggested that a coupling between hysteresis measured from the local velocity profiles and that measured from the global flow curve. They predicted a monotonic decrease of the hysteresis loop areas $A\sigma$ and Av with increasing sweep time δt, for inelastic fluids. However for viscoelastic materials they demonstrated more complicated dependences, in some cases resembling the bell-shaped plots. These experimental measurements and simulation results has been limited to the macroscopic measurements of a system and indicated that there is a characteristic time scale in different thixotropic fluids. Jamli et al. [17]determined a characteristic hysteresis time in attractive colloidal suspensions based on the hysteresis areas calculated at three different length scales: from particle-level local measurements of coordination number (microscale), to the appearance of density and velocity fluctuations (mesoscale), and up to the shear stress response to an imposed deformation (macroscale). At all length scales, the characteristic hysteresis time become shorted upon increasing the strength of the inter particle attraction, and also the maximum hysteresis area increases due to the formation of bonds, clusters and spanning networks between particles. Moreover, they suggested that suspension with stronger attractions exhibit larger sensitivity to the history of flow.

Hysteresis in different systems
System with thermal behavior showed rate dependent hysteresis due to the competition between the driving and the relaxation rates [18]. Nguyen et al. [19] reported hysteresis phenomenon in Al_2O_3-water and CuO water nanofluids beyond a critical temperature which the particle suspension properties seem to be drastically altered. This critical temperature has been found to be strongly dependent on both particle size and concentration. Demirkır et. al [20] found that the graphene-water nanofluids with relatively higher particle concentration and at higher temperatures exhibit more pronounced shear thinning behavior in descending sweep rather than ascending ones, and thus showed hysteresis.

Conclusion
We have reviewed the experimental and simulation studied on rheological hysteresis in complex fluids. Hysteresis phenomena as a rate and time dependent relaxation time can be described by a measurement of flow curve in ascending and descending stress (shear) rate sweep and the local velocity profiles measurements. In addition, hysteresis is often also accompanied by the spatial heterogeneous flows such as shear banded or plug flows.

References
[1] E. McMillen, J. Rheol., 3, 179, (1932).
[2] J. Labanda and J. Llorens, Rheol. Acta 45, 305 (2006).
[3] M. Fourmentin, G. Ovarlez, P. Faure, U. Peter, D. Lesueur, D. Daviller and P. Coussot, Rheol. Acta. 54, 647 656. (2015).
[4] R. Mendes, G. Vinay, G. Ovarlez and P. Coussot, J. NonNewtonian Fluid Mech.,. 220, 77 86. (2015).
[5] J. Adams, S. Fielding, and P. Olmsted, J. Non-Newton. Fluid Mech. 151, 101 (2008).
[6] P. Sollich, Phys. Rev. E 58, 738 (1998).
[7] J. J. Stickel, J. S. Knutsen, and M. W. Liberatore, J. Rheol. 57, 1569 (2013).
[8] A. Visintin, Rend. Semin. Mat. Univ. Padova 77, 213 (1987).
[9] J. Mewis and N. J. Wagner, Adv. Colloid Interface Sci., 2009, 147 148, 214 227.
[10] T. Divoux, D. Tamarii, C. Barentin and S. Manneville, Phys.Rev. Lett., 104, 208301(2010).
[11] T. Divoux, V. Grenard and S. Manneville, Phys. Rev. Lett.,2013, 110, 018304.
[12] R .G Larson, Y Wei, Journal of Rheology 63, 477 (2019).
[13] Kanai H, Amari T. Rheol Acta;34:303 (1995).
[14] Zhu, C., and J. E. Smay, J. Rheol. 55, 655–672 (2011).
[15] Radhakrishnan, R., T. Divoux, S. Manneville, and S. M. Fielding, Soft Matter 13, 1834–1852 (2017).
[16] Puisto, A., M. Mohtaschemi, M. J. Alava, and X. Illa, ", Phys. Rev. E 91, 042314 (2015).
[17] S jamali, R.C Armstrong, G.H McKinely, Physical Rev Lett. 123, 248003 (2019).
[18] G. Bertotti and I. Mayergoyz, The Science of hysteresis (Academic Press, New York, 2006).
[19] C.T. Nguyen, F. Desgranges, N. Galanis, G. Roy, T. Maré, S. Boucher, H. Angue Mintsa, Int. J. Therm. Sci. 47 103–111 (2008).
[20] Demirkır, H Ertürk, International Journal of Heat and Mass Transfer 149,119113.(2020)

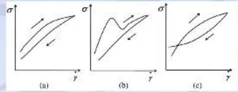

Fig 1: Different shapes of hysteresis loops [9]

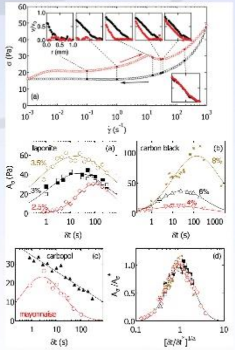

Fig 2: Flow curve of a 2.5% wt. laponite suspension: descending sweep in 90 logarithmically spaced steps of duration δt = 15.5 s (black symbols), ascending sweep (red symbols). Insets: Velocity profiles during the descending (black), ascending (red) sweeps. Area of the hysteresis loop as a function of δt for (a) laponite suspensions, (b) carbon black gels (c)a carbopol microgel and a commercial mayonnaise (d) Normalized data [11]

Article code:

2nd International Conference on Rheology
14 & 15 December 2021, Tehran, Iran

Synthesis of rough particles and investigation its rheological behavior in a Newtonian matrix

Sheyda Khazaee[1], Fatemeh Goharpey[1]
1. Polymer and Color Engineering Department, Amirkabir University of Technology, Tehran, Iran

Abstract
A reason for the recent surge of interest in studying the rheological behavior of rough particles in suspensions is that the proving of the relationship between shear thickening behavior and frictional contact among the particles due to the asperities on the surface of the particles. Surface roughness has emerged as an essential design parameter for the thickening response. For instance, one can increase the solid loading and delay undesired shear thickening by introducing a small number of particles displaying lower friction into the system be of interest for slurry processing, for example. Conversely, increasing surface roughness enables a significant reduction of the volume fraction, while retaining extreme thickening but having lower viscosities in the unthickened region of the flow curve, which could be of interest in fluid materials for vibration or impact absorption. In this project, we try to use different volume fraction of rough particles in dilute till concentrated suspension to calculate the critical shear stress in each volume fraction. And so in practical with tuning the roughness of the surface and its volume fraction, one can reach to the most proper behavior of the suspension.

Keywords: Rough particles, colloidal suspension, frictional contact, rheology, shear thickening behavior

Introduction

Concentrated suspensions (volume fraction $\varphi \geq 0.40$) have an essential contribution in a broad range of engineering applications and physical aspects, from past to present.

Hsiao et al.[1] investigated the effect of roughness on the suspension shear thickening and dilatancy behavior by using PMMA particles with varying surface roughness length scales up to 10% of the particle radius. They use AFM equipment to characterized surface asperities. They observed that in smooth particle suspension, the critical shear stress is independent of φ and only in very large amounts of volume fraction and also shear rate the system shows a weak shear thickening

In this article, at first, we present a new method for synthesis of raspberry-like poly(styrene-co-acrylic acid)/silica nanocomposite, then prepare dilute-concentrated suspensions of synthesized nanoparticles to investigate the effect of roughness on the rheology of the suspensions compared to a smooth one.

Experimental

Synthesis of smooth PS nanoparticles

PS nanoparticles were synthesized by soap-free emulsion polymerization [3] For this goal, 15gr styrene monomer with 100gr deionized water was mixed in a 250cc flask equipped with reflux system for 30min. Then 1gr acrylic acid was added to the reactor, and the reaction was mixed for 30min. At last the reactor was put in a 70°C-oil bath and KPS solution (0.1gr KPS in 15gr water), was added to the reaction medium, simultaneously. The reaction had been completed in 24h, and finally, poly(styrene-co-acrylic acid) latex was directly achieved.

Sol-gel process

Coating the functionalized PS particles with silica

The sol-gel process was used for coating the poly(styrene-co-acrylic acid) spherical nanoparticles with silica. 3cc TEOS, 40cc EtOH and 5gr PS latex were dispersed with a stirrer, and then 7cc ammonia was added to the system to activate the hydrolysis reaction of TEOS. The hydrolysis-condensation reaction had been completed in 50°C for 24h, and after centrifuge the raspberry-like PS/SiO_2 nanoparticles were obtained.

Results and discussion

FE-SEM and TEM images of synthesized raspberry-like silica nanoparticles with PS cores are shown in fig.1 with a average diameter about 500 nm.

Flow curve

In fig2 as can be seen, in all samples in the volume fraction of about φ = 20%, almost quasi-Newton behavior can be seen. Only in the range of 10^{-3} < Pe <10^{-1}, due to some weak structures in the system, some discrepancies are observed in the diagrams. It is noteworthy that this amount of deflection increased in the quite rough sample, and also the flow curve shows a plateau at higher Pe. This behavior can be attributed to the presence of surface roughness resulting in more frictional contacts and more particles colliding with each other. On the other hand, in the volume fraction of φ = 34% in all samples, we see shear thinning in almost the entire range of Pe. Here it can be said that increasing the percentage of rough particles has somewhat increased the viscosity of the system. In fact, in this percentage combination, with an increasing the percentage of rough particles in the system, the resulting structures become more robust, and this causes that by increasing the shear rate on the suspension, the structures are broken, and the shear thinning is somehow occur stronger in the system. In other words, in this case, it can be said that the hydrodynamic forces overcome the Brownian forces as well as the existing structures, leading to the arrangement of particle [4]. On the other hand, fragile shear thickening behavior can be observed in 8/2 and quite rough samples. Therefore, it can be said that the presence of a high percentage of roughness in the system, leads to an increase in frictional contacts and thus increase energy loss in the system and consequently increase the viscosity in the system [5][6]. As can be seen, the completely rough sample has a higher intensity of shear thickening, and its viscosity increases at lower values of Pe than the 8/2 sample. However, this behavior is fragile in both samples. In the volume fraction of φ = 49% in all samples, at low Pe numbers, shear thinning behavior occurs without any constant viscosity at a low shear rate. However, with increasing the roughness percentage, from the sample 5/5-0.49 and above, the shear thickening behavior is seen. This behavior becomes more visible and intensified by increasing the percentage of rough particles. In fact, as the percentage of roughness increases, the hydroclusters created by the particles, as a result of their solid-solid frictional contacts and the roughness of the surface particle, locking together and loss more of the shear stress in the system. It moves and thus further increases the viscosity of the system [7].

Although the shear thickening behavior also had be seen in samples containing a higher percentage of smooth particles, such as sample 5/5, this behavior can be more attributed to hydrodynamic forces in the system.

The morphology of hard spherical suspensions in this area is in the form of hydrocluster. In this way, the fluid between the two particles is compressed due to the increase in hydrodynamic pressure. In this case, the lubricating forces are most significant and have brought the particles closer together. In other words, they prevent the particles to moving away from each other, and the paths of the particle move closer to each other, thus creating a series of short gaps in the particles' density, which is called the hydrocluster. The resulting hydrocarbons have more stress and lead to energy loss or increased viscosity in the system. Therefore, in hard spheres, the formation of hydroclusters leads to shear thickening behavior without thixotropy and significant residuals[8][9], but here it is observed that with increasing roughness percentage, in combination with the same percentage of particles, the shear thickening behavior becomes more intense and occurs in smaller amounts of Pe. Therefore, it can be concluded that surface roughness has also been effective in intensifying this behavior in addition to the effect of lubricating hydrodynamic forces [3][10].

References

[1]L. C. Hsiao, S. Jamali, E. Glynos, P. F. Green, R. G. Larson, and M. J. Solomon, "Rheological State Diagrams for Rough Colloids in Shear Flow," Phys. Rev. Lett., vol. 119, no. 15, pp. 1–6, 2017, doi: 10.1103/PhysRevLett.119.158001.
[2]M. I. Smith, R. Besseling, M. E. Cates, and V. Bertola, "Dilatancy in the flow and fracture of stretched colloidal suspensions," Nat. Commun., vol. 1, no. 9, 2010, doi: 10.1038/ncomms1119.
[3]F. Pinto and M. Meo, "Design and Manufacturing of a Novel Shear Thickening Fluid Composite (STFC) with Enhanced out-of-Plane Properties and Damage Suppression," Appl. Compos. Mater., vol. 24, no. 3, pp. 643–660, 2017, doi: 10.1007/s10443-016-9532-1.
[4]T. Jiang and C. F. Zukoski, "Role of particle size and polymer length in Rheology of colloid-polymer composites," Macromolecules, vol. 45, no. 24, pp. 9791–9803, 2012, doi: 10.1021/ma301184t.
[5]F. Tapia, O. Pouliquen, and E. Guazzelli, "Influence of surface roughness on the rheology of immersed and dry frictional spheres," Phys. Rev. Fluids, vol. 4, no. 10, p. 104302, 2019, doi: 10.1103/PhysRevFluids.4.104302.
[6]I. R. Peters, S. Majumdar, and H. M. Jaeger, "Direct observation of dynamic shear jamming in dense suspensions," Nature, vol. 532, no. 7598, pp. 214–217, 2016, doi: 10.1038/nature17167.
[7]C. P. Hsu, S. N. Ramakrishna, M. Zanini, N. D. Spencer, and L. Isa, "Roughness-dependent tribology effects on discontinuous shear thickening," Proc. Natl. Acad. Sci. U. S. A., vol. 115, no. 20, pp. 5117–5122, 2018, doi: 10.1073/pnas.1801066115.
[8]B. J. Maranzano and N. J. Wagner, "The effects of interparticle interactions and particle size on reversible shear thickening: Hard-sphere colloidal dispersions," J. Rheol. (N. Y. N. Y)., vol. 45, no. 5, pp. 1205–1222, 2001, doi: 10.1122/1.1392295.
[9]R. V. More and A. M. Ardekani, "Effect of roughness on the rheology of concentrated non-Brownian suspensions: A numerical study," J. Rheol. (N. Y. N. Y)., vol. 64, no. 1, pp. 67–80, 2020, doi: 10.1122/1.5097794.
[10]C. Hoyle, S. Dai, R. Tanner, and A. Jabbarzadeh, "Effect of particle roughness on the rheology of suspensions of hollow glass microsphere particles," J. Nonnewton. Fluid Mech., vol. 276, no. November 2019, p. 104235, 2020, doi: 10.1016/j.jnnfm.2020.104235.

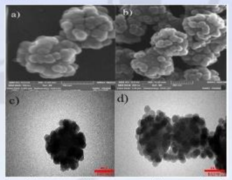

Fig. 1. a, b) FE-SEM c, d) TEM images of images of synthesized nanoparticles. The scale bar is equal to 200 nm in all nanographs.

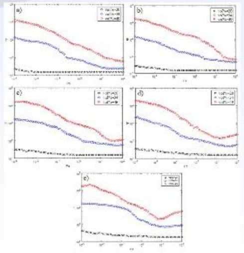

Fig. 2. Relative viscosity curve as a function of Peclet number for samples a) smooth, b) 80/20, c) 50/50, d) 20/80. and e) rough.

Article code: A-10-325-1

2nd International Conference on Rheology

14 & 15 December 2021, Tehran, Iran

Similarities in electrical and rheological percolation of the nanocomposites comprising hybrid of nanoparticles

Mohammad Heydarnejad Moghadam*, Fatemeh Goharpey

Department of Polymer Engineering, Amirkabir University of Technology, Tehran, Iran;

Abstract

The evolution of electrical conductivity and melt state storage modulus by increment in the weight percentage of nanoparticles is described by the scaling law of the percolation theory. Consistent with the percolation theory, the phenomenon transport experiences a sudden jump-like transition at the critical weight percentage of the percolation threshold and increases by power-law near the percolation threshold via a critical exponent. Herein, it is shown that the charge and mechanical load transport experience a similar percolation behavior due to the identical trend for percolation threshold and critical exponent, when the utilized nanoparticles are electrically conductive and mechanically stiff. Also, it was indicated that the composites of hybrid particles are more complex and more efficient than the composite of the single-kind nanoparticle. Interestingly, stitching hybrid components can make particles' networks extremely structured; however, it can also increase the percolation threshold.

Keywords: Hybrid-Percolation theory-Electrical conductivity-Linear rheology-Critical exponent

Introduction

It is well known that the evolution trend of many phenomena such as electrical and thermal conductivity, Young's modulus, viscosity, storage modulus in melt state by the fraction of particles can be described by the percolation theory.[1] Percolation theory claims an exponential increment of phenomenon Θ by particle fraction of ϕ after a critical fraction of ϕ_c, percolation threshold, via an exponent t, critical exponent (equation 1).

$$\Theta \sim (\phi - \phi_c)^t \quad (1)$$

Both ϕ_c and t are under the impression of the microstructure of particles, and improvement in dispersion state leads to a decrement in ϕ_c, and exponent t is an indicator of the networks' dimensionality of particles [1]. Utilizing multi-walled carbon nanotube (MWCNT) and/or graphene for the fabrication of polymer nanocomposite makes the employment of percolation theory for the investigation of the contributor networks in electrical and rheological percolation feasible as a result of the conductive and stiff nature of these particles [2].

In this study, the electrical and rheological percolation of the polymer nanocomposites comprising MWCNT, graphene, and they physically mixed and chemically stitched hybrid of them are studied in a comprehensive insight of particles' microstructure is achieved.

Experimental Section

The styrene-b-(ethylene-co-butylene)-b-styrene (grade G-1652 Kraton) is used as the polymeric matrix in this study, and the nanocomposites containing octadecyl amine (ODA) modified MWCNT (NC7000 Nanocyl) and graphene (N002 PDR angstron) and their physically mixed hybrids are obtained by the solution casting method. Furthermore, the chemically stitched hybrid is obtained by stitching MWCNTs' ends to graphenes' edges via ethylene diamine through a nucleophilic substitution reaction. Nanocomposites samples nomenclature is presented in table 1.

The AC conductivity measurements are done by an Autolab PGSTAT302N apparatus, and the nanocomposites' rheological behavior is tested by an Anton Paar Rheometer MCR 302. The values of the real part of AC conductivity and shear modulus at the lowest frequency (1 Hz and 0.007 Hz for ac conductivity and storage modulus, respectively) are used for percolation behavior studies.

Results and Discussion

Figure 1 shows the FE-SEM images of the physically incorporated and chemically stitched hybrids of MWCNT and graphene and their corresponding nanocomposites. As is evident, in the case of In the physically-mixed hybrid, Graphenes are distinct from MWCNTs' bulk, and it is manifest that there is no junction amongst them (Fig.1a). However, in the case of chemically stitched hybrid, a unified structure of MWCNT@graphene, where MWCNTs accompany the standing graphene, is visible(Fig.1b). The unified and hierarchical structure of nanoparticles in chemically stitched hybrid causes an excellent dispersion in their nanocomposite, so in all parts of the image, MWCNTs and graphenes are present simultaneously, while in the nanocomposite of physically mixed nanoparticles, MWCNTs are accumulated in the central part of the image.

In continuation, the electrical and rheological percolation is investigated. Fig.2 a and b demonstrate the values of the real part of electrical conductivity and shear modulus at the lowest frequency of experiment versus weight fraction of the graphitic content of nanoparticles. The values of percolation threshold and critical exponent also are presented in figures 2. c and d, respectively. First of all, the trend for percolation threshold is identical in s' and G'; however, the values of the rheological percolation threshold are greater than the electrical percolation threshold, which is related to the fact that construction of a conductive path needs particles with about one-nanometer distance for electron tunneling while rheologically load carrier path needs about 50 nanometers particles' distance, scaled with the gyration radius of polymer chains. Also, as is evident for both s' and G', the percolation threshold of the C-x is lower than the G-x, indicating a higher capability of MWCNTs for making conductive pathways. Adding a minor part of an inhomogeneous nanoparticle and fabrication of hybrid samples can significantly decline the percolation threshold, attributed to the improvement in dispersion state. Contrary to HC-x, the percolation threshold of CHC-x is greater than C-x, which originates from the fact that MWCNTs are attached to the graphene sheets, and they act as selective clusters, which hindered their random distribution.[3]

According to figures 2. c and d, the trend for the critical exponent in electrical and rheological percolation is entirely identical. Similar to the percolation threshold, values of critical exponent for rheological percolation are less than electrical percolation. This unusual outcome is related to the polystyrene microdomains of SEBS, which act as reinforcing material, contributing nanoparticles in establishing the load carrier network. So, the role of nanoparticles in creating the load carrier network weakens, and critical exponent decreases.

Another point that must be pointed here is the non-universal values (greater than 2.0) of electrical critical exponents. One of the reasons for this non-universality is the mechanism of charge transport on the molecular scale, which is quantum tunneling for nanocomposites of graphitic materials instead of the direct contact mechanism considered in the calculation of universal values based on percolation theory. Another reason for the values of critical exponent higher than universal values is the structured network of materials.[4] Hybrid samples are prone to create more structured networks than the composite of single-kind nanoparticles. The more structured network in hybrid samples is owing to the reduction in the inactive particles in the network. MWCNTs bridge among isolated graphene sheets and make them participate in the charge carrier network, and concurrently graphene sheets gather inactive and isolated MWCNTs in the conductive network. For the case of CHC-x, the conductive network is extremely structured, reflected from the huge decline in the inactive particles after stitching particles together.

Conclusion

Hybridization of inhomogeneous nanoparticles yields network structures with a high degree of dispersion and complexity, which makes them more efficient for reinforcement and charge conduction than the composite of single-kind nanoparticles.

References

[1] M. Sahimi and M. Sahimi, *Applications Of Percolation Theory*, vol. 242, no. 3 4. CRC Press, 1994.

[2] F. Du, R. C. Scogna, W. Zhou, S. Brand, J. E. Fischer, and K. I. Winey, "Nanotube Networks in Polymer Nanocomposites: Rheology and Electrical Conductivity," *Macromolecules*, vol. 37, no. 24, pp. 9048–9055, Nov. 2004.

[3] L. Yue, G. Pircheraghi, S. A. Monemian, and I. Manas-Zloczower, "Epoxy composites with carbon nanotubes and graphene nanoplatelets - Dispersion and synergy effects," *Carbon N. Y.*, vol. 78, pp. 268–278, 2014.

[4] M. Yoonessi and J. R. Gaier, "Highly Conductive Multifunctional Graphene Polycarbonate Nanocomposites," *ACS Nano*, vol. 4, no. 12, pp. 7211–7220, Dec. 2010.

Table 1. Nanocomposites samples nomenclature

Sample name	Fraction of MWCNT	Fraction of graphene	Type of hybrid's preparation
G-x	0	1	-
C-x	1	0	-
HG-x	1	3	Physically incorporated
HC-x	3	1	Physically incorporated
CHC-x	3	1	Chemically stitched

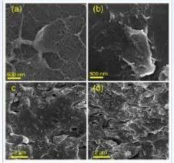

Fig.2. FE-SEM images of a) Physically incorporated hybrid of MWCNT and Graphene, b) Chemically stitched hybrid of MWCNT and Graphene, c) HC-5, and d) CHC-5.

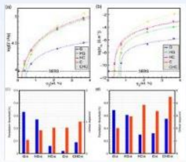

Fig.3. Rheological (a) and electrical (b) percolation behavior of diverse nanocomposites and their corresponding fitting parameters in rheological (c) and electrical (d) percolation theory.

2nd International Conference on Rheology
14 & 15 December 2021, Tehran, Iran

Rheology and Morphology of Dynamically Vulcanized Poly(lactic acid) / Polyurethane (PLA/PU) Blend in Presence of Nanoparticles

Salar Haghjoo,[1] Jafar Khademzadeh Yeganeh,*[1] and Ismaeil Ghasemi [2]
1. Department of Polymer Engineering, Qom University of Technology, Qom, Iran
2. Iran Polymer and Petrochemical Institute, Tehran, Iran

Abstract
The presented research reports preparation of tough PLA/PU blend using simultaneous peroxide (BIPB)-induced dynamic vulcanization and addition of hydrophobic spherical silica nanoparticles (NPs). NPs were localized mainly in the PU droplets and at the interface where a layer of particles was formed with a small amount dispersed in the PLA matrix. The incorporation of NPs or BIPB induced compatibilization, causing a drastic decline in the size of PU droplets in addition to improving the interfacial adhesion. The effect of BIPB and NPs on the microstructural properties of the sample was investigated through rheological evaluations

Keywords: Poly(lactic acid) - Polyurethane - Dynamical Vulcanizate - Nanocomposites.

Introduction

As a biodegradable polymer, poly(lactic acid) (PLA) has been benefited from various advantages such as excellent biocompatibility, ease of processability, high modulus and mechanical strength compared to the conventional polymers, bio-based nature, and excellent transparency which have introduced it as a promising alternative to petroleum-based polymers. However, PLA suffers from inherent brittleness, which has limited its widespread commercial applications. Blending with a rubbery polymer is the most convenient, economic, and efficient method to toughen the PLA. The object of this study is to prepare toughened PLA/PU blend by simultaneous dynamic vulcanization and NPs addition.

Experimental

PLA (2003D, D-isomer content of about 4%) was supplied from NatureWorks®, USA. PU (Desmopan 385S) was supplied from Bayer. Aerosil R805, with a hydrophobic surface supplied by Degussa Corp. Bis(t-butylperoxy isopropyl)benzene (BIPB) was supplied by Rhein Chemie.

The melt blending approach was adopted to obtain the specimens using a lab internal mixer (Brabender Plasticator, Germany) at 200 °C and a rotor speed of 80 rpm for 12 min.

Results and Discussion

SEM

Scanning electron microscopy (SEM) was performed to investigate the morphology of the samples (Figure 1,2,3). As anticipated, PLA/PU (75/25) sample showed a droplet-matrix morphology in which, PLA was the matrix. The blend exhibited a well-distinguished interface and large PU droplets and the cavities caused by interfacial debonding were visible (Figure 1). This indicates an incompatible polymer blend leading to weak interfacial adhesion between the phases. After incorporating NPs or BIPB the size of PU droplets was greatly decreased and the interfacial adhesion improved (Figure 2,3).

TEM

To explore the exact location of nanoparticles, TEM analysis was employed. NPs are mainly localized in the PU droplets and at the interface (Figure 4).

Rheological Behavior

Figure 5 shows storage modulus G'as a function of frequency for PLA/PU blend with and without nanoparticles. The neat PLA/PU blend exhibited terminal behavior with the scaling properties of approximately $G' \propto \omega^2$ which exhibited a shoulder at the storage modulus which can be attributed to the contribution of the interface to the blend elasticity and the shape relaxation of the PU droplets in the PLA matrix [1]. It can be seen that the addition of 2 wt% nanoparticles sharply enhanced the low-frequency modulus and the slope of the G' curve considerably decreased (nonterminal behavior). At low NP contents and low frequencies, the sample behavior is controlled by the particle-induced changes in polymer chain dynamics. Thus, the large-scale polymer relaxations in the nanocomposites will be efficiently restrained at the presence of the NPs which prevented the viscous flow of molecular chains and also enhanced the elastic response. This indicates a favorable interaction between nanoparticles and PLA matrix. Furthermore, in polymer blends, the elasticity of the interface contributed to the overall elasticity at low frequencies. According to SEM images, the decrease of droplet size and improved interface upon NPs introduction enhanced the modulus. However, at nanosilica loadings of 5 wt% and higher, the low-frequency storage modulus was considerably enhanced and became almost independent of frequency (a plateau is observed). This is indicative of solid-like viscoelastic behavior implying that the nanosilica has formed a percolated network which spanned the sample and restrained the long-range motion of polymer chains. Besides, the compatibilization effect of nanoparticles induced high interfacial area which increased dynamic moduli at low frequencies. At high frequencies, storage modulus was also enhanced suggesting short-range dynamics of polymer chains is restricted especially in the entanglement length scales [2]. Figure shows the dynamic moduli of the nanocomposite in presence of BIPB. Through comparison of Figure 5 and 6, it can be seen that adding BIPB enhanced the dynamic moduli. This indirectly confirms dynamic vulcanization in the samples.

Conclusion

In this study, we prepared toughened PLA/PU blend by simultaneous dynamic vulcanization and the
addition of nanoparticles. The incorporation of NPs and BIPB both induced compatibilization, subsequently the size of PU droplets was greatly decreased and the interfacial adhesion improved. On the other hand, simultaneous dynamic vulcanization and NPs addition exhibited a synergistic effect on the compatibilization of PU and PLA phases. The effect of BIPB and NPs on the microstructural properties of the samples was investigated through rheological evaluations.

References

[1] J. Khademzadeh Yeganeh, F. Goharpey, and R. Foudazi, "Rheology and morphology of dynamically asymmetric LCST blends: polystyrene/poly (vinyl methyl ether)," *Macromolecules*, vol. 43, no. 20, pp. 8670-8685, 2010.
[2] S. Moradi and J. K. Yeganeh, "Highly toughened poly (lactic acid)(PLA) prepared through melt blending with ethylene-co-vinyl acetate (EVA) copolymer and simultaneous addition of hydrophilic silica nanoparticles and block copolymer compatibilizer," *Polymer Testing*, vol. 91, p. 106735, 2020.

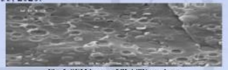

Fig .1 SEM image of PLA/PU specimen

Fig .2 SEM image of PLA/PU/BIPB specimen

Fig .3 SEM image of PLA/PU/R2 specimen

Fig .4 TEM image of PLA/PU/R5 specimen

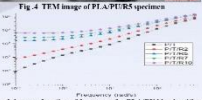

Fig .5 storage modulus as a function of frequency for PLA/PU blends with and without nanoparticles

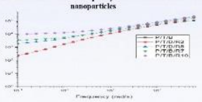

Fig .6 storage modulus as a function of frequency for dynamically vulcanized PLA/PU blends with and without nanoparticles

2nd International Conference on Rheology
14 & 15 December 2021, Tehran, Iran

Evaluation of Printability of Carbon-based Nanocomposite Samples using Rheological Study

A. Eftekhari[1], F. Goharpey[1*], M. Mehranpour[2]
1.Department of Polymer Engineering, Amirkabir University of Technology, Tehran, Iran
2. Islamic Azad University, Science and Research Branch, Tehran, Iran

Abstract The purpose of this project is to investigate of the rheological properties for 3D printing of ABS-based systems and carbon nanoparticles including Nano carbon black and carbon nanotubes. The current evaluated hybrid system is more competitive compared to its CNT-based counterparts in terms of Economical aspects. FESEM images also present an acceptable dispersion of nanoparticles with desired rheological properties. The results extracted from the frequency sweep test indicate the development of a three-dimensional physical network of nanoparticles in the printed nanocomposites due to the extended frequency-independent (non-terminal) behavior for the storage modulus. It should be noted that these hybrid samples affect the complex viscosity trend less than that of CNT-based systems, which leads to better printability and prevent nozzle blockage. Also, considering the importance of elongation viscosity in the 3D printing process, the rheological behavior under the extensional field was investigated.

Introduction

ABS, with easy processability, toughness, good dimensional stability, and also optimal chemical resistance, has been considered. Due to its good flexibility; ABS has a wide range of applications, including automotive, home appliances, and electronic parts[1]. FDM technology in 3D printing makes it possible to create electronic kits and sensors by adding small amounts of carbon nanoparticles. Since this material is a complex random copolymer made up of SAN copolymer and PB rubber phase (island-sea structure), it is important to study the rheology of this system. melt flow study is a key index in preparation of samples containing nanoparticles, so that flow obstruction in the nozzle causes poor printing and surface roughness[2]. That is why studying rheology is of increasingly importance. Rheological evaluation provides the ability to optimize nanoparticles dispersion and viscosity behavior. In this study, the optimal print was evaluated using shear and extensional mode tests.

Experimental Section

Materials. Acrylonitrile-butadiene-styrene (ABS) was supplied by Tabriz Petrochemical Co, Iran (SD150), The carbon nanotubes used in This Study were commercially available as multiwall carbon nanotubes (MWCNTs), NC7000, from Nanocyl Inc., Belgium. The multiwall had a carbon purity of 90%, average outer diameter of 9.5 nm, length up to 1.5 μm, and surface area of 250-300 $m^2 g^{-1}$. Commercially available super conductive carbon blacks, Ketjen Black EC 300J were supplied by Lion Specialty Chemicals Co., Japan. Carbon black had a DBP absorption 360 ($cm^3/100g$) and BET surface area 800 $m^2 g^{-1}$. Dichloromethane (DCM) and chloroform were Purchased from dr.Mojallali Inc., Iran.

Preparation of Nanocomposites.

Solution method was applied to prepare the masterbatch of nanocomposites. Then the masterbatch was added to neat ABS in Twin Screw Extruder Brabender DSE20 (L/D=40) at 230° and screw speed of 150 rpm and the nanocomposites achieves the desired percentages. The Production of filaments with 1.75±0.05 mm dimeter was done by single screw extruder (Noztek).

Results & Discussion

Fig.1 shows the FESEM images of fracture surfaces of samples. The droplet-matrix morphology is clearly visible in neat sample. In Figure1.b, CNT nanoparticles like worms and in Figure1.c, CB nanoparticles are visible as aggregate, which is inevitable due to the small size of CB nanoparticles. Finally, CB aggregate and individual CNT nanoparticles can be seen in figure 1.d. In the frequency sweep test (Fig.2) according to the FESEM image, a pure sample showed non-terminal behavior. In a sample containing 1.5% CB, a slight change in the storage modulus is observed compared to the 1.5% CNT sample, which is attributed to the unfavorable dispersion of nanoparticles. In the 1.5% CNT sample, the storage modulus distanced itself from the loss modulus, indicating solid like behavior. It should be noted that the unfavorable dispersion in the CB1.5 sample caused a rough surface in the printed sample, and also the printing of the CNT1.5 sample was not successful due to the nozzle blockage. The reason is the highly elastic behavior and high viscosity of the sample. Hybrid samples were prepared by replacing the amount of CB nanoparticles with CNT. By increasing the percentage of CNT nanoparticles in these samples, the storage modulus is significantly affected. However, this increase in the storage modulus of the hyb1: 1 sample is about one-third of the CNT1.5 sample, which is an advantage for 3D printing applications. Then, due to the existence of the extensional flow field in the convergent part of the nozzle and a more detailed study of the printing process, the elongation viscosity behavior was investigated[3]. The results of this test show the strain hardening behavior for all samples, which indicates the resistance of the elastic behavior of the material to extension. The maximum limit of strain hardening behavior is observed in the CNT1.5 sample, which is one of the main reasons for the interruption of printing process in this sample. On the other hand, with increasing printing speed, this behavior occurs quicker and with more slope, which leads to undesirable printing and rough surface (figure 3).

Conclusion

Rheology provides a powerful tool to evaluate the nanoparticle dispersion state through a polymeric matrix. In this study, in order to evaluate the three-dimensional network of nanoparticles, a frequency sweep test was performed. No significant amount of storage modulus and time-independent behavior was observed. Also, the results of elongation viscosity test in this regard showed the strain hardening behavior; which was the maximum value in CNT1.5 sample and proves the non-printability of this sample.

The hyb1:1 sample has a lower print modulus and also a lower viscosity than the CNT1.5 sample. This hybrid sample has desirable properties and is cost effective.

References

[1] M. G. Wyzgoski, "Acrylonitrile-Butadiene-Styrene.," vol. 1, pp. 241–243, 1974.
[2] K. Gnanasekaran *et al.*, "3D printing of CNT- and graphene-based conductive polymer nanocomposites by fused deposition modeling," *Appl. Mater. Today*, vol. 9, pp. 21–28, 2017, doi: 10.1016/j.apmt.2017.04.003
[3] M. E. Mackay, "The importance of rheological behavior in the additive manufacturing technique material extrusion," *J. Rheol. (N. Y. N. Y).*, vol. 62, no. 6, pp. 1549–1561, 2018, doi: 10.1122/1.5037687.

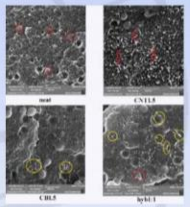

Figure1. FESEM images with 500nm magnification a) neat sample b) sample containing 1.5% CNT c) sample 1.5% CB d) sample contacting 0.75% CB and 0.75% CNT

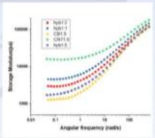

Figure2. variation of a storage modulus of nanocomposites with 1.5% nanoparticles versus frequency

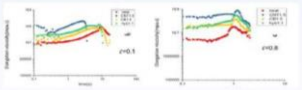

Figure3. elongation viscosity versus time at two different extension rate

*goharpey@aut.ac.ir

Article code: A-10-337-1

2nd International Conference on Rheology
14 & 15 December 2021, Tehran, Iran

Dynamic Mechanical and Rheological Properties of Liquid Crystal Elastomers Prepared *via* Thiol Acrylate Michael Addition Reaction

Parmida Harirchi[1], Mahshid Fallah-Darrehchi[1] and Payam Zahedi[1*]
[1]Nano-Biopolymers Research Laboratory, School of Chemical Engineering, College of Engineering, University of Tehran, Tehran, Iran

Abstract Liquid crystal elastomers (LCE) as newly developed stimuli-responsive materials with combined properties of orienntational order of liquid crystals and elasticity of amorphous elastomers leading to reversible shape change (RSC) property which motivating factor simulate efficient system for artificial muscles. Moreover, fiber spinning of LCEs is problematic issue due to their low M_w and necessity of crosslinking reaction. The main reason for appearance of RSC property along with actuation-active properties, two stages of crosslinking is required. In this line, we provided LCE thin films by thiol-acrylate Michael addition (TAMA) reaction to evaluate fiber production feasibility. Therefore viscoelastic response of LCE samples after first stage of crosslinking and dynamic-mechanical behavior after second stage of crosslinking was evaluated. The results showed in LCE_1 (PETMP:EDDET=50:50) specific structure has formed during 60 minutes and strain failure and fixity reached highest amount indicating that this sample could be suitable candidate for production of LCE-based fibers.

Introduction

Liquid crystal elastomers (LCEs) are the new class of responsive polymeric materials, possessing entropic elasticity combined with liquid crystal (LC) order. LCEs are responsive to various actuators including: mechanical stress, temperature variation, magnetic or electrical fields. One of the main reason of conspicuous physical properties appearance related to presence of mesogenic units into the polymeric chains as functional group or through the polymer backbone in the exposure of external stimuli. In fact, mesogens are the solid segments enabling polymeric chain parallel to a direction in which majority of LC units tend to reorient called director vector leading macroscopic shape changes at transition temperature (nematic ↔isotropic, Tni) [1]. LCEs possess reversible shape change (RSC) feature without mechanical bias or specific environment. due to two-step crosslinking process. in the first step lightly cross-linked network during the polymerization and in the second, photo-initiated crosslinking process along with induced molecular patterning by utilization of mechanical loading or magnetic fields orientation of LCEs' chains. As the suitable balance of crosslink density in both steps lead to appear RSC property of LCEs which is the base of mimicking the muscular tissue. fibrillary topology of muscle structure motivated the researchers to fabricate micro-scale fibrous LCE via melt-spinning, electrospinning, microfluidic devices and direct ink writing) [2, 3]. In all the above methods, lightly cross-linked LCE is injected through the patterned nozzle followed by photo-initiated crosslinking reaction. Therefore, the rheological properties of LCE should be determined to avoid morphological and rheological instabilities. The aim of this project is to
synthesis of LCE by thiol acrylate Michael addition reaction accepted to click chemistry and possess high yields stereoselectivity, high rate, and room temperature cure system to evaluate their properties to evaluate rheological properties as contractile shape memory fibrils to mimic muscular tissues [4].

Experimental

In order to prepare LCE samples RM257 as mesogenic monomer was purchased from whlshire Technologies, USA. 2,2'-(Ethylenedioxy) diethanethiol (EDDET) and Pentaerythritoltetra (3-mercaptopropionate) (PETMP) as crosslinking agent was provided from Sigma-Aldrich Co., (pilsburg, The Netherland). Dipropylamine (DPA was supplied from Merck Co., Germany. All the other chemicals were analytical reagent grades and were used without further purification.

To synthesize the three LCE samples which were different in terms of EDDET: PETMP molar ratio, firstly weighted monomer into the toluene was heated at 80°C for 5 minutes. Afterwards, the stoichiometry amount of EDDET and PETMP was added to the monomer mixture according to the Table 1. Then diluted DPA in toluene was added to the container to accelerate TAMApolymerization procedure mounting 0.1 % mole of RM257.

Results & Discussion

A rheometer (Anton Paar, Physica MCR 300) was used for all rheology data cone and plate geometry. After adding the PETMP storage and loss moduli as a function of time were obtained under oscillation with a strain of 3% and the frequency or 2 Hz for 1 h. As expected (Fig. 1(a)) the G' curves for all three specimens is lower than the G" curves, indicating that no cross-links have not been formed in 60 minutes. By setting the aliphatic spacer next to the cross-linker, intensification (increase of slope) of the curves was observed, which indicates the special structure. Also, all samples had a structure and this structure disappears under shear and time. To evaluate RSP property of samples six samples (two samples from each one) subjected to 100% and 200% strain at the speed of 0.2 mm/s were used. The samples were irradiated with 265 wavelengths of UV light during the extension for 7 minutes. Then the fixity parameter illustrating the RSC feature, was calculated by Eqn. (1) given tin Tab.2.

$$Fixity\ (\%) = \frac{\varepsilon_{fixed}}{\varepsilon_{applied}} \times 100$$

Fixity amounts showed that all samples have RSC property and increase in strain led to increase in fixity amount which induced that higher extension reoriented mesogenic segments more efficiently. But the fixity amount for LCE_1 revealed that this sample could completely retain shape memory. For more precision the strain failure amounts were plotted vs PETMP extent. Fig. 1(b) showed that LCE_1 possessed the highest amount of strain failure and also the tanδ graph for LCE_1 confirmed that this failure has taken place at T_g. The samples at the Ɛ=100% were selected for DMA test (DMA-Triton, Model, Tritec 2000 DMA, England) with heating ramp of 3 °C/min ranging from -60 °C to 120 °C. It can be concluded from Fig 1 (c, d) that tanδ graph had two extremums points belonging to Tg and Tni. Also by increasing the PETMP extent, the crosslinking density was increased leading to obtain higher Tg and Tni.

Conclusion

Dynamic-mechanical data and rheological studies of LCE samples prepared by TAMA reaction polymerization after first and second crosslinking processes respectively, showed that by employing the PETMP:EDDET ratio of 50:50 gel formation in practical time interval and RSC property of LCE reached highest values fulfilling most significant features of an ideal artificial muscle.

References

[1] M. Barnes and R. Verduzco, "Direct shape programming of liquid crystal elastomers," *Soft Matter*, vol. 15, no. 5, pp. 870-879, 2019.
[2] M. Barnes, S. M. Sajadi, S. Parekh, M. M. Rahman, P. M. Ajayan, and R. Verduzco, "Reactive 3D printing of shape-programmable liquid crystal elastomer actuators," *ACS Applied Materials & Interfaces*, vol. 12, no. 25, pp. 28692-28699, 2020.
[3] Z. Wang, Z. Wang, Y. Zheng, Q. He, Y. Wang, and S. Cai, "Three-dimensional printing of functionally graded liquid crystal elastomer," *Science advances*, vol. 6, no. 39, p. eabc0034, 2020.
[4] D. P. Nair *et al.*, "The thiol-Michael addition click reaction: a powerful and widely used tool in materials chemistry," *Chemistry of Materials*, vol. 26, no. 1, pp. 724-744, 2014.

Table 1. The amounts of mesogenic monomer and PETMP: EDDET for preparation of LCE samples

Sample	RM 257	PETMP: EDDET
LCE_1	0.5	50:50
LCE_2	0.5	75:25
LCE_3	0.5	100:0

Table 2. Fixity amounts for LCE samples at Ɛ=100% and Ɛ=200%

Sample	fixity @ ε=100%	fixity @ ε=200%
LCE_1	91.3	96.5
LCE_2	79.3	88.5
LCE_3	74.0	83.70

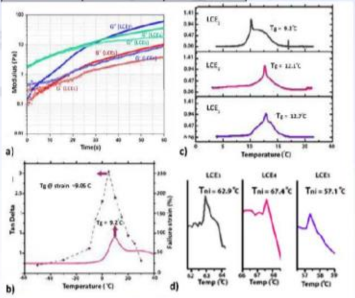

Fig 1. a) Storage and loss moduli of LCE samples, b) strain failure vs temperature for LCE_1, c) indication of Tg and (d) Tni for LCE samples by DMTA test

*phdzahedi@ut.ac.ir

A-10-339-1

2nd International Conference on Rheology
14 & 15 December 2021, Tehran, Iran

A new thermoresponsive nano-hydrogel based on cellulose nano-crystal

Farhad Jamali[1], Fatemeh Goharpey[1], Seyed Mohammad Mahdi Mortazavi[2]

1. Department of Polymer & Color Engineering, Amirkabir University of Technology, Tehran, Iran
2. Engineering Department, Catalyst Group, Iran Polymer and Petrochemical Institute, Tehran, Iran

Abstract

This study investigates a new combination of polycaprolactone-polyethylene glycol-polycaprolactone (PCL-PEG-PCL) micelles in presence of cellulose nano crystal (CNC). A specific molecular weight with no thermogelling behavior was synthesized with ring-opening polymerization (ROP) catalyzed by $Sn(Oct)_2$. 30% wt. triblock solutions prepared to investigate sol-gel behaviors in water media. Different concentrations of CNC that hydrolyzed from cotton were used. In low concentrations of CNC there was no gelling state, but with increasing CNC concentration presence of a gel was detected by RMS measurements. G' and G" crossover in the low and high frequencies indicates a new network. A new gelling state emerged by increasing CNC concentration up to 3% in which system gels in body temperature range. The thermogelling state was proved by the inverted-tube test in 30 seconds.

Keywords: PCL-PEG-PCL - Hydrogel- Thermogelling – Cellulose nano-crystal – Thermoresponsive

Introduction

Block copolymers are a class of copolymers that monomers are organized in repeated units. Each discrete portion in the chain is referred as "blocks". The arrangement of an A-B or A-B-A type of hydrophobic and hydrophilic blocks makes copolymers amphiphilic.[2] Amphiphilic block copolymers have been widely employed for different technological applications. Some of these copolymers indicate a thermogelling behavior, undergoing a sol-gel transition by changing temperature. This feature is an important fact to design thermogelling systems. Dehydration of the polymeric chain at the micellar state triggers the thermogelling as a result of increasing the temperature. CNCs are a class of nanomaterials with rod-like shape owing to their physical/mechanical properties and high aspect ratio, which are generally obtained through acid hydrolysis of cellulose. They can form gels only at high concentrations or with additives such as salt,[4] acids, polymers or through surface functionalization with cross-linkable groups. The combination of nanomaterials such as CNC with triblock hydrogels will result in improving rheological properties and adverting new features.

Experimental/Theoretical

ε-caprolactone, stannous octoate ($Sn(Oct)_2$), poly (ethylene glycol) (PEG) 2000 gr/mol, dichloromethane were purchased from Aldrich. Anhydrous toluene and diethyl ether were purchased from Dr. Mojallali Industrial Chemical Complex Co. The PCL-PEG-PCL triblock copolymers prepared by ring-opening polymerization (ROP) of caprolactone in the presence of PEG. Sn $(Oct)_2$ was used as a catalyst. For example, to synthesize the PCL-PEG-PCL (800-2000-800) triblock copolymer, the procedure was choose as reported by Bae et al.[1]
Cotton was used as a cellulose source for obtaining CNC by hydrolyzing with sulphuric acid. 5 gr cotton hydrolyzed in 64% wt. sulphuric acid in 45 °C for 45 minutes. The hydrolyzed cotton was quenched in cold water and diluted with excess deionized water to stop the reaction. Then centrifuged many times until the solution became stable. The solution was poured into a dialysis bag and the water constantly changed until it reached a neutral pH. In the next step, the resulting solution is freeze-dried to obtain solid CNCs. The nanocomposites were prepared in two steps: In the first step different concentrations of CNCs dispersed in deionized water with the help of an ultrasonic homogenizer (400 w, 20 KHz). In the second step copolymers were dissolved in the CNC colloids to form nanocomposites.

Results and Discussion

The structures of the PCL-PEG-PCL block copolymers were confirmed using ^{1}H-NMR analysis. According to Figure 1, the two characteristic peaks at 4.07 and 4.23 ppm which related to PCL block formation are resolved in the NMR spectrum. The average molecular weight of PCL block segments can be calculated by dividing the area of corresponding peak at 4.23 to the area of the peak located at 4.07.[2] By preparing a sample of 30% by weight of polymer and two different 1% and 3% by weight of CNC, it was observed that at 25 °C, 1% by weight sample of CNC, called TC1, flows during the tube-inverted test time (30 seconds) and does not show drastic behavior change with temperature and does not gel in the body temperature range. 3% by weight sample of CNC, called TC3, according to figure 2 flows at 25 °C during the test period, but unlike TC1, it does not flow in the body temperature range during the test period and shows a gel state. Rheological tests were conducted using an Anton Paar MCR-302 rheometer with cone and plate geometry with a 25 mm diameter, a cone angle of about 1 °. The dynamic moduli versus angular frequency is illustrated in Figure 3 to observe 3D structures and their change by changing the CNC percentage. For TC1 presence of a three-dimensional structure at low frequencies with the passage of G' from G " as well as the deviation from terminal behavior of G' at low frequencies can be detected.[3] But for TC3 a G' & G" cross-over in the high frequencies was observed. In the low frequencies both G' and G" show non-terminal behaviors that indicates the 3D network formation in the high percentage of CNC.

Conclusion

A novel combination of triblock micelles based on PCL-PEG-PCL and cellulose nano crystal was studied as a candidate for thermo-responsive hydrogels. Inverted-tube test shows that TC1 is sol in the temperature range of 25-37 °C. TC3 is sol at 25 °C but its behavior changes to be gel in 37 °C (body temperature). Rheological studies of the two samples showed that by increasing the CNC percentage, the presence of a 3D network will be favorable. The network of CNCs helped triblock micelles to find their new gel state and show thermo-responsive behavior.

Acknowledgment

Special thanks to the supports of Dr. Ahmadjo, and Dr. Heydarnezhad for their devoted guidance.

References

1. Bae, S. J., Suh, J. M., Sohn, Y. S., Bae, Y. H., Kim, S. W., & Jeong, B., *Macromolecules*, *12*, 5260-5265, 2005.
2. Cui, Shuquan, Lin Yu, and Jiandong Ding, *Macromolecules*, 10, 3697-3715, 2019.
3. Vidyasagar, A., Ku, S. H., Kim, M., Kim, M., Lee, H. S., Pearce, T. R., ... & Kokkoli, E., *ACS Macro Letters*, *10*, 1134-1139, 2017.
4. Bertsch, P., Schneider, L., Bovone, G., Tibbitt, M. W., Fischer, P., & Gstöhl, S., *ACS applied materials & interfaces*, 11, 38578-38585, 2019.
5. Moud, A. A., Kamkar, M., Sanati-Nezhad, A., Hejazi, S. H., & Sundararaj, U., *Colloids and Surfaces A: Physicochemical and Engineering Aspects*, *609*, 125577, 2021.

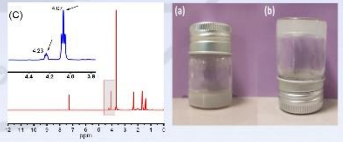

Figure 1. (a) Sol state of TC3 at 25°C, (b) Gel state at 37°C., (C) ^{1}H-NMR graph of PCL-PEG-PCL triblock.

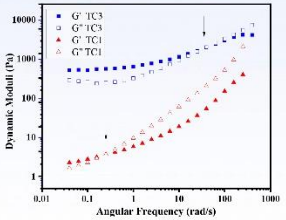

Figure 3. Frequency sweep of TC3 and TC1 sample at a constant strain 1% and 25°C.

Article code:

www.icor-sor.com

A-10-341-1

2nd International Conference on Rheology

14 & 15 December 2021, Tehran, Iran

Assessment and characterization of a dye-sensitized solar cell based on functionalized graphene nanocomposite gel polymer electrolyte

Pedram Manafi [1,2], Hossein Nazockdast *[1], Mohammad Reza Manafi [3]

1. Department of Polymer Engineering and Color Technology, Amirkabir University of Technology, Tehran, Iran.
2. Research and Development Center, Jam Petrochemical Company, South Pars Special Economic Zone (Asalouyeh), P.O. Box 11368-75118, Iran
3. Department of Applied Chemistry, Islamic Azad University, South Tehran Branch, P.O. Box: 17776-13651, Tehran, Iran.

Abstract

The long-term device instability of liquid-electrolyte-based dye-sensitized solar cells declines their ionic conductivity and performance. These issues can be resolved using the quasi-solid-state electrolytes. Despite the enhanced ionic conductivity of graphene nanoplatelets (GNP), their aggregation tendency has limited their application in quasi-solid-state electrolytes. The current study chemically modifies the GNP using polyethylene glycol (PEG) by amidation reaction to obtain a dispersible nanostructure in a PVDF-HFP/PEO polymer-blended gel electrolyte. Maximum ionic conductivity (4.11×10–3 S cm–1) was recorded in the optimal nanocomposite gel polymer electrolyte (GPE) encompassing 0.75 wt% functionalized graphene-nanoplatelets (FGNP). The power conversion efficiency of the DSSC based on 0.75 wt% of GPE was 6.46%. By incorporation of optimum FGNP content, a homogenous particle network was fabricated capable of effective mobilization of the redox-active species by its amorphous matrix

Keywords: Electrolytes, Microstructure, Rheological properties, DSSC and Graphene Nano Particles.

- Introduction

Dye sensitized solar cells (DSSCs) an electrochemical photovoltaic cell which converting solar energy to electricity with no environmental pollution and ecological destruction, have been attracted a lot of attention due to the easy fabrication, low cost cell assembly process, relatively high efficiency, scalable components, and no environmental issues [1–3]. Still leakage of liquid electrolyte is one of the remaining restrictions for its large-scale commercialization [4][5]. Various efforts have been aiming to substitute the liquid electrolyte by a polymer gel electrolyte (PGE) and solid polymer electrolyte (SPE) in order to overcome the weaknesses of liquid electrolytes [6]. Recently Gomari et al. [7] pioneerly grafted PEG onto graphene and used it in PEO electrolyte to increase the ionic conductivity by reducing the crystallinity of the nanocomposite. This study is motivated by aforementioned main concerns of DSSCs and let us to increase the efficiency of the instrument by developing a PGE. PVDF-HFP/ PEO blend has been chosen to used, due to its exceptional ion conductivity and lower crystallinity compare to the pair components. In the light of above, two types of electrolyte were prepared and compared as (i) Gel (PVDF-HFP/PEO/IL), and (ii) Gel (PVDF-HFP/PEO/IL/GNP or FGNP). Then, the influence of FG nanomaterial reinforcement on structural, rheological, and electrochemical properties of PVDF-HFP/PEO electrolyte membranes was explored.

- Experimental

The performance was further enhanced by synthesizing the ion–electron-conducting polymer composites with various contents of GNP and FGNP in PVDF-HFP/PEO: BMIMBF4: LiBF4 polymeric film. Different levels of functionalized or pristine graphene nanoplatelets (i.e., 0.1, 0.25, 0.5, 0.75, 1, or 1.5 wt% graphene relative to blend) were incorporated into the mixture containing a 10:1 w/w ratio of the BMIMBF4:LiBF4 redox complex couple and solvent. The black suspension was treated by 20 minutes of ultra-sonication while stirring to make sure on the formation of the homogenous dispersion of graphene, it was then incorporated into the PVDF-HFP and PEO mixture (60:40 w/w). The obtained mixture was further stirred at 80 °C until the complete dissolution of the polymer content followed by cooling down to the ambient temperature, which trigged the gelation process. The sample codes, as well as their composition, are listed in Table 1.

- Results and Discussion

For differentiating the linear viscoelastic region from the nonlinear, investigating the dispersive stability of NPs and the influence of IL, the strain amplitude sweep tests were carried out under the controlled frequency (1 rad s–1) and the range of 0.05–100%. The storage modulus was plotted as a function of the strain amplitude for PVDF-HFP/PEO blend, Gel and its nanocomposites including GNP and FGNP as shown in Fig 1. The linear-nonlinear transition of the viscoelastic behavior occurred at lower strain values in the Gel, Gel-GNP(1), and Gel-FGNP(0.75) as compared with the neat blend.

As can be seen, modulus reduction happens because of plasticizing effect of IL in the Gel sample. As can be seen, modulus reduction in Gel sample happens as a result of a) plasticizing effect of IL, and **b)** decreasing of physical crosslinking density. It should be noted that reduction of modulus, which happens by these two phenomena, are in competition with modulus improvement causes by gelation interactions. Thus, the linearity of the viscoelastic behavior was reduced and the storage modulus of the Gel sample was rapidly decreased after the critical strain. Also, this transition in the FGNP containing nanocomposites occurred at lower strains in comparison with pristine nanoplatelets. Such an observation could be assigned to the microstructural variations due to the
presence of the functionalized graphene nanoplatelets and the breaking of several essential elastic linkages in the 3D framework of the nanoplatelets whose contents are more dominant in the functionalized nanoplatelets. Additionally, storage modulus exhibited a rapid decline in the Gel-FGNP(0.75) implying more robust 3D network structures when FGNPs are used instead of GNPs. Therefore, more linear rheological assessments were conducted within the linear viscoelastic region (at 0.5% amplitude).

J–V plots of the as-prepared DSSCs are presented in Fig.2. The efficiency of the PVDF-HFP/PEO electrolyte was calculated at 0.61%. The photovoltaic performance, as well as other parameters, exhibited a drastic enhancement upon the incorporation of IL, GNP, and FGNP in comparison with the blend electrolyte. The highest photo-conversion efficiency (5.30%) with an open-circuit voltage of 0.636 V was recorded in Gel-FGNP(0.75). The further incorporation of FGNP declined the DSSC performance due to the lowered ionic transport and enhanced crystallinity.

As the designed DSSCs were fabricated and tested at consistent temperatures and device components, the enhancement in JSC could not be assigned to the thermal acceleration of ions in the GPE or the different photoanode properties. Improvement in the dye regeneration kinetics is under the influence of the ion diffusion and charge transport efficiencies inside the electrolyte layer. Thus, it can increase the JSC values. Consequently, the elevated JSC could be ascribed to the ionic diffusion of the redox-active species through the bridged nanoparticle network. Such a phenomenon is a consequence of PEG functionalization, through a Grotthus-type electron hopping ion-exchange mechanism.

Article code:

- Conclusion

According to the results, the ion conductivity and DSSC performance are highly dependent on the accessibility of the free ions and incorporation of optimal ratios of additives within the polymer electrolyte. The mobility of the ions could be also affected by the free volume of PVDF-HFP/PEO which can be enhanced through incrementing the amorphous domains of the samples. The PEG-functionalized graphene nanoplatelets (FGNP) were employed as the filler and incorporated into PVDF-HFP/PEO and ionic liquid systems.

- References

[1] Y. Ren, D. Sun, Y. Cao, H.N. Tsao, Y. Yuan, S.M. Zakeeruddin, P. Wang, M. Grätzel, , J. Am. Chem. Soc. 140 (2018) 2405–2408.

[2] W. Zhang, Y. Wu, H.W. Bahng, Y. Cao, C. Yi, Y. Saygili, J. Luo, Y. Liu, L. Kavan, J.-E. Moser, , Energy Environ. Sci. 11 (2018) 1779–1787.

[3] P. Ferdowsi, Y. Saygili, S.M. Zakeeruddin, J. Mokhtari, M. Grätzel, A. Hagfeldt, L. Kavan, Electrochim. Acta. 265 (2018) 194–201.

[4] J.H. Wu, S.C. Hao, Z. Lan, J.M. Lin, M.L. Huang, Y.F. Huang, L.Q. Fang, S. Yin, T. Sato, Adv. Funct. Mater. 17 (2007) 2645–2652.

Table 1 Sample codes along with their respective composition

Sample Name	Polymer electrolyte	Constituents in weight percent
PVDF-HFP/PEO	Neat Blend	60/40
Gel	PVDF-HFP/PEO: $BMIMBF_4$: $LiBF_4$	36/24: 36: 4
Gel-GNP(1)	PVDF-HFP/PEO: $BMIMBF_4$: $LiBF_4$: GNP	36/24: 36: 4: 1
Gel-FGNP(0.75)	PVDF-HFP/PEO: $BMIMBF_4$: $LiBF_4$: FGNP	36/24: 36: 4: 0.75

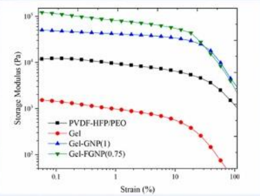

Fig 1. Storage modulus versus strain amplitudet

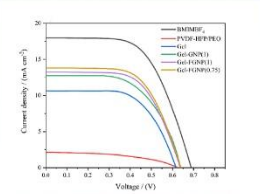

Fig 2. J–V curves of graphene-functionalized DSSCs

2nd International Conference on Rheology

14 & 15 December 2021, Tehran, Iran

Investigation on the Shear-induced Gelation Behavior of PVA/Sodium alginate/GO Nanocomposite Hydrogel

Abdolali Mehrjou[1], Ismaeil Ghasemi[2]

1. Department of Polymer Engineering and Color Technology, Amirkabir University of Technology, Iran
2. Faculty of Processing, Iran Polymer and Petrochemical Institute, Tehran, Iran

Abstract

This study aims to prepare nanocomposite hydrogel based on poly(vinyl alcohol)/sodium alginate, reinforced by incorporating graphene oxide (GO) for use in strain sensors. Small Amplitude Oscillatory Shear (SAOS) flow was used to monitor hydrogel property. Additionally, GO surface was modified using polyethylene glycol (PEG) through the formation of covalent bonds between functional groups on the GO's surface and PEG chains. In the FTIR spectrum of GO-g-PEG, the characteristic peaks of different bonds were shifted, which proves the presence of new functional groups, and can be related to the reaction of GO and PEG. The variation of storage modulus showed the formation of hydrogel, and structural strength was find. In addition, self-healing of the samples due to the presence of sodium alginate was tracked using typical self-healing experiment.

Keywords: Hydrogel – Induced gelation – Graphene oxide – Surface modification – IPN

Introduction

There is fast growing interest in using nanoparticles such as graphene oxide (GO) in hydrogels. This could be because GO is a "super gelator" in aqueous solution, with a critical gelation concentration of less than 0.5 weight percent [1]. Smart materials have attracted the attentions of academics over the last few decades due to their unique applications in a wide range of industries. One of the most promising fields of smart materials, self-healing materials, has recently become a heated topic. Self-healing hydrogels based on noncovalent reactions and dynamic covalent interactions have received a lot of attention [2].

If stress relaxation is significantly faster than the time required for structural change, SAOS measurements can be used to track microstructure evolution in dispersions. The storage modulus indicates the number of network points in the gels and grows as the gelation process progresses. As a result, several studies have used SAOS measurements to track the degree of gelation.

We used rheological analysis to investigate the gelation of aqueous dispersions containing GO and polyvinyl alcohol (PVA). Surprisingly, our research found that SAOS can cause graphene dispersions to gel. Shake gels have also been observed in polymer dispersions, including other nanoparticles. The "shake gels" revert to the solution once the flow stops. The SAOS-induced hydrogels, on the other hand, were stable in this investigation.

Furthermore, sodium alginate plays an iconic role in having a self-healable hydrogel. To be more specific, having dynamic bonds is crucial for obtaining self-healing property: Both PVA physical entanglements and sodium alginate ionic crosslinks can be broken up and repaired.

Experimental

Poly(vinyl alcohol) (PVA) was purchased from Sigma Aldrich (99 mol% hydrolyzed, $\overline{Mw}$ = 13000 g). Graphene oxide nanoplatelets (3.4-7 nm thickness) was supplied from US Research Nanomaterials Inc, with a purity of 99.5% and 6-10 layers. PEG with a molecular weight of 400 gr/mol was obtained from Merck. Sodium alginate (Guluronic Acid:Mannuronic Acid equal to 1.2:1) was purchase from Sigma Aldrich. Grafting of PEG on GO was done following the procedures reported in our previous work [3].

PVA powder was added into deionized water to prepare a solution under stirring at 80 °C for 1 h. After the PVA solution was cooled down to room temperature, 5 ml GO dispersion (5 mg/ml) was added into 5 ml PVA solution. Aqueous dispersions with two different PVA weight ratios to GO was prepared: GO concentration kept as 0.4 wt.% in the dispersions prepared with PVA:GO = 2:1 and 1:5, corresponding to 0.80 and 0.08 wt.% PVA in the dispersions, respectively. Both dispersions kept under magnetic stirring for another 1 h. It is worth mentioning that hydrogel is not formed when PVA contents is less than or equal to 0.05 wt.% in the dispersions. Next, 2 wt.% solution of sodium alginate is added to each of the dispersions to obtain a PVA/GO/sodium alginate mixture under magnetic stirring. At last, each dispersion is added to 4 wt.% aqueous solution of calcium chloride to prepare samples.

We measured G' and G" with respect to frequency at constant shear (γ=10%) to corroborate the SAOS-induced gelation. Fig. 1 shows a typical storage modulus (G') and loss modulus (G") of hydrogels with 0.8 wt.% and 0.08 wt.% PVA. These measurements have been done by a conventional frequency sweep from 0.01 rad/s to 100 rad/s in the rotational rheometer with parallel plate geometry with a gap size of 1.0 mm and a plate diameter of 50 mm.

Results and Discussion

According to the FTIR spectra of GO and GO-g-PEG presented in Fig. 2, the characteristic peak of C=O bond was moved to 1731 cm^{-1} which indicates the presence of ester groups. This peak proves the successful grafting of PEG on GO surface.

Regarding the formation of the double network hydrogel, it is clear that PVA chains are concentrated around GO nanoparticles, which are grafted to PEG long chains. As this aqueous solution is put under SAOS flow, the PVA chains create physical entanglements, and finally, they form a stable structure. Besides, sodium alginate and calcium chloride have already produced ionic bonds. The creation of physical entanglements coupled with ionic bonds leads to the formation of hydrogel nanocomposite. As shown in Fig. 1, G' and G" at first had some fluctuations until they reach a plateau. Moreover, G' is always higher than G" at all frequencies mentioned in this study. These findings suggest that SAOS may impact the gel structure. If this is the case, traditional frequency sweep dynamic moduli cannot be used to measure the structural properties of hydrogels.

We measured G' and G" with respect to time at constant frequency (ω = 1 rad/s) to validate the SAOS-induced gelation. For hydrogel (0.8 wt. percent PVA), the time evolution of G' and G" at ω = 1 rad/s is presented in Fig. 3. G' decreases over time until it reaches a plateau. Also, G' plot is always above the G" plot in Fig. 3. The behaviors of G' and G" at other frequencies are likewise indicating SAOS stress causes the GO hydrogels to restructure. The struggle between the development and breakdown of gel-networks in SAOS flow increases the number of network sites until a stable state is obtained.

Conclusion

In summary, a facile approach is presented to prepare dynamic hydrogels using poly(vinyl alcohol) (PVA), sodium alginate, graphene oxide, and water as the main components. Small amplitude oscillatory shear (SAOS) stress thickens the GO hydrogels. When the hydrogels are agitated at lower frequencies, the thickening is more noticeable. The SAOS-induced gelation described in this study differs from regular polymer gelation. These findings support the development of a new rheological theory to explain such a phenomenon.

References

1. Hu, Y.-L., et al., *Applied Physics Letters*, **100**(16): p. 161101, 2012.
2. Jing, X., et al., *Sensors and Actuators B: Chemical*, **295**: p. 159-167, 2019.
3. Karimi, S., I. Ghasemi, and F. Abbassi-Sourki, *Composites Part B: Engineering*, 2019.

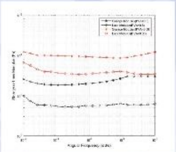

Fig 1. The storage modulus (G') and the loss modulus (G") of hydrogels with 0.8 wt.% PVA (black) and 0.08 wt.% PVA (red) by frequency sweep measurements.

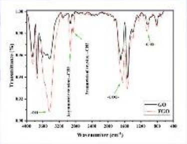

Fig 2. FTIR spectra of graphene oxide (GO) and PEG-g-GO (FGO).

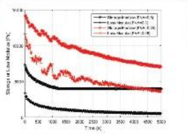

Fig 3. Time evolution of storage modulus (G') and loss modulus (G") of hydrogels with 0.8 wt.% PVA (black) and 0.08 wt.% PVA (red) at ω=1 rad/s.

A-10-389-1

2nd International Conference on Rheology
14 & 15 December 2021, Tehran, Iran

Rheology of self-assembled Polystyrene block polyacrylic acid

Farnaz Farbod, Fatemeh Goharpey
Amirkabir University of Technology

Introduction

Self-assembly of block copolymers has been widely studied for nanopatterning application including alternative way of lithography for semiconductor industry. In an attempt to reach sub 10 nm pattern periodicity, we demonstrate synthesis, characterization and self-assemblies of PS-PAA as the best candidate of BCPs for self-assembly thanks to its high chi parameter. ATRP method was used for PS-b-PMA synthesis, followed by hydrolysis with TFA. Temperature sweep and DSC analysis were used for determination of transition temperatures of BCPs.

Experimental

ATRP synthesis of BCPs were done as described elsewhere[1, 2]. PS-PAA were obtained after hydrolysis by TFA as a mild condition procedure. Successful synthesis and hydrolysis reaction process were checked and characterized by GPC, H-NMR and FTIR tests. Thin films on the pre-cleaned wafer silicones were obtained by spin coating and solvent annealing procedure were performed at room temperature under toluene THF atmosphere. Self-assembled BCPs were observed by AFM images.

Results and discussion

Temperature sweep of PS74-PAA28, PDI=1.16, was performed at 2° C/min of heating rate with fixed strain and angular frequency of 0.2% and 1 rad/s, respectively. Two sharp decreases of storage modulus, about two orders of magnitude, at 80 and 153 °C followed by two overlaps of G' and G" at 84 and 157 °C were observed. First sharp storage modulus reduction indicates an order-order transition while the second of this phenomenon implies order disorder transition. Another two order to order transition temperatures occurred at 91 and 112° C/min according to figure 1, at maximum value of tan delta and overlapping point of G' and G", respectively. Rheology experiment of temperature sweep also shows two distinct glasses transition temperature attributed to two blocks of block copolymer at 84 and 157 °C where both moduli overlap each other. In summary, as it shows in rheology test figure, important phase transition temperatures include: order to order transition temperatures (TOOT) are 80, 112, 91,153; Tg: 84; order to disorder transition temperature is (TODT): 157°C.

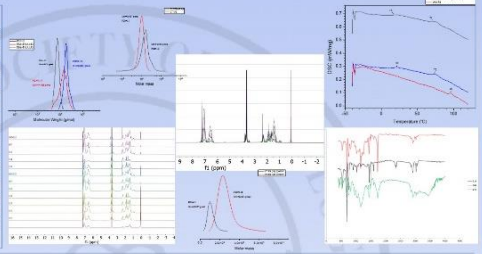

Conclusion

PS-PAA BCPs were successfully synthesized and characterized. Lamellae and HPL structure were observed with sub 10 nm feature size. Temperature sweep was conducted to determine order to disorder and order to order transition temperature which were in accordance with DSC results

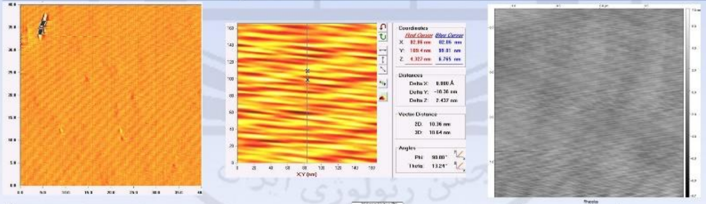

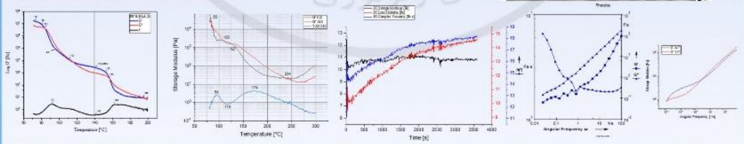

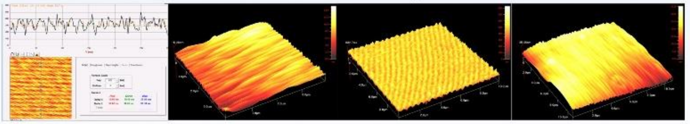

Article code:

References:

1. Abraham, S., C.-S. Ha, and I. Kim, Synthesis of poly(styrene-block-tert-butyl acrylate) star polymers by atom transfer radical polymerization and micellization of their hydrolyzed polymers. Journal of Polymer Science Part A: Polymer Chemistry, 2005. 43(24): p. 6367-6378.
2. Ma, Q. and K.L. Wooley, The preparation of t-butyl acrylate, methyl acrylate, and styrene block copolymers by atom transfer radical polymerization: Precursors to amphiphilic and hydrophilic block copolymers and conversion to complex nanostructured materials. Journal of Polymer Science Part A: Polymer Chemistry, 2000. 38(S1): p. 4805-4820.
3. Moon Jeong Park, K.C., Interplay between Cubic and Hexagonal Phases in Block Copolymer Solutions. Langmuir, 2005. 21: p. 1403-1411.
4. Che-Yi Chu, W.-F.L., Jing-Cherng Tsai, Chia-Sheng Lai, Shen-Chuan Lo, Hsin-Lung Chen, Takeji Hashimoto, Order–Order Transition between Equilibrium Ordered Bicontinuous Nanostructures of Double Diamond and Double Gyroid in Stereoregular Block Copolymer. Macromolecules, 2012. 45: p. 2471−2477.
5. Chang Dae Han, D.M.B., Effect of Volume Fraction on the Order-Disorder Transition in Low Molecular Weight Polystyrene-bZock-Polyisoprene Copolymers. 1. Order-Disorder Transition Temperature Determined by Rheological Measurements. macromolecule, 1995. 28: p. 5043-5062.

www.icor-sor.com